

**The Evolution of Binary Populations in Young Star Clusters:  
From the ONC to OB associations**

Doktorarbeit - PhD Thesis

In a u g u r a l - D i s s e r t a t i o n

zur

Erlangung des Doktorgrades

der Mathematisch-Naturwissenschaftlichen Fakultät

der Universität zu Köln

vorgelegt von

Thomas Kaczmarek

aus Köln

1. Physikalisches Institut  
Universität zu Köln

Köln, den 20. August 2012

Berichterstatter/in: Prof. Dr. Susanne Pfalzner .....

Prof. Dr. Joachim Krug .....

Tag der mündlichen Prüfung: 19. Oktober 2012

## Zusammenfassung

Beobachtungen der Doppelsternpopulationen in jungen Sternhaufen zeigen, dass kurz nach dem Ende des Sternentstehungsprozesses ein Großteil der Sterne Teil eines Doppelsternsystems sind. Im Gegensatz dazu beträgt die Doppelsternrate im Feld nur  $\sim 50\%$ . Die meisten Sterne und damit auch die meisten Doppelsterne, entstehen in dichten Sternhaufen, was zu der Frage führt, ob die Geburtsstätten der Doppelsterne für die Abnahme der Doppelsternrate verantwortlich sind. In dieser Arbeit wird eine Antwort auf diese Frage gesucht. Zu diesem Zwecke wurden numerische N-Teilchen Simulationen von Doppelsternpopulationen in Sternhaufen mit unterschiedlichen Dichten durchgeführt.

Zunächst wurde die Entwicklung von Doppelsternen in “Orion Nebula Cluster”-artigen (ONC-artigen) Sternhaufen untersucht. Es konnte gezeigt werden, dass die Entwicklung der normalisierten Anzahl an Doppelsternen unabhängig von der initialen Doppelsternrate ist. Dies ermöglicht es, die Entwicklung der Doppelsternpopulationen in ONC-artigen Haufen vorherzusagen, ohne dass weitere numerische Rechnungen erforderlich sind. Zusätzlich wurde gezeigt, dass die dynamischen Interaktionen vorrangig Doppelsternsysteme massearmer Sterne zerstören, was in Übereinstimmung mit Beobachtungen im ONC zu einer erhöhten Doppelsternrate für massive Sterne führt. Eine Kombination der dynamischen Entwicklung mit dem gas-induzierten Schrumpfen der Orbits von in Gas eingebetteten Doppelsternen wandelt eine logarithmisch gleichverteilte Verteilung der Umlaufzeiten, wie sie in jungen Sternhaufen beobachtet wird, zu einer logarithmisch normalen Umlaufzeitenverteilung um, wie sie in der Feld Population beobachtet wird.

Anschließend wurden die Rechnungen für Sternhaufen mit beliebigen Dichten verallgemeinert, indem Simulationen von Sternhaufen mit bis zu achtfach höheren Dichten als im ONC durchgeführt wurden. Es konnte nachgewiesen werden, dass auch in diesen Sternhaufen die Entwicklung der normalisierten Anzahl an Doppelsternen unabhängig von der initialen Doppelsternrate ist und das, wie zu erwarten, in Sternhaufen mit höherer Dichte mehr Doppelsterne zerstört werden. Dieser Effekt nimmt jedoch für Sternhaufen mit Dichten von mehr als  $\approx 3 \times 10^4 \text{ pc}^{-3}$  ab. Dies bedeutet, dass es eine Grenze gibt, ab der das Erhöhen der Dichte in den Sternhaufen zu keiner signifikanten Zunahme der Anzahl an zerstörten Doppelsternen führt.

Schließlich wurde untersucht, wie sich Doppelsternpopulationen in Sternhaufen entwickeln, die ihr überschüssiges Gas ausgeworfen haben und in Folge dessen schnell an stellarer Dichte einbüßen. Es wurde gezeigt, dass mit abnehmender Sternentstehungsrate eines Sternhaufens weniger weite Doppelsterne zerstört und mehr sehr weite gebildet werden. Der Vergleich der Entwicklung der simulierten Sternhaufen und der beobachteten “leaky cluster sequence” legt nahe, dass Sternhaufen mit einer Doppelsternpopulation und einer Sternentstehungsrate von 30% den beobachteten “leaky clusters” sehr gut entsprechen.



## Abstract

Observations of the binary populations in young, sparse clusters have shown, that almost all stars are part of a binary system at the end of the star formation process. By contrast, the binary frequency of field stars only  $\sim 50\%$ . Most stars, and therefore most binaries, are formed in dense star clusters. This rises the question if the natal environments lead to the observed reduction of the binary frequency. In this thesis this question is addressed using numerical Nbody simulations of binary populations in different star cluster environments.

First the evolution of binaries in ONC-like star clusters has been investigated. It was found that there the evolution of the normalised number of binaries is independent from the initial binary frequency. This allows to predict the evolution of binary populations in ONC-like clusters without the need of further numerical simulations. In addition it was found, that dynamical interactions preferentially destroy low-mass binaries resulting in a higher binary frequency for high-mass stars in the simulated clusters, in accordance with observation in the ONC. The combination of dynamical evolution with gas-induced orbital decay of embedded binaries is capable to reshape a log-uniform period distribution, as observed in young star clusters, to a log-normal period distribution as observed in the field today.

The modelling has been generalised to clusters with arbitrary densities. Performing simulations for clusters with up to eight times higher densities than before with two different initial binary frequencies, it was shown that the evolution of the normalised number of binaries remains independent of the initial binary frequency. The higher the density in a cluster the more binaries are destroyed as to be expected. However, this effect levels out for clusters with central densities exceeding  $\approx 3 \times 10^4 \text{pc}^{-3}$ . This means that there is a limit beyond which increasing the binary frequency in the clusters does not lead to significantly more binaries being destroyed.

Finally it was investigated how the binary population evolves in star clusters that have undergone instantaneous gas expulsion with a resultant fast decrease in stellar density. It was found that the lower the star formation efficiency of a cluster and therefore the faster the decrease in stellar density, the less binaries are destroyed during the evolution while at the same time the more very wide binaries are formed. Comparison of the evolution of the simulated clusters and the observed leaky cluster sequence shows that clusters including a binary population and a  $\varepsilon = 0.3$  match the observations of leaky-star clusters remarkably well.



# Contents

<b>1</b>	<b>Introduction</b>	<b>1</b>
1.1	Star clusters . . . . .	3
1.2	Evolution of star clusters . . . . .	10
1.3	Binaries . . . . .	16
1.4	Gas expulsion . . . . .	20
<b>2</b>	<b>Numerical Simulations</b>	<b>27</b>
2.1	Integration . . . . .	27
2.2	Individual time steps . . . . .	30
2.3	Neighbour treatment . . . . .	32
2.4	KS-regularization . . . . .	34
2.5	Hardware acceleration . . . . .	37
<b>3</b>	<b>Binary populations in ONC-like star clusters</b>	<b>41</b>
3.1	Introduction . . . . .	41
3.2	The influence of the cluster dynamics on the binary population . . . . .	41
3.3	Orbital decay . . . . .	53
3.4	Combination and comparison with observations . . . . .	56
3.5	Summary . . . . .	61
<b>4</b>	<b>Density-dependence of binary dynamcis</b>	<b>63</b>
4.1	Introduction . . . . .	63
4.2	Setup . . . . .	63
4.3	Evolution of the binary population in dense star clusters . . . . .	64
4.4	Evolution of the period distribution at different densities . . . . .	70
4.5	Dependence on the primary mass . . . . .	74
4.6	Evolution of the eccentricity and mass-ratio distribution . . . . .	77
4.7	Comparison with the observations . . . . .	78
4.8	Summary . . . . .	82
<b>5</b>	<b>Binary populations in supervirial clusters</b>	<b>83</b>
5.1	Introduction . . . . .	83
5.2	General evolution of star clusters after gas expulsion . . . . .	85
5.3	Simulation setup . . . . .	87

5.4	Evolution of the star clusters . . . . .	89
5.5	Binary populations in star clusters undergoing instantaneous gas expulsion . . . . .	105
5.6	Summary . . . . .	112
<b>6</b>	<b>Discussion</b>	<b>115</b>
<b>7</b>	<b>Summary and Conclusions</b>	<b>117</b>
	<b>Bibliography</b>	<b>121</b>
<b>A</b>	<b>Density-dependence of binary dynamics</b>	<b>129</b>
<b>B</b>	<b>Supervirial Cluster Evolution</b>	<b>131</b>



# 1 Introduction

The most important observations to have shaped our current picture of the binary field population were performed in the early 1990's. Duquennoy & Mayor (1991) found that the binary frequency of G-type stars in the solar neighbourhood is about 61% and the period distribution follows a log-normal distribution

$$f(\log P) = C \exp \left\{ \frac{-(\log P - \overline{\log P})^2}{2\sigma_{\log P}^2} \right\}, \quad (1.1)$$

over the period range  $\sim 10^{-1} - 10^{11}$  d, where  $P$  is the period in days ( $\overline{\log P} = 4.8 \equiv 172$  yr,  $\sigma_{\log P} = 2.3$ ) and  $C$  a normalisation constant. A year later, Fischer & Marcy (1992) analysed the binary properties of M-dwarfs in the separation range  $0.04 - 10^4$  AU corresponding to periods in the range  $\sim 10^{-2} - 10^6$  yr and found that the period distribution of M-dwarfs in the solar neighbourhood is also log-normally distributed with a peak between 9 yr and 270 yr, which is nearly identical to the findings for G-dwarfs. Although the observed binary frequency of M-dwarfs at about 33% is lower than that of G-dwarfs, the properties of the G and M-dwarf binary populations seem very similar. Observations of Raghavan *et al.* (2010) confirmed this picture. They determined the binary properties of nearby ( $d < 25$  pc) solar-type stars ( $\sim F6 - K3$ ) and found that the fraction of binary stars is 58% with a log-normal period distribution ( $\overline{\log P} = 5.03$  and  $\sigma_{\log P} = 2.28$ ).

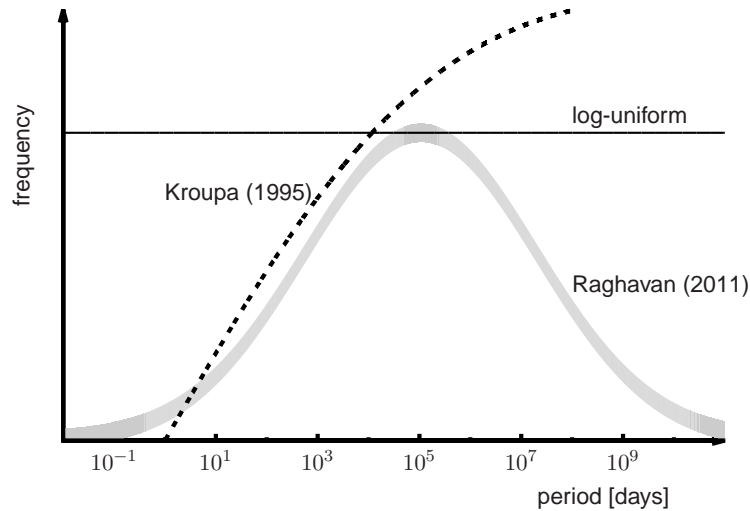


Figure 1.1: Schematic picture of possible initial period distributions. The thick grey curve displays the log-normal fit to the data of Raghavan *et al.* (2010), the thick dashed line the Kroupa (1995a), and the solid line a log-uniform period distribution, which is observed for many young star-forming regions (see text for references).

With an average age of a few Gyrs, the field population constitutes a dynamically evolved state. Therefore, dynamical processes have most likely changed the binary properties since the formation of these stars, and the current properties probably differ significantly from the primordial state. To understand the binary formation process, it is insufficient to know the properties of the (old) field population: those of the primordial binary population of to be known.

Connelley *et al.* (2008) determined the binary properties of the very young populations in Taurus, Ophiuchus, and Orion star-forming regions (excluding the much denser Orion Nebula Cluster). They found that their observed period distribution can be fitted by a log-uniform distribution, which differs significantly from the log-normal distribution in the field (see also Kraus & Hillenbrand (2007)). In these sparse young star-forming regions, it is improbable that dynamical evolution has altered the period distributions in the short period since the stars were formed (see e.g. Kroupa & Bouvier, 2003). Hence, we can assume that their properties in general match the initial conditions.

In denser regions, indications of an originally log-uniform distribution have also been found. For example, the HST observations by Reipurth *et al.* (2007) of binaries in the Orion Nebula Cluster (ONC) demonstrate that the semi-major axis distribution deviates from the log-normal distribution and is closer to a log-uniform distribution. Hence, it seems that older binary populations have a *log-normal* period distribution, while the primordial distribution is likely to be *log-uniform*.

After the binaries have been processed in the star clusters that have to be released into the field to form the binary population that is observed there today. The most likely process to unbind most binaries is the expansion of the star clusters after they have lost their remnant gas (e.g. Tutukov, 1978; Hills, 1980; Lada *et al.*, 1984; Baumgardt & Kroupa, 2007) which is also thought to be responsible for the observed leaky cluster sequence for massive clusters (Pfalzner, 2009; Pfalzner & Kaczmarek, in preparation).

From the theoretical side, the binary frequency is the most well-studied binary property (e.g. Kroupa & Burkert, 2001; Kroupa & Bouvier, 2003; Kroupa *et al.*, 2001; Pfalzner & Olczak, 2007). It also seems that the evolution of the binary frequency in the ONC depends on the initial binary frequency, whereas the evolution of the binary population does not (Kaczmarek *et al.*, 2011). However, the binary population is not only described by the binary frequency but also by the period, mass-ratio, and eccentricity distribution.

Starting with the work of Heggie (1975), it has been realised that binaries can be dynamically disrupted by three- and four-body interactions. Wide binaries are generally more affected by dynamical destruction than close ones. The existence of binaries wider than  $10^3$  AU in the field is still difficult to explain in models of their origin (Parker *et al.*, 2009).

Performing N-body simulations, Kroupa (1995a,b) showed that to reproduce the observed log-normal distribution of the field, the initial number of wide binaries has to be significantly higher than observed, if all binaries are subject to dynamical evolution in a star cluster. This rising distribution was obtained by inverse dynamical population synthesis, i.e. inverting the effects of dynamical destruction on the period distribution (see dashed line in Fig. 1.1).

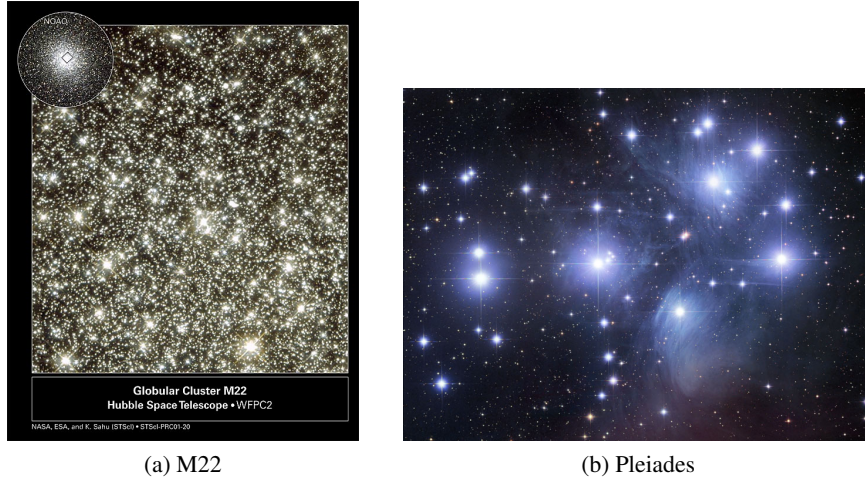


Figure 1.2: a) Image of the M22 globular cluster taken with the Hubble Space Telescope (Copyright: NASA). b) Image of the Pleiades cluster. Copyright Robert Gendler.

The scope of this thesis is to investigate how binary populations evolve in star cluster models that are motivated by observations of star clusters. In Chap. 3 the evolution of binaries in ONC-like clusters will be studied which will be generalised to cluster of arbitrary densities in Chap. 4. Finally, the evolution of binaries in star clusters after instantaneous gas expulsion will be investigated in Chap. 5 as this ends the evolution of each star cluster.

## 1.1 Star clusters

### 1.1.1 Classification

In general, the term “star cluster” denotes a group of several, interrelated stars. Obviously, this definition is very vague and comprises a wide variety of stellar groupings. For this reason, star clusters are usually divided into different groups concerning their shape, mass, age, stellar content and so on. In this section the definitions concerning gas free clusters will be introduced while embedded star clusters will explicitly be excluded, as they will be treated in Sec. 1.4.

Historically, two different types of star clusters can be distinguished based on their masses, shapes and ages - globular and open (sometimes also-called galactic) clusters. Globular clusters like M22 (see Fig. 1.2a) are very old structures which have their perfect spherical shapes and their small sizes ( $\approx 0.1$  pc). They usually consist of several  $10^4 - 10^5$  stars and have masses up to  $10^6 M_{\odot}$ . In our galaxy  $\approx 150$  globular clusters are known which can mostly be found in the galactic halo (e.g. Djorgovski & Meylan, 1993). In contrast to that open clusters like the Pleiades (Fig. 1.2b) are much younger ( $< 0.3$  Gyr) and often show serious deviations from the spherical shape that is observed for globular star clusters. Open clusters are in general much larger than globular clusters ( $\leq 10$  pc) and contain significantly less stars (up to a few thousand). In our galaxy about 1000 open clusters are known today (Dias *et al.*, 2002).

However, the detection of unbound young stellar groupings that do not survive as long as it is

observed for open or globular clusters required to introduce the so-called “stellar associations”. Stellar associations are groups of stars that are only loosely bound or even in the process of being completely dissolved in the near future. Based on the total mass of the association and the type of stars that can be found inside the associations a further distinction is applied for these systems.

T associations are the least massive associations and consist only of low-mass stars that have not reached the main-sequence yet and are still surrounded by their accretion disks. Since stars in this evolutionary phase have first been found in the Taurus-Auriga star forming region (Strom *et al.*, 1975), which is a prototype for a T association, such stars are called T-Tauri stars.

The second more massive type of associations are the so-called R associations which due to their young ages also consist of pre-main sequence stars only. However, as R associations also include intermediate mass stars, they do not only consist of T-Tauri stars but also include Herbig-Ae/Be stars (Herbig, 1960) which are the more massive counterparts of the T-Tauri stars and which produce so-called reflection nebulae by illuminating gas in their surroundings. A typical example for a R association is Mon R2 (Herbst & Racine, 1976).

The last and at the same time most massive type of stellar association are the so-called OB-associations. In contrast to the T- and R-associations these do not exclusively consist of pre-main sequence stars, but also of stars that already settled on the main-sequence, meaning that these stellar groupings are older than the previous two types. Additionally OB-associations contain very massive O and B stars in significant number, which lead to the name of this association type. The nearest OB-association from the sun is the Scorpius-Centaurus Association (Sco-OB2) which includes several thousand stars with masses up to  $20 M_{\odot}$  (Preibisch *et al.*, 2002).

As can be seen, stellar groupings can be categorised in different ways. However, an objective measure to decide if a stellar grouping is a cluster or an association is still missing. Only recently, Gieles & Portegies Zwart (2011) proposed to use the ratio of age of a stellar grouping and its crossing time  $\Pi = \text{age}/t_{\text{cr}}$  (see Sec. 1.2.1 for a definition of the crossing time of a stellar grouping) for this purpose. Following their suggestion all stellar groupings with  $\Pi < 1$  should be designated as stellar association while groupings with  $\Pi > 1$  should be regarded as star clusters. However, these definition is only based on empirical findings that cannot be substantiated with any physical considerations.

An alternative classification scheme was proposed by Pfallner (2009), who found that, at least massive clusters with more than  $1000 M_{\odot}$ , can be divide into two distinct “cluster sequences”, depending on their location in the density radius plot shown in Fig. 1.3. Stellar groupings in the first cluster sequence are called “starburst clusters” and begin their evolution as very small ( $\approx 0.1$  pc), massive ( $\approx 20000 M_{\odot}$ ) systems that slowly diffuse with time so that after  $\approx 20$  Myr their sizes have grown to about 1 pc while their total masses remain almost the same. Examples for starburst clusters are the young Arches and Quintuplet clusters, which both are in near vicinity to the galactic centre. However, also the much older  $\chi$ -Perseus cluster, which is usually categorised as OB-association, has to be designated as being an (old) starburst cluster if the definition by (Pfallner, 2009) is adopted.

The stellar groupings in the second sequence are called “leaky clusters” and begin their evolution

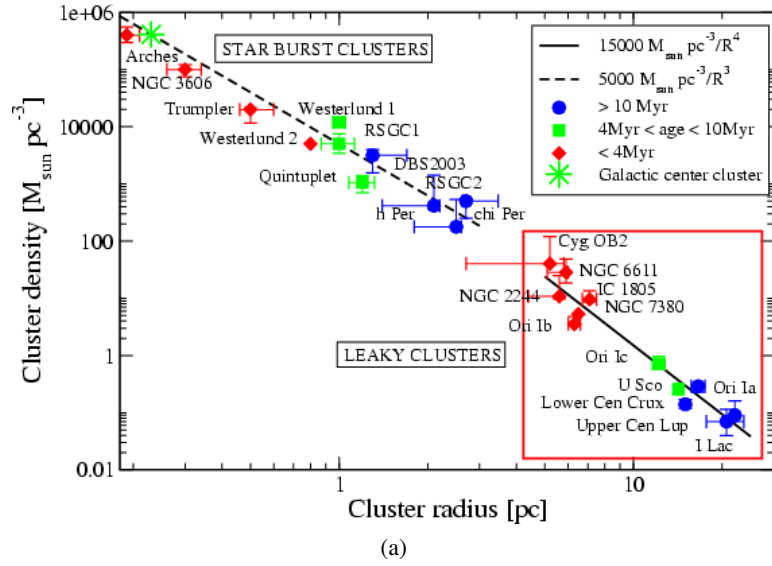


Figure 1.3: Observed cluster density as function of the cluster radius for clusters more massive than  $10^3 M_{\odot}$ . Taken from Pfalzner (2009).

with the same masses as the starburst clusters but much larger sizes of about 2 pc. During the next 20 Myr the leaky clusters expand to sizes of about 13 pc but at the same time loose a significant fraction of their masses. Examples for leaky star clusters are Cygnus OB2 and Scorpius OB2, which are usually designated as being OB associations.

The evolution of leaky star cluster and the evolution of a primordial binary population inside these clusters will be investigated in Chap. 5. Therefore, the naming convention proposed by Pfalzner (2009) will be applied throughout this thesis.

### 1.1.2 Models

The most fundamental way to characterise star clusters is to give the complete  $6N$ -dimensional phase-space vector of the cluster consisting of the position and velocity vectors of all stars in the cluster. However, as star clusters consist of up to several ten-thousand stars this is impracticable when comparing both observations and simulations of star clusters because of the high number of parameters involved and the dramatic changes of the phase-space vector on short-timescales. Therefore it is convenient to define equilibrium models that describe the clusters with a significantly reduced set of parameters.

In this section of the thesis the most important models of star clusters that are used in theoretical and observational studies of star clusters will be introduced.

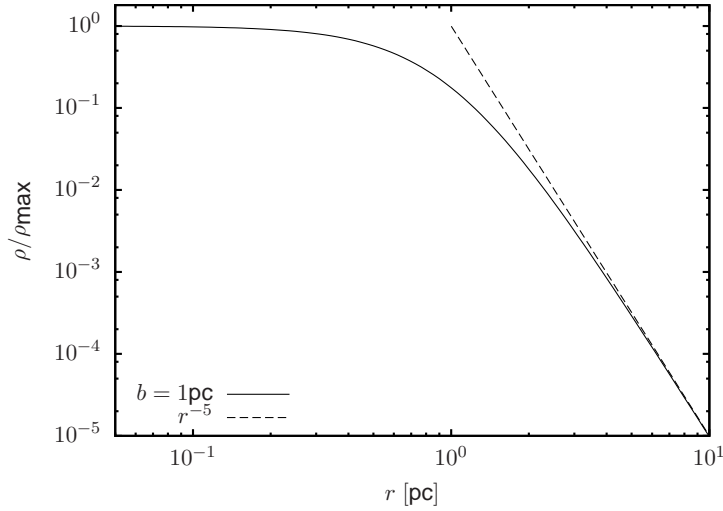


Figure 1.4: Stellar density distribution resulting from a Plummer model cluster with scale-length  $b = 1$  pc (solid line).

### Plummer model

One of the most often used star cluster models is the so-called Plummer-model whose potential is given by

$$\Phi = -\frac{GM}{\sqrt{r^2 + b^2}} \quad (1.2)$$

with the **Plummer scale length**  $b$  and total mass  $M$ . The density distribution resulting from this potential is

$$\rho(r) = \frac{3M}{4\pi b^3} \left(1 + \frac{r^2}{b^2}\right)^{-5/2}. \quad (1.3)$$

From this it can easily be seen, that the Plummer model extends without any borders which of course is not physical.

Originally Plummer (1911) used this potential to fit the observed density profiles of globular clusters. Today, the Plummer model is often used for simulations of star clusters in general - regardless if the clusters under consideration are several Gyr old or much younger (e.g. Aarseth *et al.*, 1974; Kroupa, 1995a; Goodwin & Bastian, 2006; Parker *et al.*, 2009; Allison *et al.*, 2009; Kouwenhoven *et al.*, 2010, and many more). The reason the Plummer model is used that often to set up star clusters in simulations is that, in comparison to other star cluster models (see below), the Plummer model can be described by a set of analytic equations which allows to set up the clusters very easily (Aarseth *et al.*, 1974).

Fig. 1.4 shows the density distribution (Eq. 1.3) of a Plummer model cluster with scale length  $b = 1$  pc. As can be seen the Plummer model is characterised by a central core, within which the density is constant. Outside the core, the density of the Plummer density profile starts to decline and for radii  $> b$  the density drops of as  $r^{-5}$ .

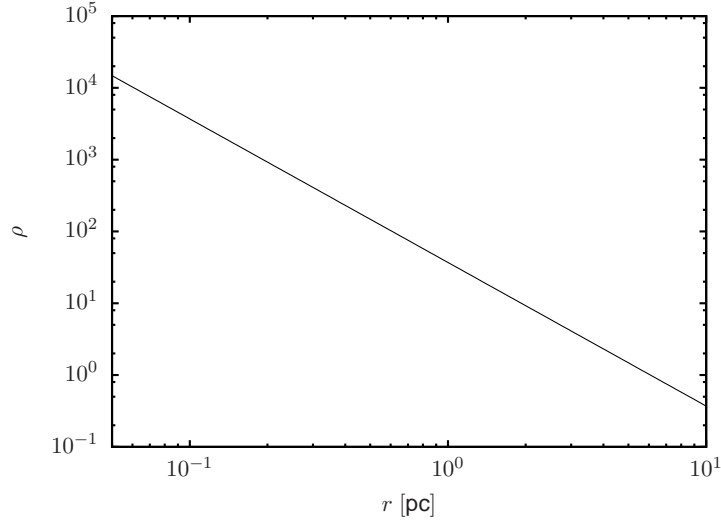


Figure 1.5: Stellar density distribution of the singular isothermal sphere.

### The isothermal sphere

The present standard picture of star formation states, that stars form out of self-gravitating molecular clouds (Larson, 2003), which can be approximated as being isothermal spheres. As also the star clusters form out of this molecular clouds, it seems reasonable to assume that also star clusters can be approximated as being isothermal spheres.

The gravitational potential of the so-called **singular isothermal sphere** (singular due to the singularity at the cluster centre) is given by

$$\Phi(r) = 2 \sigma^2 \ln(r) + \text{const.} \quad (1.4)$$

where  $\sigma = \sqrt{k_B T / m}$  is the velocity dispersion inside the cluster. Applying Poisson's equation yields the stellar density distribution

$$\rho(r) = \frac{\sigma^2}{2\pi G r^2}. \quad (1.5)$$

The mass of the cluster inside a given radius  $r$  is given by

$$M(r) = \frac{2\sigma^2 r}{G}. \quad (1.6)$$

The velocities of the stars in the isothermal spheres are given by the **Maxwellian velocity distribution**

$$dn \propto \exp\left(-\frac{|\mathbf{v}|^2}{2\sigma^2}\right) d^3\mathbf{v} \quad (1.7)$$

independently of the position in the sphere.

Fig. 1.5 shows the stellar density distribution of an isothermal sphere. In contrast to the Plummer model, which exhibits a central core, within which the density is constant, the isothermal sphere has a

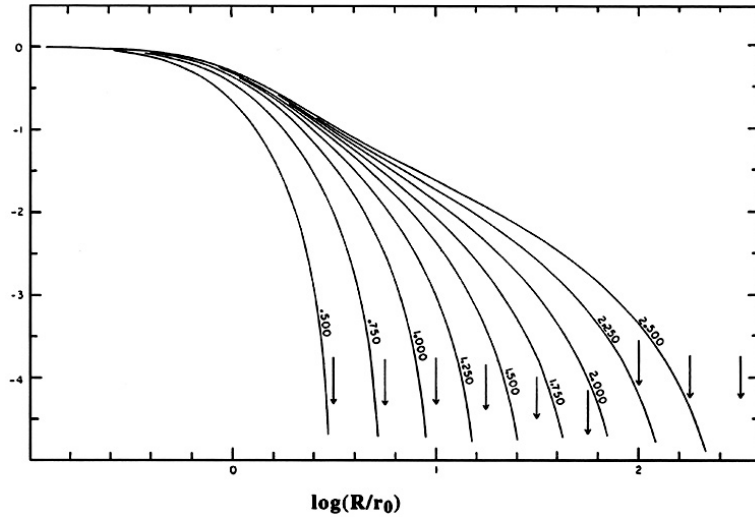


Figure 1.6: Projected density profiles for the King models (from King, 1967). The curves show the logarithm of the projected density (normalised to the central value) for selected values of the concentration parameter  $c$  (marked along the curves). For each case an arrow provides the location of the relevant truncation radius  $r_t$ .

central cusp, within which the density remains raising in contrast to a core where the density becomes constant (see Sec. 1.1.2). As a result, the density in the central parts of an isothermal sphere are very high leading to many stellar interactions.

The isothermal sphere has so far not often been used in investigations of the dynamics of star clusters. One of the reasons for this is that the singular isothermal sphere due to its central singularity features very high densities in its centre, which can lead to numerical problems if such a cluster is simulated. Another reason isothermal spheres in simulations are not used in general for simulations is that strictly speaking, isothermal spheres do not have any boundaries regarding the size and mass. However, observed star clusters obviously are finite objects. As a result, even if a cluster is set up as isothermal sphere in virial equilibrium, the cluster will expand making it a not a good candidate if the evolution of clusters in equilibrium shall be investigated.

However, isothermal spheres have also been used successfully in star cluster simulations. For example the cluster model introduced by Olczak *et al.* (2006) uses a modified version of the isothermal spheres to model the initial state of the Orion Nebula Cluster. This cluster model has been proven to evolve to the same state as is observed in the ONC today (see also Olczak *et al.*, 2008, 2010) and is used in Chap. 3 for investigating the evolution of a primordial binary population in ONC-like clusters.

### King models

The isothermal sphere and Plummer model can be used straight-forwardly to set up star clusters in simulations, because they can be described with simple analytic functions (e.g. Aarseth *et al.*, 1974, and Sec. 1.1.2 and Sec. 1.1.2). However, strictly speaking, both models are only applicable for clusters that are either very young (isothermal sphere) or very old (Plummer). A star cluster model that is



applicable to star clusters of any age is the family of King models, which were initially introduced to fit the density profiles of globular clusters (King, 1962), but can also be used for much younger cluster like the ONC (Hillenbrand & Hartmann, 1998).

Theoretically, the King models can be derived by limiting the distribution function of the isothermal sphere by setting it to zero outside the desired tidal radius of the cluster, which sets the size of the cluster (see Binney & Tremaine, 2008, for a complete introduction into King models). Integrating this distribution function over the complete velocity space yields the density as a function of the cluster potential of the King model clusters which is given by

$$\rho_K(\Psi(r)) = \rho_1 \left[ e^{\Psi(r)/\sigma^2} \operatorname{erf} \left( \frac{\sqrt{\Psi(r)}}{\sigma} \right) - \sqrt{\frac{4\Psi(r)}{\pi\sigma^2}} \left( 1 + \frac{2\Psi(r)}{3\sigma^2} \right) \right], \quad (1.8)$$

where  $\Psi(r)$  is the relative potential of the cluster,  $\sigma$  a parameter that should not be mistaken for the velocity dispersion of the cluster and erf the Error function. As can be seen In comparison with the corresponding density distributions of the Plummer and isothermal sphere model, the density distribution of King model cluster is much more complicated and to setup a star cluster in the simulations one has to numerically integrate the Poisson equation for  $\Psi$  (for more details see Binney & Tremaine, 2008).

Basically, the King models can be parametrised by the ratio of  $W_0 = \Psi(0)/\sigma$  or their concentration

$$c = \log_{10}(r_t/r_0), \quad (1.9)$$

where  $r_t$  is the tidal radius of the cluster, beyond which the cluster ends and

$$r_0 = \sqrt{\frac{9\sigma^2}{4\pi G\rho_0}} \quad (1.10)$$

is the King radius of the cluster, which gives the size of the core of the model. The concentration therefore gives the ratios of the cluster core size to its initial size where higher values of  $c$  denote more concentrated clusters. In the limit  $W_0 \rightarrow \infty$ ,  $c \rightarrow \infty$  the King models go over to the isothermal spheres, while for lower values of  $W_0$  and  $c$ , the resulting clusters become less extreme. For example, the ONC can be fitted by a King model cluster with  $W_0 = 9$  ( $c \approx 2.1$ ) while the Plummer model can be approximated by a King model with  $W_0 = 4$  ( $c \approx 0.8$ ). Fig. 1.6 shows a series of King models with concentration factors in the range from 0.5 – 2.5. As can be seen the size of the core with respect to the size of the complete cluster decreases the larger  $c$  becomes.

In contrast to the Plummer and isothermal model, where the velocity dispersion is constant throughout the cluster, the velocity dispersion in King model clusters is a function of the distance to the cluster centre. The larger the distance to the cluster centre is, the lower is the velocity dispersion.

## 1.2 Evolution of star clusters

Although on first sight star clusters appear to be rather static objects, they undergo serious evolution during their lifetimes. In the following section some important processes acting in and on star cluster will be summarised.

### 1.2.1 Two-body relaxation

The simplest way to treat self-gravitating stellar systems like star clusters is to assume, that they are “collisionless systems” in which the trajectories of the stars are dictated by the smoothed out potential of the complete system. While this approximation can safely be applied for galaxies ( $N \approx 10^{11}$ ,  $t_{\text{cross}} = 100\text{Myr}$ ,  $t_{\text{relax}} \approx 4 \times 10^7\text{Myr}$ , age  $\approx 10\text{Gyr}$ ), it fails to explain the evolution of star clusters as there the gravitational interactions between the stars with their neighbours becomes important. The reason for this is that due to this stellar encounters the trajectories of the stellar members are deflected from the path they would have if no encounters would have taken place, although this changes are mostly very small (the effect of strong encounters will be discussed in Sec. 1.2.5).

However, during their lifetime the stars in a cluster will undergo many of such weak encounters which means that after some time all stars in the cluster will have left their initial trajectories and follow paths that are specified by their neighbours instead of the gross cluster potential. The time-scale after which this happens can be calculated by determining the number of times a star has to cross the star cluster so that the many small interactions have changed the velocity of the star by an amount comparable to its initial velocity (e.g. Binney & Tremaine, 2008). This time is called **relaxation time** of the cluster and can be approximated by

$$t_{\text{relax}} \simeq \frac{0.1N}{\ln N} t_{\text{cross}}, \quad (1.11)$$

where  $N$  is the number of particles in the systems and  $t_{\text{cross}} = R/v$  is the **crossing time** of the system ( $R$  is the diameter of the system and  $v$  the mean velocity of the stars). The crossing time gives the average time a star in the cluster needs to cross the complete cluster and is the shortest time, within which significant dynamical changes in the clusters, like changes of the cluster shape, can occur. Instead of calculating this relaxation time, often the **half-mass relaxation time** (e.g. Binney & Tremaine, 2008) is given because it can be constrained easier by observation than the regular relaxation time. It is calculated by

$$t_{\text{th}} = \frac{0.78\text{Gyr}}{\ln(\lambda N)} \frac{1M_{\odot}}{m} \left( \frac{M}{10^5 M_{\odot}} \right) \left( \frac{r_h}{1\text{pc}} \right) \quad (1.12)$$

where  $\ln(\lambda N)$  is the so-called Coulomb logarithm,  $m$  the mean stellar mass in the cluster,  $M$  the total mass and  $r_h$  the half-mass radius. The Coulomb logarithm is often found in formulae for scattering rates from  $1/r$  potentials, such as the gravitational potential of a point mass or the electrostatic potential of a point charge.

Two-body relaxation is of major importance for the evolution of stellar systems with ages that

exceed the relaxation time of the system. Therefore two-body relaxation had a significant influence on old globular clusters ( $N \approx 10^5$ ,  $t_{\text{cross}} = 0.5\text{Myr}$ ,  $t_{\text{relax}} = 0.5\text{Gyr}$ , age  $\approx 10\text{Gyr}$ , based on values from Harris (1996)), and old open clusters ( $N \approx 10^2$ ,  $t_{\text{cross}} = 1\text{Myr}$ ,  $t_{\text{relax}} = 15\text{Myr}$ , age  $\approx 0.3\text{Gyr}$ , based on values from Piskunov *et al.* (2007)), while it has not been of great importance for much younger cluster like the Orion Nebula Cluster ( $N = 4000$ ,  $t_{\text{cross}} = 0.3\text{Myr}$ ,  $t_{\text{relax}} = 15\text{Myr}$ , age  $\approx 1\text{Myr}$ , based on values from Hillenbrand & Hartmann (1998)). However, this does not mean that stellar encounters are of no importance in these clusters. As will be shown later, strong encounters can remove stars from star clusters (Sec. 1.2.5), alter the properties of stellar disks in star clusters (Pfalzner *et al.*, 2006; Olczak *et al.*, 2006, 2010; Steinhausen *et al.*, 2012) and alter binary system, which is investigated in this thesis.

### 1.2.2 Thermodynamics of self-gravitating systems and Core collapse

In analogy to ideal gases, the temperature of a given stellar system can be defined by the relation

$$\frac{1}{2}m\bar{v}^2 = \frac{3}{2}k_B T, \quad (1.13)$$

where  $m$  is the stellar mass,  $\bar{v}$  the mean velocity of the stars and  $k_B$  is Boltzmann's constant. In general the mean velocity in a stellar cluster depends on the location of the star in the stellar cluster, therefore also the temperature in general depends on the position (the isothermal sphere displays an exception). The mass-weighted mean temperature is  $\bar{T} = \int d^3\mathbf{x}\rho(\mathbf{x})T / \int d^3\mathbf{x}\rho(\mathbf{x})$ , where  $\rho(\mathbf{x})$  is the density, and the total kinetic energy of a system of  $N$  identical stars is therefore

$$K = \frac{3}{2}Nk_B\bar{T} \quad (1.14)$$

In a stationary system the virial theorem then states that the total energy of the system is  $E = -K$ , so

$$E = -\frac{3}{2}Nk_B\bar{T}. \quad (1.15)$$

Therefore the heat capacity of an self-gravitating stellar system is

$$C = \frac{dE}{d\bar{T}} = -\frac{3}{2}Nk_B, \quad (1.16)$$

which is negative. This means that the system increases in temperature if it loses energy.

This causes self-gravitating stellar systems to collapse into singularities if they are in contact with heat baths which have a lower temperature than the self-gravitating system because energy is flowing from the hotter system into the cooler heat bath. On contrary self-gravitating stellar systems will expand if they are in contact with heat baths that have a higher temperature.

It turns out that star clusters usually also show this behaviour which leads to a phenomenon called **core collapse**. The mean stellar velocity in star clusters (the isothermal sphere again marks an excep-

tion) usually depends on the position within the cluster with the stars in the cluster core having higher speeds than in the outer cluster parts. This means that the temperature in the cluster core is higher than in the cluster outskirts. Therefore energy will flow from the cluster core to the outer cluster parts in the form of ejected stars. As this energy flow increases the temperature within the cluster core due to the negative heat capacity, it decreases in size to return to virial equilibrium. Because the temperature gradient of the core and the outer cluster parts steepens due to this process, it accelerates itself potentially leading to the formation of a singularity at the cluster centre.

Early simulations of the evolution of globular clusters using the Fokker-Planck or fluid approximations did not include any processes to stop core collapse (e.g. Hénon, 1961; Sabbi *et al.*, 2011, translation) so that they all led to the formation of a singularity after about 16 initial half-mass relaxation times (Eq. 1.12). However, this time should only be taken as a crude estimate of the “core-collapse” time, as it heavily depends on the cluster density profile and mass function, that is used for the computations.

In more realistic computations core collapse does not proceed to this extreme state. To halt core collapse, an energy source is needed that pumps energy into the core. Due to the negative heat capacity of self-gravitating system, the temperature of the core decreases so that the temperature gradient between the cluster core and the outer cluster parts diminishes. If both temperatures become the same, the heat flow vanishes and the core collapse has stopped.

A natural energy source, that could halt the core collapse in star clusters are binary stars. Their interactions with other core members have been already recognised by Hénon (1961) as possible process to stop core collapse, however it took almost 20 years until Sugimoto & Bettwieser (1983) were able to consistently include their influence on the evolution of star clusters into the computations.

### 1.2.3 Influence of the galactic potential

The stellar cluster models described in Sec. 1.1.2 are often assumed to be isolated to simplify the calculations. In reality however, star clusters are embedded in their parent galaxies. Therefore stars do not only feel the gravitational potential resulting from the other stars in the cluster, but also the potential of the overall galaxy, which has important implications for the structure of star clusters.

To derive the radius beyond which a star will no longer be bound to its star cluster but to the hosting galaxy it is convenient to change to a coordinate system that rotates with an angular velocity  $\Omega$  so that the galaxy and the cluster are standing still. In this coordinate system, the usual total energy is not conserved but the Jacobi integral

$$\begin{aligned} E_J &= \frac{1}{2}mv^2 + \Phi(x) - \frac{1}{2}m|\Omega \times \mathbf{x}|^2 \\ &= \frac{1}{2}mv^2 + \Phi_{\text{eff}}(\mathbf{x}), \end{aligned} \quad (1.17)$$

with  $\Omega = [0, 0, \Omega]$  and the term  $-\frac{1}{2}m|\Omega \times \mathbf{x}|^2$  being something like the “potential energy” giving rise to the centrifugal forces present in the rotating coordinate system.

Next one has to determine the saddle point of  $\Phi_{\text{eff}}$  that lies between the cluster and the galaxy. This means that at  $(x_{\text{cl}} - r_J, 0, 0)$  the potential has to fulfill the following condition

$$\left( \frac{\partial \Phi_{\text{eff}}}{\partial x} \right)_{x=x-r_J} = 0 \quad (1.18)$$

The effective potential generated by the cluster and the galaxy separated by a distance  $d$  can be written as

$$\Phi_{\text{eff}}(x) = -G \left[ \frac{m_{\text{gal}}}{|\mathbf{x} - \mathbf{x}_{\text{gal}}|} + \frac{m_{\text{cl}}}{|\mathbf{x} - \mathbf{x}_{\text{cl}}|} + \frac{1}{2} \frac{m_{\text{gal}} + m_{\text{cl}}}{d^3} |\mathbf{e}_z \times \mathbf{x}|^2 \right] \quad (1.19)$$

Combining Eq. 1.18 and Eq. 1.19 then gives

$$0 = \frac{1}{G} \left( \frac{\partial \Phi_{\text{eff}}}{\partial x} \right)_{x_{\text{cl}}-r_J} = \frac{m_{\text{gal}}}{(d-r_J)^2} - \frac{m}{r_J^2} - \frac{m_{\text{gal}} + m_{\text{cl}}}{d^3} \left( \frac{d}{1 + m_{\text{cl}}/m_{\text{gal}}} - r_J \right) \quad (1.20)$$

In the current context  $m_{\text{cl}} \ll m_{\text{gal}}$  so that  $r_J \ll d$  and it is possible to expand  $(D - r_J)^{-2}$  in powers of  $r_J/D$ :

$$0 = \frac{m_{\text{gal}}}{d^2} \left( 1 + \frac{2r_J}{D} + \dots \right) - \frac{m_{\text{cl}}}{r_J^2} - \frac{m_{\text{gal}}}{d^2} + \frac{m_{\text{gal}} + m_{\text{cl}}}{d^3} r_J \quad (1.21)$$

So to the first order in  $(r_J/D)$  it follows that

$$r_J = \left[ \frac{m_{\text{cl}}}{m_{\text{gal}}(3 + m_{\text{cl}}/m_{\text{gal}})} \right]^{1/3} d \approx \left( \frac{m_{\text{cl}}}{3m_{\text{gal}}} \right)^{1/3} d \quad (1.22)$$

The here derived radius  $r_J$  is often called the **Jacobi limit** or the **Jacobi radius**. It displays a rather good estimate of the tidal radius  $r_t$  of an star cluster in it's host galaxy

#### 1.2.4 Stellar mass loss

At the end of their life most stars loose significant amounts of their mass due to stellar winds or in the extreme case through supernova explosions. Most of this material is likely to escape the cluster as the velocities of the winds (for massive stars they can be up to  $\approx 2000 \text{ km s}^{-1}$ ) usually exceeds the escape velocity of the cluster (for example  $v_e = \sqrt{\frac{GM}{r}} \approx 3 \text{ km s}^{-1}$  for the ONC) which results in a loss of cluster mass without the need of reducing the number of stars in the cluster (disregarding supernovas which do remove stars).

Usually the effect of lowering the stellar mass in the cluster is to widen the stellar orbits of the stars without changing the shape of the orbits because the timescale of the mass loss is much longer than the crossing time of the cluster, so that it can adapt to the new potential adiabatically (see Sec. 1.4). As long as the cluster is treated to be isolated, it could grow without any boundaries without loosing any stars (neglecting supernovas or the like). If however, the cluster is placed into the tidal field of an galaxy, the cluster will loose stars if they pass the tidal or Jacobi radius  $r_J$  of the cluster (see Sec. 1.2.3).

### 1.2.5 Evaporation and ejection

Encounters of stars in a star cluster potentially remove stars from the cluster by two distinct processes. (i) A single, strong encounter with another star or with a binary can raise the energy of one star by such an amount, that it directly leaves the star cluster. This process is called **ejection**. (ii) Multiple, weak encounters of a star with many other stars can gradually raise the energy of the star, so that it can leave the star cluster. This process is called **evaporation**.

To be able to estimate the importance of these two processes, the ejection and evaporation time-scales will be given, which denote the time each process would need to completely dissolve the cluster

$$t_{\text{dissolution}} = - \left( \frac{1}{N} \frac{dN}{dt} \right)^{-1}. \quad (1.23)$$

The ejection time-scale of an isolated cluster with a Plummer density distribution consisting of single-mass stars only was determined by Hénon (1960) to be

$$t_{\text{ej}} \approx 10^3 \ln(\lambda N) t_{\text{rh}} \quad (1.24)$$

where  $\ln(\lambda)$  is before mentioned Coulomb logarithm and  $t_{\text{rh}}$  is the half-mass relaxation timescale (see Eq. 1.12). Including a mass function in the calculations significantly increases the effectiveness of the ejection process as massive stars tend to eject a high number of lower mass stars. Hénon (1969) found that the ejection timescale is reduced by a factor of about 30 when including a mass function in the calculations.

While the ejection timescale can, in principle, be evaluated analytically, the determination of the evaporation timescale requires using numerical calculations. The reason for this is that while for the ejection only a single encounter has to be considered, evaporation emerges from millions of encounters of a star with the other stars in the cluster which, in very small steps, rise the energy of the star so that it possibly can leave the cluster. Using Fokker-Planck calculations Spitzer (1987) determined the evaporation timescale of an isolated single-star cluster to be

$$t_{\text{evap}} = 300 t_{\text{rh}}, \quad (1.25)$$

which is about 30 times shorter than ejection time scale ( $\ln(\lambda N) \approx 10$  for typical clusters). However, the timescale given in Eq. 1.24 and Eq. 1.25 should be treated with caution because the calculations used to acquire them did not include all physics present in star clusters, which might have an effect on these. For example by including the effect by an external tidal field on the cluster both timescales can be reduced by a factor of ten (Spitzer, 1987).

### 1.2.6 Energy equipartition and mass segregation

All processes that have been discussed so far in this chapter can work in clusters, that consist only of single stars. However, not all stars have the same mass, but show a wide range of masses from the Hydrogen-burning limit ( $0.08M_{\odot}$ ) to the theoretically accepted maximum stellar mass of  $150M_{\odot}$  up to which stars are stable. However, stars with even higher masses have been detected recently (Crowther *et al.*, 2010).

By allowing the stars in a cluster to have different masses, the kinetic energy of a star will not only depend on the position of the star, but also on its mass. Encounters will therefore tend to establish energy equipartition between the lighter stars and the more massive ones. However, energy equipartition in self-gravitating systems does not work exactly the same way as in ideal gases, where only the kinetic energy has to be considered. To enlighten this, consider a self-gravitating system with potential  $\Phi(x)$  consisting of two populations of stars with masses  $m_1$  and  $m_2$  and  $m_2 \gg m_1$ . The mean energy per star in both population is then given by  $\langle E \rangle_i = m_i \langle 1/2v^2 + \Phi(\mathbf{x}) \rangle_i$  where  $\langle \rangle_i$  denotes the average over the complete population  $i$  and  $v$  is the average velocity of the stars. Encounters do not lead to  $\langle E \rangle_1 \rightarrow \langle E \rangle_2$  on throughout the cluster but only locally. This means that if the energy of the heavier stars is higher than the energy of the less massive stars at a given location  $\mathbf{x}$  (so they have higher kinetic energies), then they will transfer part of their energy with the lower mass stars. However, by loosing orbital energy the heavier stars will sink deeper into the potential  $\Phi(\mathbf{x})$  so that they have to speed up to keep their new energy after the energy transfer conserved. That means that due to energy equipartition, the kinetic energy of massive stars increases in contrast to what would be assumed at first glance.

Energy equipartition therefore leads to the massive stars being more centrally concentrated than the lower mass stars in the cluster. This state is often called “mass segregation” and is observed in many star clusters (Hillenbrand & Hartmann, 1998; de Grijs *et al.*, 2002; Gouliermis *et al.*, 2004). Since also very young cluster like the ONC show evidence for mass segregation the question arises, if star clusters are born in a mass segregated state or if the energy equipartition is responsible.

Performing Nbody simulations of star clusters in virial equilibrium Bonnell & Davies (1998) could show that the degree of mass segregation, that is observed in the ONC today can only be explained if the cluster was already initially mass segregated. In contrast to that Allison *et al.* (2009) found, that no initial mass segregation is needed to explain the mass segregation of the ONC, if the cluster was initially in a clumpy, subvirial state. Olczak *et al.* (2011) could even generalize this by dropping the need for a clump structure of the clusters.

Because energy equipartition causes an inward motion of massive stars, it can significantly speed up the core collapse. While in the single-mass case, core collapse occurred after about  $16t_{\text{rh}}$  (see Eq. 1.12, it can appear after  $2 - 4t_{\text{rh}}$  if a proper mass function is used in the simulations.

### 1.3 Binaries

Binary stars are pairs of stars, that are energetically bound, meaning that their internal or binding energy is smaller than zero:

$$\begin{aligned} E_{\text{int}} &= \frac{1}{2} (m_1 \mathbf{v}_1^2 + m_2 \mathbf{v}_2^2) - \frac{Gm_1 m_2}{|\mathbf{r}_{12}|} \\ &= \frac{1}{2} \mu \dot{\mathbf{r}}_{12}^2 - \frac{Gm_1 m_2}{|\mathbf{r}_{12}|} < 0, \end{aligned} \quad (1.26)$$

where  $m_1, m_2$  are the masses of the stars,  $\mathbf{v}_1, \mathbf{v}_2$  are the velocities in their centre of mass rest frame and  $\mathbf{r}_{12}$  the separation vector between the two stars. The orbits of the two stars follow Kepler ellipses with the eccentricity

$$e = \sqrt{1 + 2 \left( \frac{L^2 E_{\text{int}}}{G^2 (m_1 + m_2)^2} \right)}, \quad (1.27)$$

where  $\mathbf{L} = \mathbf{r}_{12} \times \mathbf{p}_{12} = \mathbf{r}_{12} \times \mu \dot{\mathbf{r}}_{12}$  is the angular momentum vector of the orbit. For binaries the eccentricity is always  $< 1$ . The semi-major axis of the orbit is given by

$$a = \frac{L^2}{GM(1 - e^2)} \quad (1.28)$$

With this the periastron distance  $r_p$  (minimum separation between the two stars) and the apoastron distance  $r_a$  (maximum separation) are given by

$$r_p = a(1 - e), \quad (1.29)$$

$$r_a = a(1 + e). \quad (1.30)$$

Currently several binary formation scenarios are discussed by the community which can be divided into three groups: i) scenarios based on the fragmentation of collapsing cores, ii) fragmentation inside a protostellar disk and iii) dynamical formation. The first two scenarios are obviously linked to the star formation process itself and binaries formed by either of these scenarios can therefore be safely be regarded as being primordial. However, also dynamically formed binaries can be regarded as being primordial as long as they are formed during as long the star formation proceeds in the cluster.

The first formation scenario for binaries occurs very early in the star formation process, when subclumps inside molecular clouds begin to collapse (which are then called collapsing cores), because the local gaseous pressure support is not able to balance out the force of gravity which occurs if the subclumps have masses exceeding the local Jeans mass. The first core fragmentation scenario has been investigated by Hoyle (1953), who assumed that during the collapse of the cores, further fragmentation of the core occurs, as long as the gas remains optically thin and is able to efficiently cool. The reason for this is that the Jeans mass decreases with increasing density and increases with temperature.



More recent core fragmentation scenarios have found that collapsing, bound gas clumps will fragment depending on product of the ratio of the thermal to gravitational energy  $\alpha = 5c_s^2 R/GM$  and the ratio of rotational to gravitational energy  $\beta = \Omega^2 R^3/3GM$ , where  $c_s$  is the sound speed,  $R$  the core radius,  $M$  the core mass and  $\Omega$  the orbital frequency of the core. Initially it was thought that cores with  $\alpha\beta < 0.12$  will inevitably fragment Inutsuka & Miyama (1992), however it turned out that the cores must additionally obey  $\alpha < 0.5$  to be able to fragment (Tsuribe & Inutsuka, 1999).

Another class of binary formation scenarios relying on the fragmentation of the cores are the so-called turbulent fragmentation scenarios. These scenarios assume that turbulence can lead to overdensities or filamentary structures within the bound cores, that will collapse and form a separate entity inside the core. Recent work by Offner *et al.* (2009) and Offner *et al.* (2010) implies, that the turbulent fragmentation is the dominant mode of low-mass binary formation.

The next family of binary formation scenarios is based on the fragmentation of massive protostellar/accretion disks. As these form after the core has already collapsed significantly, the disk fragmentation scenarios take place later in the formation of the stars than the before mentioned core fragmentation scenarios. Disk fragmentation has recently gathered more attention as it is now becoming obvious, that the feeding of the disk by the surround envelope of the star (Kratter *et al.*, 2008, 2010) is a efficient way to induce instabilities in the disk and that protostellar disks can be much more massive, that has been thought before (Andrews & Williams, 2007). Both findings significantly improve the efficiency for the formation of binaries in disks, making it more important as it has been expected before.

Disk fragmentation is a promising process to explain close binaries, that are only rarely formed in the core fragmentation scenarios. The reason close binaries can form through disk fragmentation is that the new stars forming in the disks have directly from the beginning relatively small separations to the central star (several 100AU) and can wander inside the disk, as it has already been found for planets (Goldreich & Tremaine, 1979).

The last family of binary formation scenarios is based on the dynamics of stars in their natal environments, namely star clusters (Lada & Lada, 2003). The so-called competitive accretion model (Bate, 2000; Bonnell *et al.*, 2003; Clark & Bonnell, 2004; Bonnell *et al.*, 2008) states that during the formation of a star cluster, many stars form which will accrete from the overall gas present in the cluster. During this period binaries will form by processes already mentioned above (e.g. via core and disk fragmentation mentioned above) or by other processes like the disk-assisted capture Moeckel & Bally (2007)). An additional way to form binaries also after the star formation has been completed is the formation of binaries during a three-body interaction (Heggie, 1975). To form a binary during such an interaction, the initially positive binding energy of two unbound star, has to be lowered below zero. This is accomplished by transferring the superfluous energy to the third star, which will afterwards leave the system with a increased velocity.

As has been shown above, the formation of stars and binaries is associated with dense molecular clouds and is not accessible by observations because the extinction due to the gas in this regions is

too high. Therefore it is not possible to determine directly by which formation scenarios the binaries actually form. However, what can be done is to observe the binary populations resulting from the star formation process and compare them to the predictions from the theory.

The most important observations to have shaped our current picture of the binary field population were performed in the early 1990's. Duquennoy & Mayor (1991) found that the binary frequency of G-type stars in the solar neighbourhood is about 61% and the period distribution follows a log-normal distribution

$$f(\log P) = C \exp \left\{ \frac{-(\log P - \overline{\log P})^2}{2\sigma_{\log P}^2} \right\}, \quad (1.31)$$

over the period range  $\sim 10^{-1} - 10^{11}$  d, where  $P$  is the period in days ( $\overline{\log P} = 4.8 \equiv 172$  yr,  $\sigma_{\log P} = 2.3$ ) and  $C$  a normalisation constant. A year later, Fischer & Marcy (1992) analysed the binary properties of M-dwarfs in the separation range  $0.04 - 10^4$  AU corresponding to periods in the range  $\sim 10^{-2} - 10^6$  yr and found that the period distribution of M-dwarfs in the solar neighbourhood is also log-normally distributed with a peak between 9 yr and 270 yr, which is nearly identical to the findings for G-dwarfs. Although the observed binary frequency of M-dwarfs at about 33% is lower than that of G-dwarfs, the properties of the G and M-dwarf binary populations seem very similar. Observations of Raghavan *et al.* (2010) confirmed this picture. They determined the binary properties of nearby ( $d < 25$  pc) solar-type stars ( $\sim F6 - K3$ ) and found that the fraction of binary stars is 58% with a log-normal period distribution ( $\overline{\log P} = 5.03$  and  $\sigma_{\log P} = 2.28$ ).

While these studies draw a very consistent picture of binaries it is not compatible to observations in star cluster. The most serious differences are that the binary frequency is much higher in (sparse) clusters (Leinert *et al.*, 1993; Ghez *et al.*, 1993; Reipurth & Zinnecker, 1993; Kraus & Hillenbrand, 2007) and the period distribution seems to be log-uniform in young clusters (Kouwenhoven *et al.*, 2007; Kraus & Hillenbrand, 2007; Reipurth *et al.*, 2007; Connelley *et al.*, 2008). In contrast observations of the binary frequencies in dense star clusters like the ONC (Prosser *et al.*, 1994; Petr *et al.*, 1998; Duchêne, 1999; Simon *et al.*, 1999; Beck *et al.*, 2003; Köhler *et al.*, 2006; Reipurth *et al.*, 2007) have shown, that the binary frequency in these clusters is comparable to the binary frequency in the field.

These findings rise the question why the binary populations in the star clusters and the field differ. A possible explanation is that the binaries, are influenced by the natal environment. A process naturally acting in star clusters that is capable to change binaries are the before mentioned three-body interactions. The general effect of three-body interactions onto a binary can be expressed by the relative energy change of the binary,  $\Delta$ ,

$$\Delta = \frac{E'_{\text{int}} - E_{\text{int}}}{E_{\text{int}}}, \quad (1.32)$$

where the primed variables denote the values after the scattering event. If  $\Delta > 0$  the internal energy of the binary has become more negative which means that it is harder bound than before the interaction. From the conservation of energy it follows that the energy of the third body  $E_3$  increases during the interaction, so that its final velocity exceeds its initial velocity,  $V' > V$ . The inverse process with

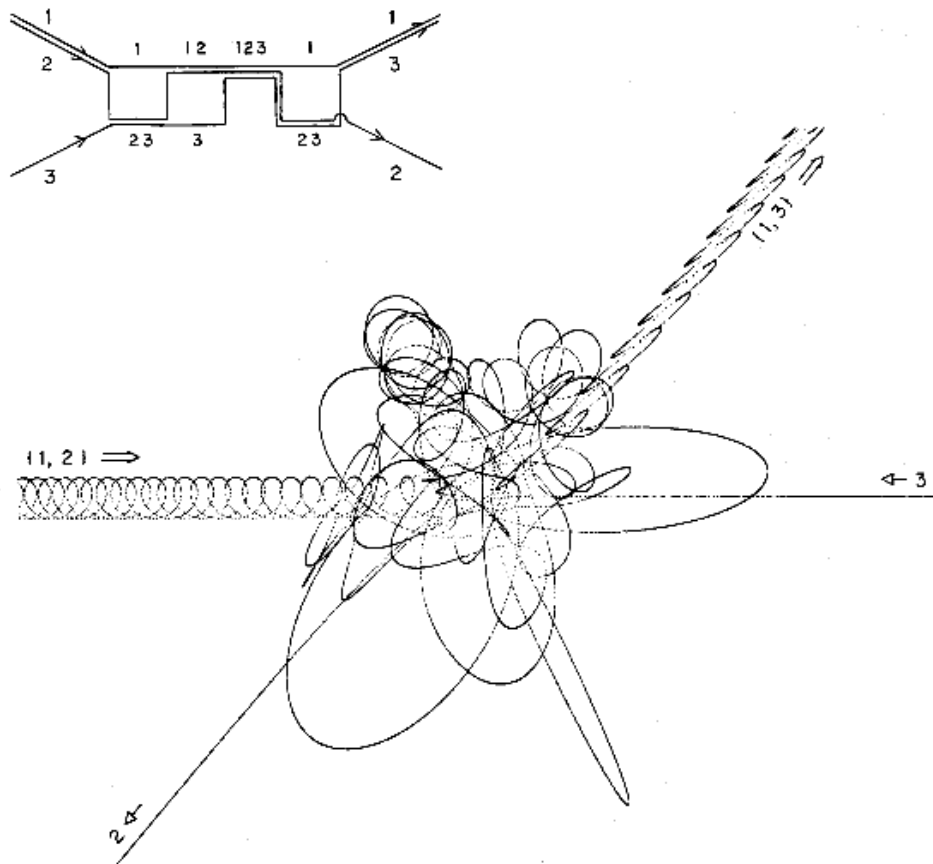


Figure 1.7: From Hut & Bahcall (1983). A three-body scattering event. It is a resonant exchange and the sequence of integrations is summarised in the pictogram at the upper left.

$\Delta < 0$  leads to a less tightly bound binary and a slower third body ( $V' < V$ ).

One can introduce two types of binaries based on the relation of binding energy and relative kinetic energy (Heggie, 1975; Hills, 1975). Binaries with  $|\mathcal{E}| > (m_1 + m_2)m_3V^2/(m_1 + m_2 + m_3)$  are called hard binaries which are hardened by three-body scatterings and binaries  $|\mathcal{E}| < (m_1 + m_2)m_3V^2/(m_1 + m_2 + m_3)$  are called soft because of their fragility to such encounters.

**Soft binaries** become softer in a three-body interaction. Here three different processes can be distinguished. First, in a fly-by the “intruder” gets close to the binary, softens it ( $\Delta < 0$ ) and escapes to infinity again. The second process is called ionisation which happens when the “intruder” causes a relative velocity change large enough, that the binary becomes unbound. The third process is the exchange process (see Fig. 1.7) where the intruder changes place with one of the binary components due to a very close encounter.

The effect of three-body scattering on **hard binaries** is that the binary gets even harder. Two different regimes for three-body scatterings can be distinguished, one for *close interactions*  $r_p \leq a$  ( $r_p$  is the minimum separation of the third body and the binary,  $a$  the semi major axis of the binary) and one for *wide interactions* where  $r_p \gg a$ .

In the close interaction case the amount of energy exchanged in an interaction is of the order of  $|\mathcal{E}|$ .

Also here two different outcomes are possible. First the intruder may get a positive amount of energy of order  $|\varepsilon|$  which vastly increases the speed of the intruder and hardens the binary considerably. In contrast, if the intruder loses energy in the interactions, it will become bound to the binary and another interaction will take place. Such interactions can occur repeatedly for a long period and lead to rather stable configurations called resonances. In this case exchanges of a binary component and the intruder are common. The probability for an exchange in an equal mass system is  $2/3$ , in an unequal mass system it is by far more probable that the lowest mass component is ejected in this process.

The same processes take place in the wide interaction case, but the amount of exchanged energy is greatly reduced. Also an exchange interaction is not possible in the resonance case which is now not called resonance anymore but “hierarchical”.

However, as three-body and even higher order interactions occur very often in star clusters during their lifetimes, it is not possible to calculate the changes of the binary population in the clusters analytically but numerical simulations have to be performed. Several authors studied the evolution of binary populations in star clusters of different kind (e.g. Aarseth, 1971; Kroupa, 1995a; Kroupa *et al.*, 1999; Kroupa & Burkert, 2001; Kroupa & Bouvier, 2003; Pfalzner & Olczak, 2007; Parker *et al.*, 2009; Kouwenhoven *et al.*, 2010). Numerical investigations of the dynamical evolution of binaries in star clusters started in the 70’s with the development of the first N-body codes (e.g. Aarseth, 1971). The early works concentrated on the formation of binaries in star clusters with initially pure single stellar systems. Only in recent years simulations have been performed to investigate the evolution of a primordial binary population. For example, Kroupa *et al.* (1999) simulated the evolution of ONC-like star cluster models where all stars initially were part of a binary system, i.e. a primordial binary frequency of 100%. They showed that the cluster evolution destroys wide binaries quite efficiently leading to a reduction in the initial binary fraction as the cluster evolves.

A different approach to calculate the evolution of star clusters is to use the Fokker-Planck equation, which describes the evolution of the distribution function of a star cluster due to encounters in the cluster. In cases where only single stars are present in the clusters, the diffusion coefficients, which give the mean changes of the distribution function due to encounters, can be acquired quite easily. However, if also binaries are present in the clusters the cross sections of the different outcomes of three body interactions have to be known which have been determined by several authors by calculating immense numbers of three-body interactions (Hut, 1983b; Hut & Bahcall, 1983; Hut, 1983a, 1993).

This thesis displays a continuation of these studies with the focus on the creation of the field binary population in cluster models being motivated by observed clusters.

## 1.4 Gas expulsion

The generally accepted view of cluster formation is that star clusters originate from Giant Molecular clouds (GMCs). With typical masses of  $10^5 - 10^7 M_{\odot}$  and typical diameters of 10 – 100pc GMCs

display immense reservoirs for star formation. However, observational evidence exists that only a minor fraction of the total cloud mass is actually converted into stars. One reason for this is that the vast majority of the material in the GMC is supported against gravitational collapse either through turbulence or magnetic fields (Arons & Max, 1975; Blitz, 1993; Myers & Goodman, 1988). Only in the densest parts of the clouds, the so-called dense cores gravity dominates. This means that only a minor fraction of an entire GMC is capable to form stars, so that the overall star formation efficiency (SFE) in a GMC is at most a few percent (Lada & Lada, 2003; Clark & Bonnell, 2004).

However, even within the dense cores the SFE does not reach 100% because the star formation process turns out to be rather ineffective. The radiation and stellar winds of newly formed (proto-) stars heat up the surrounding gas making it more difficult for the gas to collapse into new stars or accrete onto already formed ones. In fact material can even become unbound and leave the cluster if a sufficient amount of energy is pumped into the gas. The energy needed to remove all gas from a cluster is approximately (Adams, 2000)

$$E = k \frac{GM^2}{R} \approx 4 \times 10^{46} \text{erg} \left( \frac{M}{1000M_{\odot}} \right)^2 \left( \frac{R}{1\text{pc}} \right)^{-1}, \quad (1.33)$$

with  $k$  being a numerical constant of the order one describing the structure of the gas cloud. So to unbind all gas in a typical massive young star cluster ( $M_{\star} = 15000M_{\odot}$ ,  $R = 10\text{pc}$ ) with an assumed SFE of 30% an energy of more than  $E \approx 10^{49}\text{erg}$  has to be inserted into the gas. Stellar winds and the ionizing radiation of young stars are not capable to release enough energy to instantly free all gas from the cluster and therefore turn out not to be the major processes that remove the gas from massive clusters. In contrast, supernova explosions can easily unbind the complete amount of gas from the clusters as their energy input is about  $10^{51}\text{erg}$  (Khokhlov *et al.*, 1993). Lower mass clusters, in which no massive star formation takes place and which are therefore void of supernovas, are observed to become gas-free (Palla & Stahler, 2000) at some point. In those clusters the stellar winds and the ionizing radiation of the young stars become more important.

Summarising the formation and early evolution of star clusters is characterised by an transition from a system consisting mainly of gas and a minor fraction of stars to a system that more or less exclusively consists of stars. During this transition, the potential of the clusters changes significantly possibly accompanied with severe changes of structure of the clusters. To study this in more detail several studies have been performed to determine which fraction of stars stays bound after the gas has been removed from the clusters and how this fraction depends on the gas expulsion process, the star formation efficiency, the cluster density profile and so on.

The most basic description of the gas expulsion process starts from the evolution of the energies of clusters in virial equilibrium before gas loss (Hills, 1980). Before a cluster loses its gas component, the kinetic and potential energy of the cluster are given by  $T_0 = \frac{1}{2}M_0 \langle v_0^2 \rangle$  and  $W_0 = GM_0^2/2R_0$ , where  $M_0 = M_{\text{stars}}(0) + M_{\text{gas}}(0)$  is the initial total mass of the cluster,  $\langle v_0^2 \rangle = GM_0/2R_0$  the velocity dispersion of the stars and  $R_0$  the effective radius of the cluster. For equal mass stars,  $R_0$  would be given by

the mean particle distance in the cluster.

Directly after the removal of the gas, the total energy of the cluster is given by

$$E = T + W = \frac{1}{2} \left[ \varepsilon M_0 \langle v_0^2 \rangle - \left( \frac{G\varepsilon^2 M_0^2}{R_0} \right) \right] = \frac{1}{2} \left[ M \langle v_0^2 \rangle - \left( \frac{GM^2}{R_0} \right) \right], \quad (1.34)$$

where  $\varepsilon = M/M_0$  is the star formation efficiency of the cluster and  $M, R$  are the mass and radius of the cluster after the gas has been removed. The further evolution of the clusters depends on the timescale on which the gas is removed from the cluster. If the gas loss happens on timescales longer than the crossing time, as would be expected by the gradual gas loss through stellar radiation and stellar winds, the stars adapt to the slowly changing gravitational potential so that the cluster will remain in virial equilibrium. If however, the gas is removed instantaneously through supernovas, the stars will have no time to adapt to the diminished potential so that the velocity dispersion of the cluster will be the same as before the gas loss. This means that the clusters will be in a supervirial state and the clusters will have to expand to evolve towards a new virial equilibrium state. As soon as this is reached, the potential energy of the cluster is given by

$$E = -W/2 = -\frac{GM^2}{4R}. \quad (1.35)$$

Combining equations 1.34 and 1.35 with the correct velocity dispersion then gives the final cluster radii after gas loss (Hills, 1980; Mathieu, 1983)

$$\frac{R}{R_0} = \frac{M_0}{\varepsilon M_0}, \quad \text{for slow gas loss,} \quad (1.36)$$

$$\frac{R}{R_0} = \frac{\varepsilon}{2\varepsilon - 1}, \quad \text{for fast gas loss.} \quad (1.37)$$

From Eq. 1.37 it follows that all clusters with SFEs less than 0.5 become unbound due to the loss of their gas component if the gas loss happens very quickly Hills (1980). This findings lead Mathieu (1983) to the conclusions, that bound clusters can only form in environments, in which the SFE is locally very high ( $> 50\%$ ) if the gas is removed fast or at slightly lower SFEs ( $\gtrsim 30\%$ ) which requires slow gas removal.

Comparing the number of observed embedded clusters within 2kpc to the predicted number of clusters expected for a constant star formation rate (Fig. 1.8), Lada & Lada (2003) discovered that almost 90% of all embedded clusters have to disperse within 10Myr after their formation and even 96% within 100Myr. This obvious lack of open clusters is known as ‘‘infant mortality’’. The early destruction of star cluster is easily explained by the gas expulsion process if the majority of clusters forms with SFEs less than 50%. Later on star cluster can disperse due to collisions with GMCs (e.g. Spitzer, 1958; Gieles *et al.*, 2006), due to tidal interactions with the hosting galaxy (e.g. Spitzer, 1987; Gieles & Baumgardt, 2008) or due to stellar mass loss (e.g. Vesperini *et al.*, 2009). Gas expulsion therefore seems to be of major importance for the evolution of star clusters.

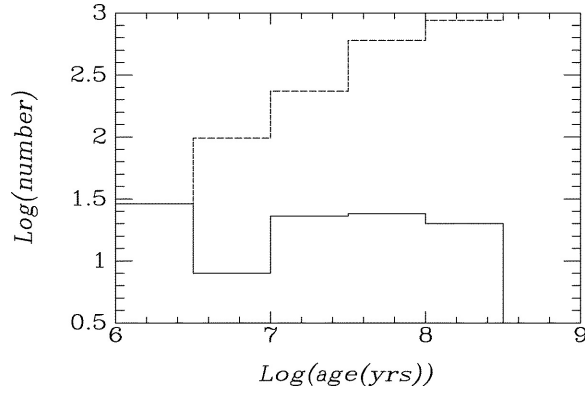


Figure 1.8: Observed number of embedded and open clusters within 2kpc of the sun (solid line) and predicted number of clusters for a constant rate of star formation (dashed line) as function of age. Taken from

The evolution of star clusters after gas loss was investigated in more detail by performing N-body simulations. One of the first of such studies has been published by Lada *et al.* (1984) who simulated the evolution of Plummer-model clusters with half-mass radii in the range  $0.2 - 0.7$  pc containing 50 or 100 stars that were initially embedded in a gas cloud in virial equilibrium. In their simulations they varied the gas removal timescales in the range from  $\approx 10^4 - 10^6$  yr modelling both, fast and slow gas removal. In this calculations the gas has been included as background potential. They found that star clusters with SFEs less than 50% are not necessarily completely dissolved due to the gas removal, but loose a major part of the stellar population leaving behind a smaller bound cluster. The fraction of stars that remain bound depends on the timescale over which the gas loss happens, the longer the gas loss timescale is, the larger is the fraction of stars that remains bound.

In addition, Lada *et al.* (1984) performed simulations of clusters in which the stellar component had zero velocities representing a cluster which is highly subvirial. The fraction of stars that remained bound was significantly higher than in the simulations of the cluster initially in virial equilibrium.

Baumgardt & Kroupa (2007) performed a parameter study of star clusters loosing gas over different timescales. In addition, they investigated the effect of the galactic tidal field using the so-called 'Near-Field Approximation' which assumes that the size of the cluster is much smaller than its distance to the Galactic centre. They simulated the evolution of 20000 equal mass stars in Plummer-model clusters at different galactocentric orbits. They showed while for very short gas-removal time-scales a SFE of at least 40% is needed for a bound cluster to survive, the SFE limit lowers to 33% if the timescale of gas removal is prolonged. The galactic tidal field has the general effect to reduce the fraction of stars remaining bound after gas expulsion. However, the effect of the tidal field begins to become important if  $R_{\text{hm}}/r_J > 0.06$  where  $R_{\text{hm}}$  is the half-mass radius and  $r_J$  the Jacobi- or tidal radius of the clusters, which determines the boundary at which stars are bound to the cluster or to the galaxy (see Sec. 1.2.3).

The N-body simulations presented so far have modelled the potential of the gas as a background potential whose structure is not influenced by the stellar component of the cluster. Simulating the evo-

lution of King-model clusters containing 1000 stars embedded into gas with two different approaches Geyer & Burkert (2001) showed that this approximation is in fact an acceptable representation of the gaseous component. First they performed pure N-body simulations with a background potential and afterwards SPH simulations which modelled the evolution of the gaseous component correctly. Both simulations gave very similar results, so that the approximation of an background potential can be regarded as valid.

Geyer & Burkert (2001) only simulated the gravitational interactions between the stellar and gas component, and gas removal was not treated in a self-consistent way. Instead they either increased the temperature of the complete cloud so mimicing the heating of the gas due to the massive OB stars in the clusters or by increasing the temperature of the innermost 0.2 pc of the gas by a factor of 200 to model the effects of a supernova. Pelupessy & Portegies Zwart (2012) included stellar winds and supernova intrinsically. The stellar winds and supernova are modelled by the generation of new SPH particles that are ejected from the stars according to their calculated mass losses. In their simulations, which comprised 1000 stars in Plummer-model clusters, the stellar winds blow out the cluster centre within 9Myr and the first supernova then removes the remaining gas on a very short timescale. Since gas is already lost before the supernova explodes, the cluster expands already before all gas is lost. However, as it is currently not known, which fraction of energy released by the stellar winds and supernova that heats the gas, Pelupessy & Portegies Zwart (2012) also performed simulations in which less energy is converted into heat. In this simulations, the stellar winds are not capable to remove any gas from the cluster so that the supernovae account for a considerable amount of mass loss. These results imply that the gas expulsion timescale significantly depends on the rate at which the energy released through stellar winds and supernovas is turned into internal heat of the gas cloud.

The effect of the gas expulsion might not only depend on the overall SFE and the expulsion timescale but as well on the differences in the distributions of stars and gas in the cluster. Adams (2000) studied the evolution of clusters, in which the stellar component had a King profile (see Sec. 1.1.2) and the gas component an almost isothermal density distribution, to study which effect a spatially varying SFE within a cluster would have on the cluster evolution after gas expulsion. In this setup, the SFE in the centres of the clusters is higher than in the outer parts of the clusters. This results in a larger fraction of stars remaining bound after gas loss compared to previous studies. He showed that the bound fraction after gas loss can approximately be fitted by  $f_b = 2\varepsilon - \varepsilon^2$  with  $\varepsilon$  being the star formation efficiency in the cluster.

Another study investigating the influence of different density profiles of the stellar and gas component in star clusters is that by Chen & Ko (2009). They performed Nbody simulations of Plummer-like star clusters embedded in Plummer-like gas spheres which grow in size to model the gas loss from the clusters. They found that the SFE is not a proper parameter to characterise the outcome of gas expulsion if the density profiles of the gas and stellar component differ in different star clusters. They find that the initial stellar to gas mass ratio at a given Lagrange radius (e.g. at the half-mass radius) or



the initial kinetic energy are better measures. The density profiles of the stellar and the gas component differ only if forces inside the clusters are present, that only influence the gas within the cluster. Such a force could be mediated by magnetic fields inside the cluster, however it is currently not known which importance magnetic forces actually have in embedded star clusters.

The influence of gas expulsion has not only been investigated theoretically, but has also been considered when interpreting young star cluster observations. For example several studies (Smith & Gallagher, 2001; Mengel *et al.*, 2002) of young star clusters have shown, that the dynamical cluster masses, determined by measuring the velocity dispersion and the radial extent of the cluster and assuming that the clusters are in virial equilibrium, do not match the masses determined using the observed luminosities of the clusters. This has been interpreted as these clusters constituting of an irregular number of high-mass stars implying a non-standard IMF of these clusters. Bastian & Goodwin (2006) interpret these deviations by the star clusters being out of virial equilibrium due to gas expulsion. They performed Nbody simulations of star cluster loosing 50% of their mass due to gas loss. Since their resulting star clusters also show the same signatures as the observed ones, the increased dynamical cluster mass compared to the real mass of the cluster and “tail of stars” at wide cluster separations they concluded that the postulation of an abnormal IMF in these clusters is obsolete.

To generalize these results Goodwin & Bastian (2006) performed N-body simulations of Plummer-model clusters with equal-mass stars which undergo instantaneous gas loss with SFEs in the range 0.1 to 1.0. They showed that the dynamical mass is higher if the SFE in the cluster is lower. The expression for the dynamical mass of a cluster

$$M_{\text{dyn}} = \eta \frac{R_{\text{hm}} \sigma_{1D}^2}{G}, \quad (1.38)$$

with  $M_{\text{dyn}}$  the calculated dynamical mass,  $R_{\text{hm}}$  the half mass radius (or the half-light radius) and  $\sigma_{1D}$  the one-dimensional velocity dispersion of the cluster and  $\eta$  being a numerical constant  $\approx 10$  is only applicable for cluster in virial equilibrium. Applying it to supervirial clusters (i.e. clusters with a too large velocity dispersion) artificially rises the mass of the cluster. Comparing their results with observations of star clusters (see Fig. 1.9) revealed that this effect is important for a multitude of clusters.

In recent work the opinion about the importance of gas expulsion for cluster survival is controversially discussed. Gieles & Portegies Zwart (2011) have shown that the deviation of the dynamical and luminosity masses of star clusters does not necessarily need to be explained by gas expulsion, but could also result from massive binaries in the clusters. Since massive stars are very luminous and are often found to be in binary systems (see Sec. 1.3) they bias the measurements of the velocity dispersions to high values. These statements are supported by observations of NGC 3603 (Rochau *et al.*, 2010), Westerlund I (Mengel & Tacconi-Garman, 2007) and the Arches (Clarkson *et al.*, 2011) which all show that these cluster have rather small (corrected) velocity dispersions which would not be expected if the cluster would have undergone a strong gas expulsion event recently.

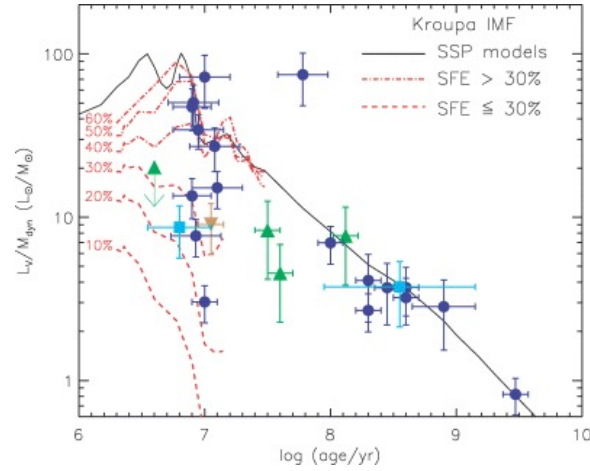


Figure 1.9: Evolution of the dynamical to luminosity mass ratio vs age of observed clusters (data-points) and resulting from the simulations by Goodwin & Bastian (2006). Taken from Goodwin & Bastian (2006).

On the theoretical side the studies of Kruijssen *et al.* (2012) and Smith *et al.* (2011) indicate that gas expulsion might be of less importance as has been found before. Kruijssen *et al.* (2012) analysed the response of subclusters forming on gas expulsion SPH simulations by Bonnell *et al.* (2003, 2008) which studied the fragmentation of molecular clouds and the formation of stars in this fragments. They found that the gas content in the subclusters significantly reduces during the simulations because of accretion of gas onto the stars and subcluster shrinkage. As this depletion of gas happens on timescales of the order of the free-fall time of the subclusters, gas expulsion in these subclusters will not disturb them significantly.

A comparable study has been performed by Smith *et al.* (2011) who investigated the evolution of embedded substructured star clusters including 1000 equal-mass stars with the help of Nbody simulations that loose their gas instantaneously after 3Myr. Their simulations show that the clumpiness of the star clusters helps the clusters to survive the gas expulsion because the star clusters evolve towards a more compact constellation before the gas is expelled (see also Allison *et al.*, 2009). As the gas potential does not change during this time the SFE within the cluster boundaries raises, therefore increasing the fraction of stars, that remained bound after the gas loss.

In summary, many studies have investigated the influence of gas expulsion on the evolution of star clusters. However, each study focused on a special stellar distribution function and so that no systematic study of the influence of it is available right now. In addition, the clusters simulated by most authors display clusters of relatively low masses ( $M_{cl} < 10^4$ ) if they include a realistic IMF or use equal mass stars to extend the number of simulated stars. In Chap. 5 a systematic study of the influence of the stellar density profile on the outcome of the gas expulsion process of massive clusters ( $M_{cl} = 1.5 \times 10^4 M_{\odot}$ ) consisting of stars drawn from the Kroupa (2002) IMF will be presented. Additionally simulations including a primordial binary population have been taken out to investigate, if these could influence the evolution of these clusters.

## 2 Numerical Simulations

Astronomical observations only show a snapshot of the evolution of star clusters because both the dynamical timescales and lifetimes of stellar systems are very long in human scales (see Sec. 1.2.1). Therefore it is necessary to use theoretical tools of any sort, if one want to understand the evolution of star clusters.

Ideally, this would lead to an elementary algebraic expression describing the dynamics of each star in the star cluster. However it turns out, that only the two-body problem can be solved using elementary functions by the well known Kepler laws (see Sec. 1.3). In addition a few special realisations of the three-body problem can be solved analytically. In these cases one of the stars has negligible mass in comparison to the other stars (restricted three-body problem) although their solutions are much more complex than for the two body problem. The complexity of the solutions increases even further, if the general three-body problem (all stars are of comparable masses) or if more than three stars are studied. As Karl Sundmann showed in the beginning of the last century, also in this case, a analytic solution can be found in form a converging series (also called the Sundmann-series), however, this series does not converge fast enough so that today, the evolution of star clusters is studied by numerical integration of the equations of motion of all stars in the cluster.

In the here presented work I used the high-precision code NBODY6 to study how a binary population evolves in star clusters off different type. The here used version of the code displays the recent version in a row of codes which have been developed by Sverre Aarseth since the early 1960's. Initially being written to simulate the evolution of clusters with a very limited number of stars (Aarseth, 1963) improvements of the numerical techniques and of the computing hardware allow simulating up to several  $10^5$  stars for several Myr(e.g. Banerjee *et al.*, 2012) nowadays. In this chapter the most important techniques used by NBODY6 to improve the runtime but also to improve the accuracy of the simulations will be introduced.

### 2.1 Integration

The equations of motion of a given self-gravitating system of  $N$  particles can be expressed as

$$m_i \ddot{\mathbf{r}} = \mathbf{F}_{g,i} = \sum_{j \neq i}^N \frac{G m_i m_j}{|\mathbf{r}_i - \mathbf{r}_j|^2} \frac{\mathbf{r}_i - \mathbf{r}_j}{|\mathbf{r}_i - \mathbf{r}_j|}, \quad i = 1, \dots, N \quad (2.1)$$

where  $G$  is the gravitational constant and  $\mathbf{F}_g$  the Newtonian gravitational force.

If the initial conditions of the stellar system are given by  $\mathbf{r}_i(t=0)$ ,  $\mathbf{v}_i(t=0)$  it is possible to calculate the evolution of the system numerically by advancing the system in discretised time steps  $\Delta t$ . This

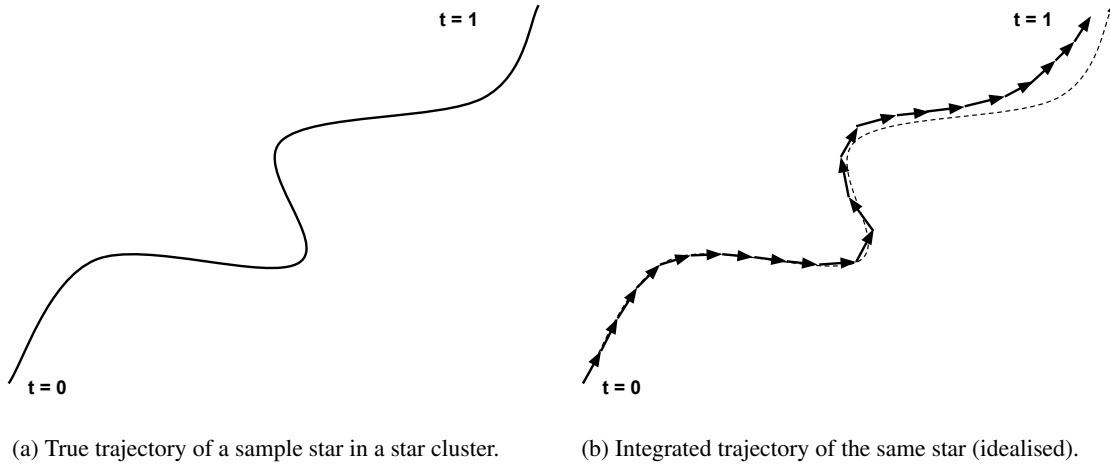


Figure 2.1: Integration of a stellar trajectory.

may be accomplished by truncating the Taylor-series of  $\mathbf{r}(t)$  and  $\mathbf{v}(t) = \dot{\mathbf{v}}(t)$  after the first order and sequentially calculating

$$\begin{aligned}\dot{\mathbf{r}}_i(t + \Delta t) &= \ddot{\mathbf{r}}_i(t) \cdot \Delta t + \dot{\mathbf{r}}_i(t), \\ \mathbf{r}_i(t + \Delta t) &= \dot{\mathbf{r}}_i(t) \cdot \Delta t + \mathbf{r}_i(t),\end{aligned}\tag{2.2}$$

where  $\ddot{\mathbf{r}}$  is given by the gravitational forces (Eq. 2.1) due to all other stars in the system. This simple integration method is known as Euler integration.

The outcome of the integration is displayed schematically in Fig. 2.1. Fig. 2.1a shows the true trajectory of a sample star in a star cluster which changes the direction of its movement multiple times due to the interaction with other stars in the cluster, which are not shown for simplicity. The integrated trajectory is shown in Fig. 2.1b which is not a continuous line anymore but has been divided into several segments where each segment corresponds to the distance the star travels during a time-step.

As can be seen the integration of the stellar trajectory does not necessarily lead to a perfect reproduction of the real trajectory of the star. This behaviour leads to (unphysical) changes in total energy and total angular momentum of the stellar system. This is why the conservation of energy or the angular momentum is often used to determine the quality of the integration.

Reasons for deviations trajectories can be manifold and some techniques used by NBODY6 to reduce the errors in the calculations will be introduced in the following sections. However, it turns out that even the integration method that is used significantly affects the quality of simulations. For example, the Euler integration is known to perform rather badly in comparison with other integration methods like the leap-frog integration or higher-order methods like the Runge-Kutta method.

The integration method used by NBODY6 is the so-called Hermite integrator which was introduced by Makino (1991). The motivation to introduce this new integration scheme was the availability of

GRAPE (GRAVity PipE) special cards, which present special purpose computers which were able to calculate gravitational forces very fast. To put this into numbers, the fastest “regular” supercomputer in the first TOP500 list of supercomputers had a peak performance of 131 Gflops ( $131 \times 10^9$  floating point operations per second) distributed over 1024 cores (<http://www.top500.org/list/1993/06/100>). At the same time, the special purpose computer HARP-1 (Makino *et al.*, 1993) of 150 Mflops, available to a single application. Two years later it’s successor GRAPE-4 (Makino *et al.*, 1997) managed to be the first TFlops computer. Nowadays, the GRAPE cards have been replaced by the much cheaper GPU cards, that initially were developed for video gaming. However, as also these cards provide immense computing power (e.g. Nvidias GTX580 used for the simulations in Chap. 5 has a peak performance of 1581.1 Gflops/s ) they can also be used for scientific computations. GRAPE boards and GPUs are only capable to compute gravitational forces and cannot be used to perform any other computations needed to be taken out during a ordinary N-body simulation like integration or IO processes.

Therefore basic idea of the Hermite integrator was to compute the forces and their first derivatives on the GRAPE boards and perform all other tasks on the host machine. However, this approach would result in a second-order integration scheme which is too inaccurate when performing high precision calculations as intended here. Therefore, the Hermite integrator introduces a correction term based on the second and third derivatives into the calculations, which raises the order of the integration to four. It turns out that this correction terms can be calculated using the force and it’s first derivative alone so that no explicit computation of any additional derivatives is needed.

The Hermite integration scheme works as follows. The Taylor series of the force and it’s first derivative up to the third order and second order respectively reads as

$$\mathbf{F} = \mathbf{F}_0 + \mathbf{F}_0^{(1)}t + \frac{1}{2}\mathbf{F}_0^{(2)}t^2 + \frac{1}{6}\mathbf{F}_0^{(3)}t^3 \quad (2.3)$$

$$\mathbf{F}^{(1)} = \mathbf{F}_0^{(1)} + \mathbf{F}_0^{(2)}t + \frac{1}{2}\mathbf{F}_0^{(3)}t^2, \quad (2.4)$$

where the variables without subscripts denote the new values of the variables while variables with subscript zero denote the current values of the variables and the superscripts denote the order of the derivation of the variable. Solving Eq. 2.4 for  $\mathbf{F}_0^{(2)}$  and introducing this in Eq. 2.3 results in the third order derivative of the force:

$$\mathbf{F}_0^{(3)} = 6 \left[ 2(\mathbf{F}_0 - \mathbf{F}) + (\mathbf{F}_0 + \mathbf{F}_0^{(1)})t \right] / t^3 \quad (2.5)$$

Now solving Eq. 2.5 for  $\mathbf{F}_0^{(2)}$  gives the second order derivative of the force as

$$\mathbf{F}_0^{(2)} = 2 \left[ -2(\mathbf{F}_0 - \mathbf{F}) - (2\mathbf{F}_0^{(1)} + \mathbf{F}^{(1)})t \right] / t^2. \quad (2.6)$$

This means that both the second and the third order derivative of the force can be calculated using the

force and its first derivative alone, which can be computed fastly on the GRAPE boards.

The integration process itself works like this. At the beginning of each new time step, the coordinates and velocities of all stars are predicted by

$$\begin{aligned} \mathbf{r}_i &= \left[ \left( \frac{1}{6} \mathbf{F}_0^{(1)} \Delta t_i' + \frac{1}{2} \mathbf{F}_0 \right) \Delta t_i' + \mathbf{v}_0 \right] \Delta t_i' + \mathbf{r}_0 \\ \mathbf{v}_i &= \left( \frac{1}{2} \mathbf{F}_0^{(1)} \Delta t_i' + \mathbf{F}_0 \right) \Delta t_i' + \mathbf{v}_0. \end{aligned} \quad (2.7)$$

where  $\Delta t_i = t - t_i$  is the time since the last time step. Afterwards the second and third order derivatives of the force are obtained by Eq. 2.6 and Eq. 2.5 and combined to form the corrections for the coordinates and the velocities of the stars:

$$\begin{aligned} \Delta \mathbf{r}_i &= \frac{1}{24} \mathbf{F}_0^{(2)} \Delta t_i^4 + \frac{1}{120} \mathbf{F}_0^{(3)} \Delta t_i^5, \\ \Delta \mathbf{v}_i &= \frac{1}{6} \mathbf{F}_0^{(2)} \Delta t_i^3 + \frac{1}{24} \mathbf{F}_0^{(3)} \Delta t_i^4 \end{aligned} \quad (2.8)$$

Besides making use of the fast calculation of the forces on the accelerator cards, the Hermite integration scheme has proven to be a very stable integration scheme, that conserves the energy of the system very well (in this thesis simulations with energy errors of more than  $1 \times 10^{-3}$  over the complete simulations time of up to 30Myr have been excluded from the diagnostics). Additionally, the Hermite scheme is much simpler than many other integration schemes (e.g. Runge-Kutta).

## 2.2 Individual time steps

An important input parameter for a simulation is the time step width for the integrator  $\Delta t$ . Basically, the time step width does not only determine the overall runtime of a simulation (the shorter the time-step width the longer the simulation runtime) but does also influence the quality of the simulation results (the shorter the time-step width the more accurate the calculations get). So the problem comes up to choose an initial time-step width, that the simulation time is shortest for a given accuracy.

However, while it might be possible to provide such a single time-step width in the set up for simulations with small particle numbers or of homogeneous systems, this is not possible in simulations of star clusters. The reason for this is that star clusters are inhomogeneous structures within which the strength of the interactions between the stars varies significantly. For example the forces acting on the stars in the dense cluster centre are very strong due to the small inter-star distances while in the sparse cluster outskirts, the forces acting onto a star are much smaller. So, while the stars in the cluster centre require very small time-step so that their trajectories can be calculated correctly, the time-step for stars in the cluster outskirts can be much longer.

The solution of this problem is to introduce individual time-steps into the calculations, so that the trajectory of each star can be integrated as often as needed. The time-step width of an individual star should thereby depend on the strength of the forces acting on the star and be the smaller the stronger

the forces are. In NBODY6 the time-step width of a individual star is calculated by

$$\Delta t_i = \left( \frac{\eta |\mathbf{F}| |\mathbf{F}^{(2)}| + |\mathbf{F}^{(1)}|^2}{|\mathbf{F}^{(1)}| |\mathbf{F}^{(3)}| + |\mathbf{F}^{(2)}|^2} \right)^{1/2} \quad (2.9)$$

where  $\eta$  is a dimensionless accuracy parameter.

Including individual time-steps into the calculations means that only one particle is integrated in an integration cycle. However, as the force on this particle depends on the current separations to the other particles in the simulation, their positions have also to be known at each integration cycle. To reduce the computational effort, instead of calculating the positions of all other stars to highest precision, their position are predicted using the Hermite scheme to order  $F^{(1)}$  (see Eq. 2.7) using the forces and their first derivatives already known from their last integration step. Afterwards the current force on the particle that is to be integrated is calculated using the predicted locations of all other particles and it's position and velocity is corrected to highest level. Since in this calculations only the force on the star under consideration has to be calculated and all other calculations involve multiplications and additions, that can be performed very fast on computers, this scheme significantly improves the runtimes of star cluster simulations.

It turned out that applying each particle a individual time step given by Eq. 2.9 is not the optimal way to handle individual time-steps. In fact, it is favourable to quantize the time-step so that a higher number of stars can be integrated at a common time step. The quantization of time is achieved by

$$\Delta t_n = \Delta t_1 / 2^{n-1}, \quad (2.10)$$

where  $\Delta t_1$  is the maximum time step width in the simulation and  $n$  is the level of the current time step. At the beginning of the simulation, each particle gets it's block time step by simply computing it's time step width by Eq. 2.9 and truncating it to the nearest time-step given by Eq. 2.10. During the simulation the block-time step of a particle is determined by again calculating it's individual time-step width  $\Delta t_i$  and checking it against it's current block time step  $\Delta t_b$  which can lead to three possible results

1. Reduction by a factor 2 if  $\Delta t_i < \Delta t_b$
2. Increase by 2 if  $\Delta t_i > 2\Delta t_b$  and  $t$  commensurate with  $2\Delta t_b$
3. No change if  $\Delta t_b < \Delta t_i < 2\Delta t_b$

So decreasing the time-step of a particle is possible at each integration cycle while increasing the time-step is only possible if the current simulation time is a multiple of  $2\Delta t_b$ . This behaviour is necessary to keep the order within the simulations as otherwise particles would be integrated on 'odd' time-steps (see. Fig. ).

NBODY6 includes a block-time time-step scheme.

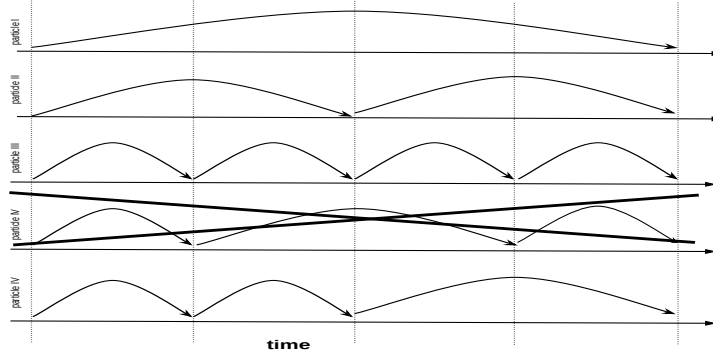


Figure 2.2: Block time-steps.

### 2.3 Neighbour treatment

Simulating the evolution of star clusters involves calculating the trajectories of a large number of particles which vary due to the forces by all other particles. This means that the force sum Eq. 2.1 has to run over all particles for each particle to be integrated resulting in an computational cost of order  $O(N^2)$  corresponding to very long computation times for large number of particles.

Therefore it is advantageous to include computational schemes, that help to reduce the computational effort during the simulations. One scheme of this sort is the Ahmad-Cohen neighbour scheme (Ahmad & Cohen, 1973) which is based on dividing the forces acting on a particle in a *regular* ( $\mathbf{F}_R$ ) and *irregular* ( $\mathbf{F}_I$ ) part:

$$\mathbf{F} = \mathbf{F}_I + \mathbf{F}_R \quad (2.11)$$

The regular forces originate from the contribution of particles, that are far away from the particle under consideration while the irregular forces originate from near neighbours of the particle. Due to this separation into 'far' and 'near' particles the regular and irregular forces have quite different characteristics. The irregular forces strongly influence the particle and vary on very short timescales while the regular forces influence the particle more mildly and do not vary much with time. This means that it should sufficient to obtain reasonable results for the trajectory of a particle to calculate the irregular forces much more often than the regular forces.

NBODY6 adapts this scheme by calculating the irregular and regular forces on two different time step widths  $\Delta t_n$  and  $\Delta t_d$  with  $\Delta t_n \ll \Delta t_d$  and  $\Delta t_d$  being a multiple of  $\Delta t_i$  (see Fig. 2.3 and Makino & Aarseth (1992)). The workflow of the AC-neighbour scheme looks like this. At the beginning of the simulation all forces and their derivatives are calculated and the positions and velocities of all stars are calculated using the Hermite integration scheme. Since  $\Delta t_n < \Delta t_d$  the next time step will be an irregular time-step so the contribution due to the nearest neighbours are calculated to highest order while the contribution by the distant particles is only predicted using the forces and their derivatives known from the last regular time step. So the total force on a particle at a arbitrary irregular time step



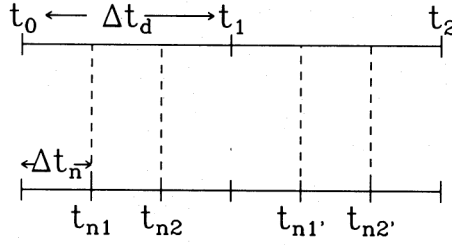


Figure 2.3: The time step scheme applied in the Ahmad-Cohen neighbour scheme. From Makino & Aarseth (1992).

is calculated by

$$\mathbf{F}(t_{ni}) = \mathbf{F}_I(t_{ni}) + \mathbf{F}_R(t_i) + \mathbf{F}_R^{(1)}(t_i)(t_{ni} - t_i), \quad (2.12)$$

where  $t_i$  denotes the time of the last regular force calculation and  $t_{ni}$  is the current time (see. Fig. 2.3). Equivalently, the first derivative of the total force is calculated by

$$\mathbf{F}^{(1)}(t_{ni}) = \mathbf{F}_I^{(1)}(t_{ni}) + \mathbf{F}_R^{(1)}(t_i) \quad (2.13)$$

Calculating the forces in this manner is only possible since the regular forces should not have changed significantly during the small time steps  $\Delta t_i$ . This scheme is repeated for the next irregular time steps until the next regular time step is reached, where all forces and their derivatives are calculated to highest order.

The selection of particles that contribute to irregular forces is of crucial importance for the AC-neighbour scheme as neglecting a neighbour in the irregular force calculation would lead to significant errors in the calculations. The selection of the nearest neighbours is taken out during each regular force step and is achieved by selecting all particles that are within the “nearest-neighbour sphere” with radius  $R_s$  as being contributors to the irregular force. However, only taking these particles is not sufficient because particles that are outside the neighbour sphere at the last regular time step might travel into the neighbour sphere of the particle during the following irregular time steps. Therefore, in addition to the stars within the neighbour sphere, particles within a buffer zone with radius  $2^{1/3}R_s$  that fulfil the condition  $(\mathbf{r}_i - \mathbf{r}_j) \cdot (\mathbf{v}_i - \mathbf{v}_j) < 0.1R_s^2/\Delta t_d$  are additionally included into the neighbourlist.

The AC-neighbour scheme can significantly speed up the calculations provided that the number of nearest neighbours  $N_{nb}$  is small compared to the total number of particles  $N$  in the simulation. In fact it turns out that relatively small neighbour number as 50 are sufficient to correctly calculate the evolution of star cluster with up to 40000 stars. However, the code include internal refinement mechanisms which can compensate for wrongly chosen parameters. For example if the number of nearest neighbours would be chosen to small, the code would automatically decrease the regular time-step width so that the accuracy of the calculations is assured.

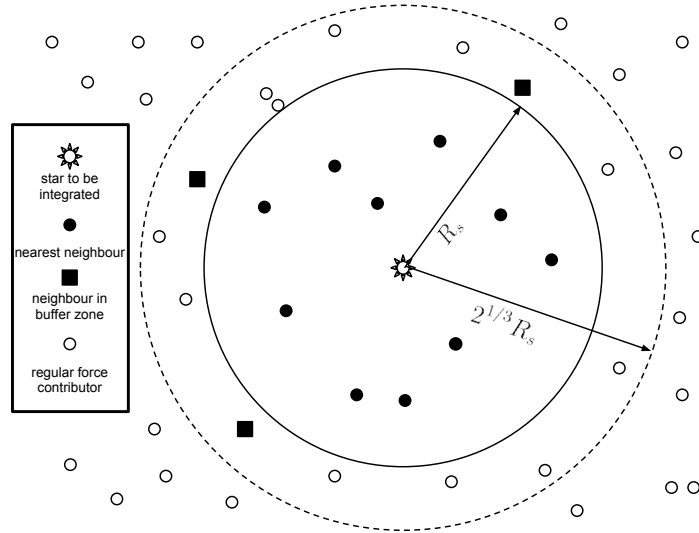


Figure 2.4: Locations of neighbours in the Ahmad-Cohen neighbour scheme.

## 2.4 KS-regularization

Even if no primordial binaries are present at the beginning of a star cluster simulations tight binaries may form due to three-body interactions even if the simulations has been set up without any binaries (e.g. Aarseth, 1963; Pfalzner & Olczak, 2007; Fujii & Portegies Zwart, 2011). These tight binaries can lead to numerical difficulties that have to be solved to maintain the accuracy of the simulation code. Firstly, the time-steps for integrating this strongly interacting systems has to be to be very short to be able to resolve it's internal orbit (see. Sec. 2.2) which is not desirable since this would significantly slow down the overall simulation. Additionally even very small numerical errors, that occur when directly integrating tight binaries with very small separations, so that the singularity at zero separations comes into play, can lead to significant deviations from the real evolution from the real evolution of the system. For example integrating a binary with an eccentricity of  $e = 0.9$  using the basic Hermite-scheme leads to deviations of the semi-major axis per orbit of about  $-1.3 \times 10^{-6}$  so that significant changes would be apparent after about  $10^4 - 10^5$  orbits (Aarseth, 2003). As binaries with period of years or even less than days may occur during the simulations this motivates, why special care has to be taken for this extreme systems.

A possible solution for this problem is to regularize their equations of motion to remove the singularity at zero separation (Bettis & Szebehely, 1972; Aarseth, 1972). In NBODY6 this regularization is realized using the Kustaanheimo-Stiefel method (Kustaanheimo & Stiefel, 1965). The basic idea behind regularization and the KS-regularization scheme will be introduced here shortly.

In general the equation of relative motion of a binary system within a star cluster is given by

$$\ddot{\mathbf{R}} = -(m_k + m_l) \mathbf{R}/R^3 + \mathbf{F}_{kl}, \quad (2.14)$$

where  $\mathbf{F}_{kl} = \mathbf{F}_k - \mathbf{F}_l$  is the external perturbation of the binary due to the other stars in the cluster. As

the first step to regularize these equations a differential time transformation of the form

$$dt = R d\tau. \quad (2.15)$$

is introduced. Denoting derivations with respect to the fictitious time  $\tau$  by primes and substituting the new differentiation operators

$$\begin{aligned} \frac{d}{dt} &= \frac{1}{R^n} \frac{d}{d\tau} \\ \frac{d^2}{dt^2} &= \frac{1}{R^{2n}} \frac{d^2}{d\tau^2} - n \frac{R'}{R^{2n+1}} \frac{d}{d\tau} \end{aligned} \quad (2.16)$$

into Eq. 2.14 yields a new set of equations of motion

$$\mathbf{R}'' = R' \mathbf{R}' / R - (m_k - m_l) \mathbf{R} / R^{3-2} + R^2 \mathbf{F}_{kl}, \quad (2.17)$$

which does not include the  $R^{-2}$  singularity for  $R \rightarrow 0$  anymore making it more convenient to use than Eq. 2.14.

The essential idea of regularization is now to additionally transform the coordinates of the system. In one dimension this is an easy task to be done. Setting  $t' = x$  and neglecting external forces for the moment for simplicity reduces Eq. 2.17 to

$$x'' = x'^2/x - (m_k + m_l). \quad (2.18)$$

This equation can be further simplified by substituting the binding energy per unit mass of the binary

$$h = \frac{1}{2} \dot{\mathbf{R}}^2 - (m_k + m_l)/R \quad (2.19)$$

into Eq. 2.18 with using  $\dot{x} = x'/x$  from Eq. 2.16

$$x'' = 2hx + (m_k + m_l), \quad (2.20)$$

which displays the equation of motion of an displaced harmonic oscillator. Finally introducing new coordinates by  $u^2 = x$  and an additional use of the energy equation Eq. 2.19 yields

$$u'' = \frac{1}{2} hu, \quad (2.21)$$

which now represents the motion of an ordinary harmonic oscillator in one-dimension. So by applying the regularization it is possible to integrate the motion of two point masses that might collide on a line their. Additionally, the computational effort is reduced as it is possible to integrate the motion of the

two particle with a constant time-step

$$\Delta\tau = \eta_U / |2h|^{1/2} \quad (2.22)$$

where  $\eta/2\pi$  is a specified fraction of the /physical/ period.

Of course, the solution for the motion of two particles in one-dimension is not applicable in real star cluster simulations, although it can be regarded as an extreme case of an binary with an eccentricity approaching unity. Therefore it is necessary to generalise the regularization for dimensions exceeding one which has been performed for two dimension by Levi-Civita (1920). To regularize the 2D-motion, he mapped the problem to the complex plane using a  $2 \times 2$  matrix. The extension of this to three dimensions proved to be much harder and was applied by Kustaanheimo & Stiefel (1965). They realized that a direct application to three-dimensions is not possible because Levi-Civita's approach was based on a mapping in the complex plane. However, using 4-dimensions with the fourth dimension being zero.

The transformation in two and four dimensions is performed via a matrix multiplication of the form

$$\mathbf{R} = \mathcal{L}(\mathbf{u})\mathbf{u} \quad (2.23)$$

with  $\mathbf{R}$  the separation vector of the binary and  $\mathbf{u}$  being the transformed separation vector. The matrices  $\mathcal{L}$  look like

$$\mathcal{L}_{LC}(\mathbf{u}) = \begin{bmatrix} u_1 & -u_2 \\ u_2 & u_1 \end{bmatrix}; \quad \mathcal{L}_{KS}(\mathbf{u}) = \begin{bmatrix} u_1 & -u_2 & -u_3 & u_4 \\ u_2 & u_1 & -u_4 & -u_3 \\ u_3 & u_4 & u_1 & u_2 \\ u_4 & -u_3 & u_2 & -u_1 \end{bmatrix} \quad (2.24)$$

With this, the components of the non-transformed separation vector can be calculate by

$$\begin{aligned} R_{1,LC} &= u_1^2 - u_2^2, \\ R_{2,LC} &= 2u_1u_2, \\ R_{1,KS} &= u_1^2 - u_2^2 - u_3^2 + u_4^2, \\ R_{2,KS} &= 2(u_1u_2 - u_3u_4), \\ R_{3,KS} &= 2(u_1u_3 + u_2u_4), \\ R_{4,KS} &= 0 \end{aligned}, \quad (2.25)$$

The choice of  $R_{4,KS} = 0$  is necessary for calculations in three dimensions. With this the separations are given by

$$R_{LC} = u_1^2 + u_2^2; \quad R_{KS} = u_1^2 + u_2^2 + u_3^2 + u_4^2. \quad (2.26)$$

With this the equations of motion take the form

$$\begin{aligned} \mathbf{u}'' &= \frac{1}{2}h\mathbf{u} + \frac{1}{2}R\mathcal{L}^T\mathbf{F} \\ h' &= 2\mathbf{u}' \cdot \mathcal{L}^T\mathbf{F} \\ t' &= \mathbf{u} \cdot \mathbf{u}. \end{aligned} \quad (2.27)$$

Again these equations behave well for  $R \rightarrow 0$ . To convert from the transformed time  $\tau$  to the physical time, a Taylor series of the form  $\Delta t = \sum_n \frac{1}{k!} t_0^{(k)} \Delta \tau^k$  is carried out. It turns out that for  $n = 6$  all needed differences are already calculated when using the Hermite, resulting in no significant additional computational effort when calculating it. Also binary properties can be calculated very fast. The semi-major axis of the regularized binary can then be calculated by  $a = \frac{1}{2}(m_k + m_l)/h$ . The eccentricity can be obtained by  $e^2 = (1 - R/a)^2 + 4(\mathbf{u} \cdot \mathbf{u}')^2 / (m_k + m_l)a$ .

NBODY6 uses the KS-regularization to regularize the orbits of tight binaries that are not strongly perturbed by the other stars in the cluster. So, during the simulation the code checks for bound systems, that are not strongly perturbed (the limit at which binaries are marked as not being strongly perturbed by the other stars can be set in the simulation input file). If such a system is found, it's global coordinates are transformed using Eq. 2.23 and it's internal evolution is calculated using the regularized equations of motion Eq. 2.27.

What remains to be calculated is the global movement of the binary in the star cluster. For this purpose both stars are removed from the simulation and replaced by the corresponding center of mass particle. The equation of motion of this particle is given by the mass weighted sum of perturbations

$$\ddot{\mathbf{r}}_{\text{cm}} = (m_k \mathbf{F}_k + m_l \mathbf{F}_l) / (m_k + m_l), \quad (2.28)$$

with  $k, l$  being the indices of the regularized stars. The global coordinates of both stars can be calculated by

$$\begin{aligned} \mathbf{r}_k &= \mathbf{r}_{\text{cm}} + \mu \mathbf{R} / m_k, \\ \mathbf{r}_l &= \mathbf{r}_{\text{cm}} - \mu \mathbf{R} / m_l, \end{aligned} \quad (2.29)$$

with  $\mu = m_k m_l / (m_k + m_l)$ .

To summarise the advantages of regularizing the orbits of tight binaries are

- the equations of motion become regular and behave well for  $R \rightarrow 0$
- the number of integration steps per orbit is significantly reduced
- the numerical stability of even circular orbits is significantly increased

A disadvantage when including regularization in the calculations is the need for coordinate transformations. However, since these transformations do not require any costly operations like taking square roots the additional effort to be taken is only minor and the above mentioned advantages outweigh these additional effort to be taken.

## 2.5 Hardware acceleration

The simulation of the evolution of realistic star clusters involves the integration of the equations of particles due to the mutual interactions. As this include the calculation of the forces on each particle

due to each other particle, this results in an computational cost of  $O(N^2)$  implying the immense effort to be taken if a large number of particles (say of the order  $10^{4-5}$ ) has to be integrated. The numerical techniques described so far can help reducing this effort, however they can not drop the dependency on very fast computers if the simulations should be finished in reasonable times.

This explains why the first calculations regarding the evolution of star clusters included very small number of particles. E.g. von Hoerner (1960) was only capable to calculate the evolution of up to 32 particles and the first version of the here used NBODY code was used to study the evolution of up to 100 particles (Aarseth, 1963) already using the individual time-step scheme described in Sec. 2.2.

Luckily, the computing power available for calculations increased with time as following Moore's law. Moore's law states that the number of logical components per CPU doubles about every two years which could be taken as an doubling of the computer power. However, it turned out, that just by increasing the number of logical components on a chip will not always lead to an increase in the computing power. Nowadays, the computing power, especially of supercomputers like JUROPA or JUGENE (located in the Jülich Supercomputer Centre, Germany) is not increased by making the CPU more powerfull, but by increasing the number of CPUs introducing the need that the codes to be run can be executed in parallel. Alternatively, so-called 'accelerators' can be introduced into the computers, that are capable to perform specific calculations much faster than ordinary CPUs, which have to be capable to perform a very broad range of calculations. A supercomputer adopting this approach is the Tianhe-1A located at the National Supercomputing Center in Tianjin, China.

Over the years, NBODY has been adopted to benefit from the hardware capabilities at the given time. The first mayor reconstruction due to improved hardware took place in the early 1990's. At this time the GRAPE accelerator boards built in Japan (Sugimoto *et al.*, 1990) became available offering the fast computation of the gravitational force. In contrast to normal CPUs, which are capable to perform (almost) any calculation, the GRAPE boards where especially manufactured to calculate gravitational forces between particles, nothing else. However, these calculations are performed very fast on the GRAPE boards (1990: 40 MFlops, 2002: 64 TFlops) so it appeared reasonable to change from the until then used polynomial integration scheme to the Hermite scheme (see Sec. 2.1). It turned out, that the Hermite integration scheme also brought benefits for calculations even if no GRAPE cards are used concerning the stability and maintainability of the code, so that it is still used in the current version of NBODY6. However, the GRAPE boards remained to be rather exotic computers as they could not be applied to other research fields making them unattractive for general purpose supercomputer centres and due to their high costs.

To broaden the user-community Spurzem (1999) parallized the NBODY6 to be usable on modern supercomputers which usually consist of a collection of CPUs. The parallelization of the code has been achieved by parallizing the several DO LOOPS in the code, including the Hermite integration and energy calculation using the Message Passing Interface (MPI). Since no domain decomposition has been included, this means that during the calculations the particles have to be communicated between the different CPUs quite often leading to a rather moderate scaling of the code making

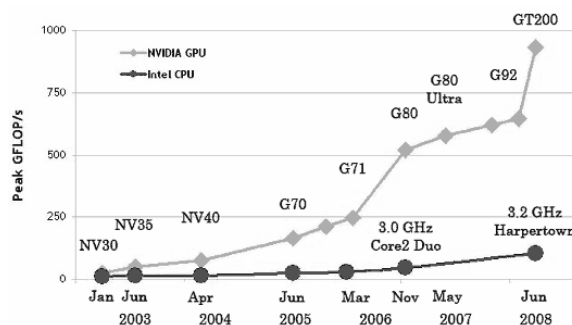


Figure 2.5: Evolution of the peak performance of Nvidia GPUs and CPUs from 2000 till 2008 [from: [www.ixbt.com/video3/images/cuda/gflops.png](http://www.ixbt.com/video3/images/cuda/gflops.png)]

simulations with more than about 10 CPUs not affordable.

In recent years accelerator cards got back in the focus of the NBODY6 community again. However, instead of using very specialised (and expensive) hardware manufactured by a small group, this time the widely used Graphic Processor Units (GPUs) are used to speed up the calculations. As their name already implies, GPUs are intended to be calculate to compute computer graphics very fast (especially 3D-graphics), especially for video games. Since these have become more complex with time and there is a large user community willing to pay for ever faster hardware great efforts have been taken to improve the GPUs that far that they outmatch usual GPUs significantly today (see Fig. 2.5) making them very attractive for simulating NBODY6 systems.

As already mentioned, GPUs were initially constructed to process 3D-graphics only. So if programmers wanted to write code to be run on GPUs they had to use the shading languages like OpenGL or Cg which however were intended to manipulate textures in 3D-graphics to make the rendered images look more nicely. As the first major manufacturer NVidia released an programming Application Programming Interface (API) called Compute Unified Device Architecture (CUDA) with which it became possible to (easily) program GPUs also outside the 3D computer graphics branch. However, CUDA programs are only executable on NVidia GPUs so that CUDA programmers are forced to use graphic cards by this vendor. In contrast to this the later released OpenCL language is supported by a wide variety of vendors (Intel, AMD, ARM, and NVidia).

With this it became possible again to perform even large Nbody simulations on ordinary PCs if a GPU is installed in the system. To make use of the GPU NBODY6 uses the CUDA API to calculate the regular forces (see. Sec. 2.3) which can significantly speed up simulations with particle numbers exceeding about  $10^3$  particles. For simulations with less than  $10^3$  particles, using the GPU turns out to be less beneficial than performing the simulations with the CPUs alone because in this cases copying the needed data to the GPU takes more time than is saved by performing the simulations on the GPU (see below).

The high speed of GPUs is based in it's highly parallel architecture. A modern GPU does not consist of one central computing unit, but instead of several multiprocessors which themselves consist of many thread processors (see Fig. 2.6) resulting in a very high total number of processors available

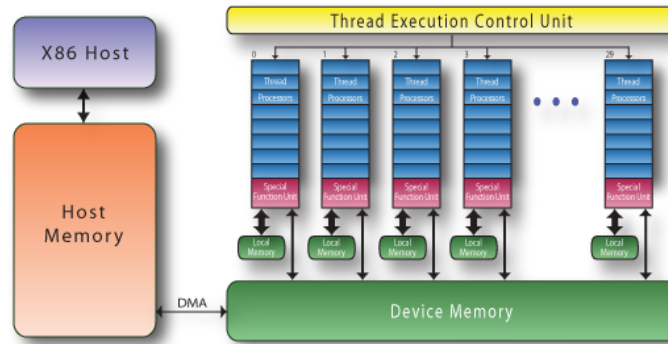


Figure 2.6: Schematic architecture of modern GPUs [from: [www.pgroup.com/lit/articles/insider/v1n1a1.htm](http://www.pgroup.com/lit/articles/insider/v1n1a1.htm)]

for the calculations. The thread processors within a single multiprocessor run the same program at the same time, however do this on different (internal) data sets (Single Instruction Multiple Data). In the case of NBODY6 the calculations performed on the thread processors are the determination of the force forces onto each particle which includes the calculations of all interparticle distances. Since the thread processors in a multiprocessor share a common, very fast memory these calculations can be performed very fast and lead to a significant reduction of the computing time if compared to the ordinary computation on a single CPU or even several CPUs, if a parallel version of the force calculation is used.

The bottleneck of this architecture is the connection to the main program, running on the CPU of the host computer. This connection is realised via the PCI-Express bus, which is slow in comparison to the internal memory connections within the GPU or within the host computer. So, if a program has to update the data on the GPU very often a serious slow-down of the program is imminent if the speed up due to the fast calculation on the GPU is not sufficient to compensate the slow communication between the CPU and the GPU.

To summarise over the years NBODY6 has been adapted to take the advantage of the most recent hardware to improve the run-time of simulations. While in the beginning this meant that very expensive hardware had to be available (either GRAPE boards or massively parallel supercomputers) the rise of GPUs made it possible again to perform also large simulations on ordinary PCs.



## 3 Binary populations in ONC-like star clusters

### 3.1 Introduction

Observations of the binary populations in young star clusters and the much older, already evolved field have shown, that there are remarkable differences between the binary populations of these two environments that represent two different evolutionary phases of a usual stars life. While there are hints that the period distribution of binaries in young star clusters is log-uniform (e.g. Kouwenhoven *et al.*, 2007; Reipurth *et al.*, 2007; Connelley *et al.*, 2008) the period distribution of binaries in the solar neighbourhood is found to be log-normally distributed (Duquennoy & Mayor, 1991; Raghavan *et al.*, 2010). This finding is striking as most if not all stars in the solar neighbourhood, including all single, binary and higher-order multiples, originate from star clusters which serve as “hatcheries” for stars (Lada & Lada, 2003).

The aim of this chapter is to investigate i) how a star cluster environment can change a binary population with a log-uniform period distribution and ii) which influence the initial binary frequency in the cluster has on the evolution on the binary population itself. In addition, it is studied, if the cluster environment is capable to convert the log-uniform period distribution to the log-normal one as it is observed in the solar neighbourhood. Therefore, an additional physical process acting in embedded star cluster, the gas-induced orbital decay of embedded binaries as described by C. Kornreich (formerly Hövel) in her Diploma thesis entitled "Gas-induced orbital decay of binary systems in young embedded clusters", will be combined with the pure dynamical effects that have been taken into account so far.

### 3.2 The influence of the cluster dynamics on the binary population

#### 3.2.1 Definitions

Before discussing the evolution of a binary population in ONC-like star clusters, I want to give some essential definitions needed when studying binary populations. These definitions will also be applied in the rest of the thesis and are therefore of crucial importance.

The most simple, and here used, measure of the binary population of a star cluster is the number of binaries ( $N_b$ ) within the cluster. Here, a pair of stars is called a binary system if the system is bound and the two stars are at the same time nearest neighbours. In this definition, a star that is part of a multiple system can be part of several “binary” systems simultaneously since two stars do not have to be mutually nearest neighbours. Using this definition triple or other higher order multiples are not handled separately by our diagnostic but are counted as multiple binary systems. The normalised

number of binary systems  $\mathcal{N}_b$  is defined as

$$\mathcal{N}_b(t) = \frac{N_b(t)}{N_b(0)}, \quad (3.1)$$

where  $N_b(0)$  denotes the initial and  $N_b(t)$  the number of binary systems within the cluster at time  $t$ . Another, often used binary populations in star clusters is the binary frequency  $b_f$

$$b_f(t) = \frac{N_b(t)}{N_s(t) + N_b(t)}, \quad (3.2)$$

where  $N_s(t)$  denotes the actual number of observed single stars and  $N_b(t)$  the actual number of binary systems.

### 3.2.2 Method and cluster setup

As here the evolution of binary populations in ONC-like clusters is to be studied, all simulations performed in this chapter have been set up using the standard ONC model cluster as described in Olczak *et al.* (2010). This means that all clusters were set up with 4000 stellar systems, where stellar systems correspond to either single stars or binary systems. This means that for a simulation with a primordial binary frequency of 100% the dynamical evolution of 8000 stars is calculated. The masses  $M$  of the 4000 stellar systems were sampled from the initial mass function given by Kroupa (2002). The minimum and maximum masses of the stellar systems have been chosen as  $M_{\min} = 0.08M_{\odot}$ , corresponding to the hydrogen-burning limit, and  $M_{\max} = 50M_{\odot}$  the mass of the most massive stellar system in the ONC -  $\theta^1\text{C Ori}$ .

Observations of the stellar content in the ONC have shown that the stellar radial density profile of the outer part of the cluster can be approximated by an isothermal sphere (i.e.  $\rho_{\text{present}} \propto 1/r^2$ , see e.g. Jones & Walker (1988); Hillenbrand (1997)) with the exception of the cluster core ( $R_{\text{core}} \approx 0.2\text{pc}$ ), which has a much flatter density profile ( $\rho_{\text{present,core}} \propto r^{-0.5}$ , Scally *et al.* (2005)). To account for this, an initial density profile of the form

$$\rho_0(r) = \begin{cases} \rho_0 (r/R_{\text{core}})^{-2.3} & , \quad r \in (0, R_{\text{core}}] \\ \rho_0 (r/R_{\text{core}})^{-2.0} & , \quad r \in (R_{\text{core}}, R] \\ 0 & , \quad r \in (R, \infty] \end{cases} \quad (3.3)$$

has been adopted where  $\rho_0 = 3.1 \times 10^3 \text{pc}^{-3}$ ,  $R_{\text{core}} = 0.2\text{pc}$ , and  $R = 2.9\text{pc}$ . Olczak *et al.* (2010) demonstrated that this initial radial density profile evolves towards the currently observed one after about 1Myr of dynamical evolution, the estimated age of the ONC (Hillenbrand, 1997). The velocities of the stellar systems are sampled from a Maxwellian velocity distribution and scaled so that the cluster resides in virial equilibrium.

Observations of the ONC indicate that the cluster is mass-segregated (e.g. Hillenbrand, 1997). Nu-

merical simulations by Bonnell & Davies (1998), comparable to the cluster models studied here, demonstrated that this mass segregation cannot be due to dynamical evolution of the cluster but is likely primordial. Following their suggestion, the most massive stellar system is initially placed at the cluster centre and the three next most massive stars within a sphere of radius  $R = 0.6R_{\text{hm}}$  centred on the cluster centre, where  $R_{\text{hm}}$  is the half-mass radius of the cluster.

The primordial binary population used here is based on the observations by Kouwenhoven *et al.* (2007). They compared observations of the Scorpius OB II association with simulated observations of their binary population model to eliminate observational selection effects and biases that affect real observations of star clusters. Their analysis shows that the binary frequency in Scorpius OB II is above 70% with a confidence of  $3\sigma$ . The closest agreement with observations is obtained for models with a binary frequency of 100%. The model of Kouwenhoven *et al.* (2007) was chosen here since it is a well-studied binary population, close to its initial conditions.

In contrast to the field population that exhibits a log-normal period distribution of G and M-dwarf binaries (Duquennoy & Mayor, 1991; Reid & Gizis, 1997), the younger population in Sco OB II has a flat distribution of the semi-major axis in logarithmic space (Kouwenhoven *et al.*, 2007)

$$f_a(a) \propto a^{-1} \quad \Leftrightarrow \quad f_{\log_{10}a}(\log_{10}a) = \text{const.}, \quad (3.4)$$

where  $a$  is the semi-major axis of the binary system.

A flat distribution of the semi-major axes in logarithmic space corresponds to a similar distribution of periods  $P$  with the relation

$$\overline{\log_{10}a} = \frac{2}{3}\overline{\log_{10}P} - \frac{1}{3}\log\left(\frac{4\pi^2}{GM_T}\right), \quad (3.5)$$

$$\sigma_{\log_{10}a} = \frac{2}{3}\sigma_{\log_{10}P}, \quad (3.6)$$

where  $G$  is the gravitational constant and  $M_T$  the total mass of a binary system.

A flat binary period distribution has not only been observed in Sco OB II but also in other regions (e.g. Connelley *et al.*, 2008; Reipurth *et al.*, 2007) and has been used in several theoretical studies involving the evolution of primordial binary frequencies (Heggie & Aarseth, 1992; Ivanova *et al.*, 2005; Hurley *et al.*, 2007).

The mass ratio distribution is given by

$$f_q(q) \propto q^{\gamma_q}, \quad \gamma_q \sim -0.4, \quad (3.7)$$

where  $q = M_{\text{sec}}/M_{\text{prim}}$  is the mass-ratio of a binary with primary mass  $M_{\text{prim}}$  and secondary mass  $M_{\text{sec}}$ . To adopt this functional form in the models, the binary system masses were sampled from the Kroupa (2002) IMF and then split into two components using Eq. 3.7.

The eccentricity of the binary systems in Sco OBII was found by Kouwenhoven *et al.* (2007)

to be thermally distributed, in agreement with the eccentricities of long-period binaries in the field. Following Kroupa & Burkert (2001) who illustrated that the dynamical evolution is not capable of changing the eccentricity distribution significantly, a thermal period distribution was applied to all simulations.

Observations show that the binary frequency varies among low-mass stars in the field (35 – 42%) (Fischer & Marcy, 1992; Reid & Gizis, 1997), Sun-like stars in the solar neighbourhood ( $\sim 60\%$ ) (Duquennoy & Mayor, 1991), and the high binary frequency in low-mass star-forming regions such as Taurus ( $\sim 100\%$ ) (Duchêne, 1999). To account for the large spread among the different environments I set up and investigated cluster models initially with 30%, 50%, 75%, and 100% binaries.

The statistical significance of the results was improved by performing 100 simulations per initial binary frequency. Only those that fulfilled the following conditions were considered in the subsequent diagnostic process:

- after 1 Myr of cluster evolution, the most massive stellar system in the simulations has to be within 0.3pc of the cluster centre.
- the cluster density profile after 1 Myr of cluster evolution has to agree with the cluster density profiles observed by Hillenbrand (1997) and McCaughrean *et al.* (2002).

### 3.2.3 Results

Figure 3.1 shows the initial semi-major axis distribution averaged over 100 simulations each. Although the semi-major axis distributions have been set up log-uniformly in the range  $4.6 \times 10^{-2} \text{AU} - 4.6 \times 10^4 \text{AU}$ , the distribution is only flat up to about  $2 \times 10^3 \text{AU}$  and declines afterwards to zero. The apparent lack of wide binary systems in the  $2 \times 10^3 - 4.6 \times 10^4 \text{AU}$  range is due to the generating algorithm. In the code, binary systems are formed in isolation and then placed in the cluster environment. The wider a binary, the higher the probability that (at least) one of its components has a closer neighbour among the other cluster members. According to the definitions (see Sec. 3.2.1), this chance neighbour is now the potential companion and most probably not bound. As a result, the number of wide binaries is lower than it was initially intended to. However, this is a common problem found in many investigations of this type.

Observations of binary populations in different environments usually use the binary frequency as the main observable of a binary population since it allows easy comparison between different environments and different observing campaigns. Often theoretical studies use this simple observable for ease of comparison with observational data (see for example Kroupa, 1995a; Kroupa *et al.*, 2001; Kroupa & Bouvier, 2003; Ivanova *et al.*, 2005; Hurley *et al.*, 2007; Sollima, 2008). Fig. 3.2a shows the evolution of the normalised binary frequency ( $b_f(t)/b_f(t=0)$ ) during the first three Myr of cluster evolution in the simulations. This normalisation allows direct comparison of the evolution of the binary frequencies for simulations with different initial binary frequencies.

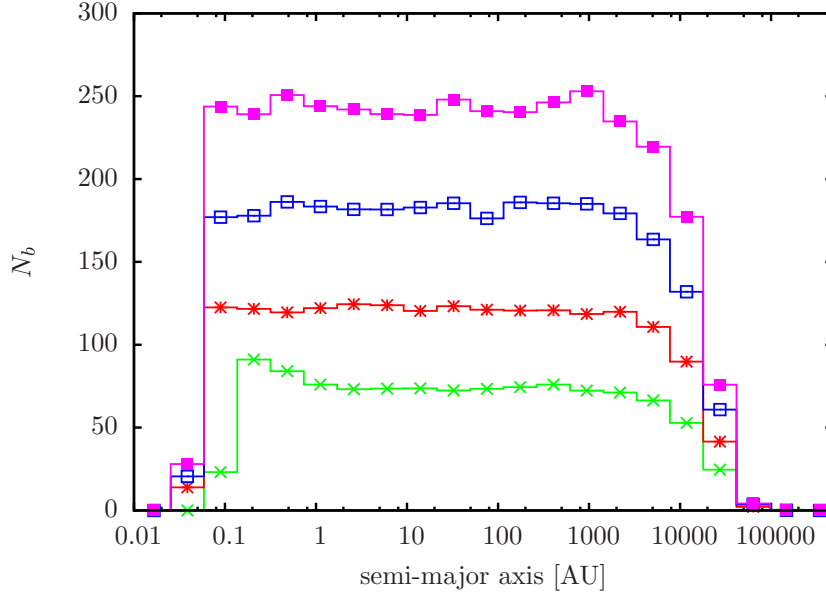


Figure 3.1: Initial semi-major axis distribution for all simulated clusters. Green, red, blue and purple lines denote simulations with initially 30%, 50%, 75%, and 100% binaries, respectively.

As expected from previous studies (Kroupa, 1995a; Kroupa & Bouvier, 2003; Parker *et al.*, 2009), dynamical evolution reduces the binary frequency with time in all simulations. This can be explained by the destruction of wide binary systems by means of three-body encounters as explained in Sec. 1.3. During such an encounter between a binary system and a single star, the energy transfer can lead to tightening or widening of the binary. Heggie (1975) and Hills (1975) have shown, that binaries with binding energies less than the mean kinetic energy of star in the cluster usually widen while binaries exceeding the mean kinetic energy tighten due to encounters. As the number of newly formed binaries in ONC-like star clusters is not capable to counterbalance the destruction of wide binaries (e.g. Pfalzner & Olczak, 2007) the binary frequency in the clusters decreases with time.

In addition, Fig. 3.2a shows that the evolution of the binary population depends on the initial binary frequency - the higher the initial binary frequency, the higher the fraction of binaries that are destroyed during cluster evolution. This finding could lead to the conclusion that the evolution of binary populations is stronger in clusters with a higher initial binary frequency. In short, the evolution of the binary population in star clusters seems to depend on the initial binary frequency. However, because the calculation of the *binary* frequency depends on the number of *single* stars (see Eq. 3.2) it is probably not an unbiased measure of the evolution of the binary population. The normalised number of binary systems  $\mathcal{N}_b$  (see Eq. 3.1) does not suffer from such a shortcoming and its evolution is shown in Fig. 3.2b.

Again normalised number of binaries also decreases with time, however, in contrast to the normalised binary frequency the evolution of the normalised number of binary systems with time does *not* depend significantly on the initial binary frequency. The 1% difference among the data is of the

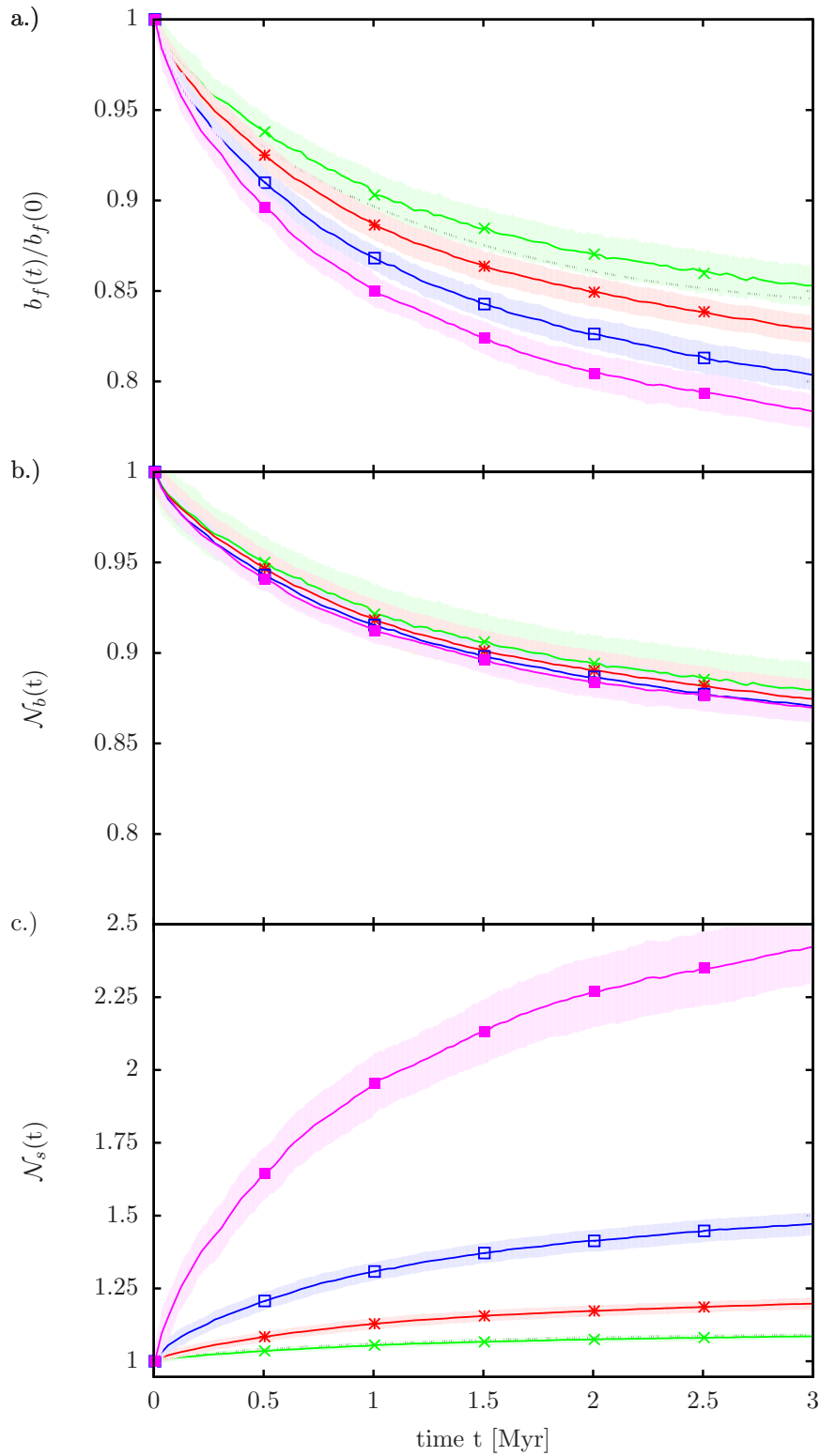


Figure 3.2: Evolution of the normalised binary frequency, normalised number of binary systems and normalised number of single stars with time. Green, red, blue and purple lines denote simulations with initially 30%, 50%, 75%, and 100% binaries, respectively.

order of the statistical error in the simulation. How can this difference in the evolution of the binary frequency and the binary population be explained? It is the evolution of the single star population in the star clusters that significantly affects the evolution of the binary frequency. Its evolution is shown in Fig. 3.2c.

In contrast to the binary frequency and the number of binaries, the number of single stars in the star cluster obviously increases with time because each dissolution of a binary system creates two new single stars. The evolution of the normalised number of single stars depends even more strongly on the initial binary frequency.

The reason why the evolution of the single star population depends on the initial binary frequency can be understood by the use of some basic arithmetics alone. First, it is assumed that the evolution of the number of binary systems can be described by a function  $\alpha(t, b_f)$  that may depend on the time of evolution, initial binary frequency, and other parameters, so that  $N_b(t) = \alpha(t, b_f)N_b(0)$ , where  $N_b(t)$  is the number of binary systems at time  $t$ . Dividing this by the initial number of binary systems one obtains the evolution of the normalised number of binary systems

$$\mathcal{N}_b(t) = \frac{\alpha(t, b_f)N_b(0)}{N_b(0)} = \alpha(t, b_f). \quad (3.8)$$

Based on the findings of Fig. 3.2b one can also assume, that the evolution of the normalised number of binary systems does not depend on the initial binary frequency, so that the function  $\alpha$  can be expressed as  $\alpha(t, b_f) \approx \alpha(t)$ . Because the dissolution of a binary system leads to the generation of two new single stars, the evolution of the number of single stars can be written as

$$N_s(t) = N_s(0) + 2[1 - \alpha(t)]N_b(0), \quad (3.9)$$

where first summand represents the initial number of single stars and the second summand gives the number of newly formed single stars. Applying the relation  $N_b(0) = \frac{b_f(0)}{1-b_f(0)}N_s(0)$  and dividing by the initial number of single stars  $N_s(0)$ , the evolution of the normalised number of binary systems is given by

$$\mathcal{N}_s(t) = 1 + 2(1 - \alpha(t))\frac{b_f(0)}{1 - b_f(0)}. \quad (3.10)$$

Hence, in contrast to the normalised number of *binary* systems (Eq. 3.8), which depends only on  $\alpha$ , the normalised number of *single* stars depends explicitly on the initial binary frequency in the cluster. Consequently, using Eqs. 3.8 and 3.10, an analogous dependence for the normalised binary frequency is given by

$$\frac{b_f(t)}{b_f(0)} = \frac{N_b(t)}{N_s(t) + N_b(t)} \frac{1}{b_f(0)} = \frac{\alpha(t)}{\frac{1-b_f(0)}{b_f(0)} - \alpha(t) + 2} \frac{1}{b_f(0)} \quad (3.11)$$

In summary, the simple model (Eqs. 3.8-3.11) describes the evolution presented in Fig. 3.2 very well: it is the evolution of the single star population that is very sensitive to the initial binary frequency,

while the binary population evolves independently of the initial binary frequency. The normalised number of binary systems (Eq. 3.1) introduced here is therefore the most simple measure of the evolution of a binary population *independent* of the initial binary frequency.

As a consequence, Eq. 3.11 can be used now to calculate the initial binary frequency and is given by

$$b_f(0) = \frac{b_f(t) - \alpha(t) + 1}{\alpha(t)}. \quad (3.12)$$

This finding has a fundamental consequence: if it is possible to determine the explicit form of the function  $\alpha(t, b_f, \dots)$ , it is possible to predict the past and future number of binary systems from the present number of binaries in a given cluster environment. Again assuming that  $\alpha(t, b_f, \dots) = \alpha(t)$ , one finds that  $\alpha_{\text{fit}}(t) = at^b + ct + 1$  with  $a = -0.35 \pm 0.04$ ,  $b = 0.89 \pm 0.01$ , and  $c = 0.27 \pm 0.04$ , provides an excellent fit to the data in an ONC-like cluster in Fig. 3.2b. However, the here used approach neglects the potential effects of other parameters such as the stellar density, this will be investigated in Chap. 4 will explicitly treat the influence of the cluster density on the evolution of the binary population.

Assuming an age of 1Myr for the ONC (Hillenbrand, 1997) for illustrative purposes, one obtains  $\alpha(1\text{Myr}) = 0.92$  using the given fit. Assuming a present-day binary frequency of 60%, motivated by observations that find a consistency between the binary populations of field G dwarfs (Duquennoy & Mayor, 1991) and the ONC (Petr *et al.*, 1998; Köhler *et al.*, 2006), the initial binary frequency in the ONC should have been  $\approx 74\%$ .

Figure 3.3 shows the fraction of binary systems per semi-major axis bin that is destroyed after 1Myr of cluster evolution. It is evident that only binaries with semi-major axis wider than about  $\approx 30\text{AU}$  are destroyed during cluster evolution. This dependence on the semi-major axis was previously reported in other studies of the evolution of binary populations (e.g. Kroupa, 1995c) and can be explained by the outcome of three-body encounters (see above): to dissolve a binary system in a three-body interaction, the velocity of the intruder must be larger than the orbital velocity of the binary system. With this, a lower limit to the semi-major axis of destroyed binaries in the cluster can be estimated. Following Kroupa & Bouvier (2003), the “thermal period” at which destruction still is possible is estimated as  $\log_{10} P_{\text{th}} \approx 4.75$  from

$$\log_{10} P_{\text{th}} = 6.986 + \log_{10} m_{\text{sys}} - 3 \log_{10} \sigma_{3D}, \quad (3.13)$$

using the least massive equal-mass system  $m_{\text{sys}} = 0.16M_{\odot}$  and assuming a typical relative velocity equal to the cluster velocity dispersion in the simulations  $\sigma_{3D} \approx 3\text{km s}^{-1}$ . A period of  $\log_{10} P_{\text{th}} \approx 4.75$  corresponds to a minimum semi-major axis of about 53AU.

This estimate is in good agreement with the results of the simulations in Fig. 3.3. However, in the simulations, there is no sharp transition between stable and destroyed systems because the thermal period  $P_{\text{th}}$  depends strongly on the system mass (Eq. 3.13). The periods of the binaries in the simulations have been sampled independently of the binary system masses. As a result, the fraction of binaries



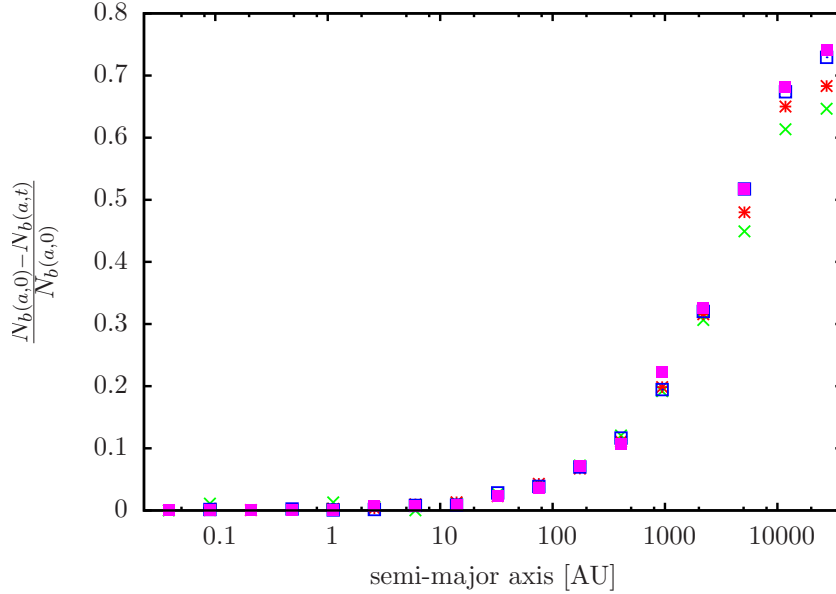


Figure 3.3: Fraction of binary systems per semi-major axis bin that is destroyed after 1Myr of cluster evolution. Green, red, blue and purple lines denote simulations with initially 30%, 50%, 75%, and 100% binaries, respectively.

destroyed by the dynamical evolution of the cluster decreases with binary mass as demonstrated in Fig. 3.4. The fraction of destroyed binaries clearly decreases with binary mass.

The solid line in Fig. 3.4 represents a fit of the function  $f(m_{\text{sys}}) = a \log_{10} m_{\text{sys}} + b$  to the data of the simulations with initially 75% binaries in the range from  $m_{\text{sys}} = 0.16M_{\odot}$  up to  $10M_{\odot}$ . For higher masses, the results suffer from low number statistics and have therefore been excluded from the fit.  $f(m_{\text{sys}})$  also fits the data of the simulations with the other  $b_f$  demonstrating that the evolution of the binary population is independent of the initial binary frequency.

The strong mass dependence of the binary destruction is further illustrated in Fig. 3.5a. It shows the evolution of the normalised number of binaries with primary masses either exceeding  $2M_{\odot}$  (thin lines) and lower than  $2M_{\odot}$  (thick lines) in clusters with various initial binary frequencies. The boundary of  $2M_{\odot}$  between high and low-mass primaries was chosen in accordance with the study of Köhler *et al.* (2006), who performed a high spatial resolution infrared study of the binary population in the ONC and found the binary frequency of high-mass stars to be significantly higher than for low mass stars. Clearly, a larger fraction of low-mass binaries is destroyed during the dynamical evolution of the cluster.

However, a consistent comparison of the simulations and the observations by Köhler *et al.* (2006) must focus on the frequency and not the number of binaries. Figure 3.5b shows the evolution of the frequency of binaries with high and low-mass primaries using the same symbols as in Fig. 3.5a. Clearly the binary frequencies of the high and low-mass primaries evolve quite differently. The former decreases much more slowly with time than the latter and does not depend on the initial binary frequency. In contrast, the evolution of binaries with low-mass primaries *does* depend on the

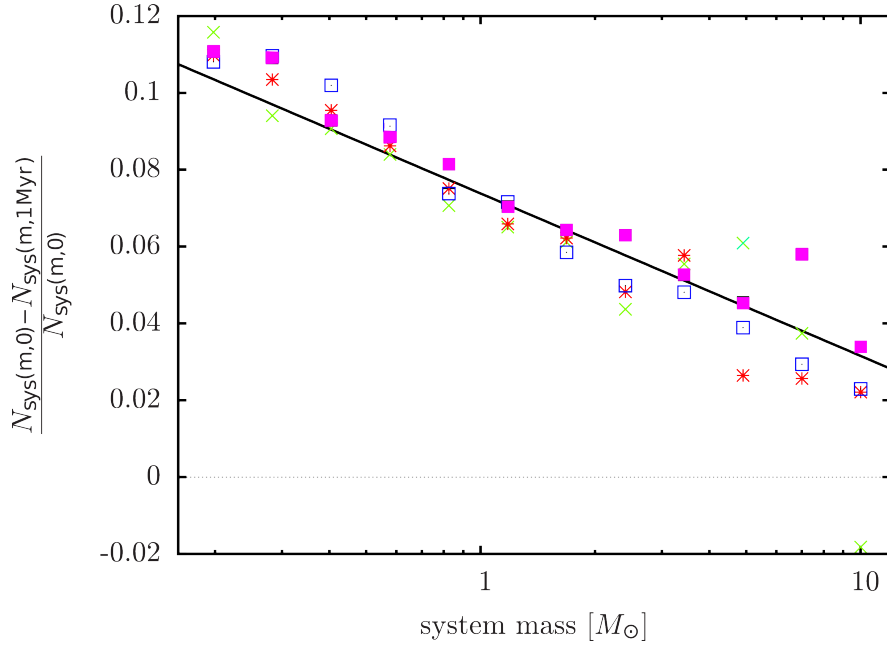


Figure 3.4: Fraction of binaries per binary system mass bin that are destroyed after 1 Myr of cluster evolution. The solid line is the fit of the function  $f(m_{\text{sys}}) = a \log_{10} m_{\text{sys}} + b$  to the data with initially 75% binaries. Green, red, blue and purple lines denote simulations with initially 30%, 50%, 75%, and 100% binaries, respectively.

initial binary frequency.

The differences in the evolution are explained by two mechanisms. First, binaries with low-mass primaries are preferentially destroyed by dynamical interactions in the cluster because of their lower binding energy (Fig. 3.5a). Secondly, the destruction of a binary with a high-mass primary either results in two new single high-mass stars or in a new high and a new low-mass star. The latter possibility means that the number of single low-mass stars increases, hence the frequency of binaries with low-mass primaries decreases relative to the former case. Simultaneously, the frequency of binaries with a high-mass primary does not decrease as fast as implied by Eq. 3.11 because of the smaller increase in the number of single high-mass stars. Hence, the possible generation of a high- and a low-mass star in the destruction of a binary with a high-mass primary accelerates the reduction of the binary frequency of low-mass stars and decelerates the reduction of the binary frequency of high-mass stars.

To emphasise the different evolution of binaries with high and low-mass primaries Fig. 3.5c shows the difference between the binary frequencies of high and low mass stars over time,  $\Delta_{\text{hl}} b_f(t)$ , relative to its initial value  $\Delta_{\text{hl}} b_f(0)$ . This normalization accounts for the possible initial difference of the binary frequencies of high and low-mass stars, so that all values are zero initially.

In all simulations, the difference of the binary frequency of high and low-mass stars increases with time because the binary frequency of low-mass stars decreases faster than the binary frequency of high-mass stars (Fig. 3.5b). However, the amount of increase depends strongly on the initial

binary frequency in the cluster with the lowest initial binary frequency (30%) resulting in the smallest increase of less than 2% after 3Myr while in simulations with the maximum initial binary frequency (100%) the difference increases by more than 10%. Under the assumption that initially the frequency of binaries with low- and high-mass stars was the same in the ONC, this in combination with the observed, significant difference of the binary frequencies of high and low mass (Köhler *et al.*, 2006) implies that the binary frequency in the ONC initially was very high with values well above 75%. If the initial binary frequencies were lower initially the observed difference must have been part of the initial conditions of the binary population.

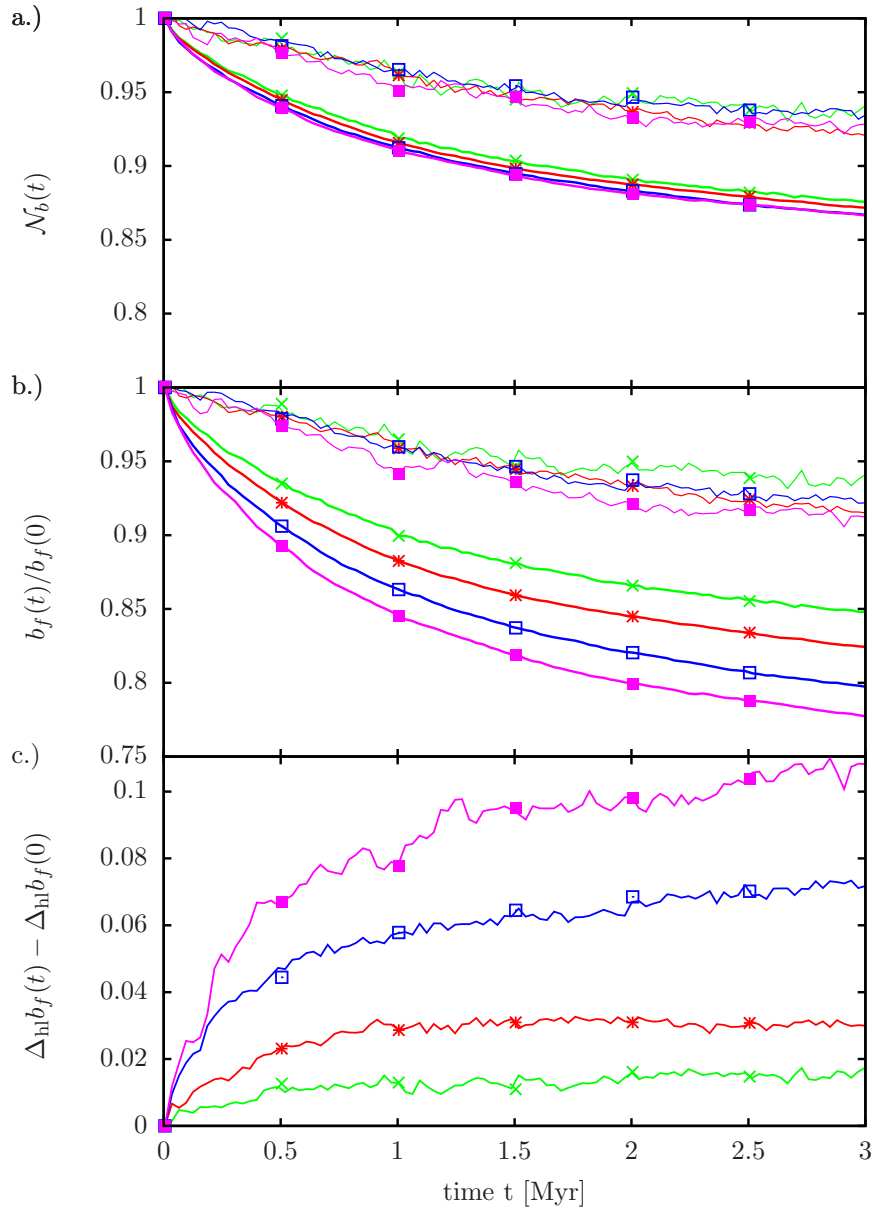


Figure 3.5: Panel a: Evolution of the normalised number of binary systems with primary masses exceeding  $2M_\odot$  (thin lines) and binaries with masses below  $2M_\odot$  (thick lines) with time. Panel b: Evolution of the normalised binary frequencies of binaries with high- (thin lines) and low-mass (thick lines) primaries with time. Panel c: Evolution of the difference of the binary frequency of high- and low-mass stars with time. The difference at each time-step has been reduced by the initial difference of the binary frequencies to improve the readability. Green, red, blue and purple lines denote simulations with initially 30%, 50%, 75%, and 100% binaries, respectively.

### 3.3 Orbital decay

Up to now, only the effect of the dynamical evolution of the clusters on the binary populations has been taken into account within the simulations. However, in real star clusters also other processes are acting which are capable to significantly change a binary population. One of these processes is the gas induced orbital decay introduced by Stahler (2010). Due to this process, the orbits of binaries shrink which can finally lead to the merging of the two stars.

In the following section, it will be investigated, if the gas induced orbital decay and the dynamical evolution of the star clusters in combination are able to reshape a log-uniform period distribution, as it is observed in young star clusters, to a log-normal period distribution, as it is observed in the field. This study has been performed in collaboration with C. Korntreff, who performed the orbital decay simulations. The work described in Sec. 3.3 was performed by C. Korntreff. For more details on the orbital decay process, see the related papers by Stahler (2010) and Korntreff *et al.* (2012).

#### 3.3.1 Method

In its early embedded phases, clusters consist of the already formed stars and a large gas component from which additional stars can potentially form. These stars remain embedded in their natal gas cloud until it is removed by strong winds, the radiation of the massive stars, or supernova explosions. During this embedded phase, dynamical friction occurs between the stars and binary systems with the ambient gas. For binaries this dynamical friction results in a shrinkage of the binary orbit, and possibly the merging of the two stars. Stahler (2010) derived an analytic expression for the temporal development of the separation  $a$  for a single isolated binary system on a circular orbit, which is given by

$$a = a_0 \left( 1 - \frac{t}{t_c} \right), \quad (3.14)$$

where  $a_0$  is the initial binary separation and  $t_c$  is the so-called coalescence time, which is given by

$$t_c = \frac{15}{32\pi} \frac{(1+q)^2}{q} \frac{c_s^5}{\rho_0} \frac{a_0}{G^3 M_{\text{sys}}^2}, \quad (3.15)$$

where  $G$  is the gravitational constant,  $c_s$  the sound speed,  $q$  the mass ratio, and  $M_{\text{sys}}$  the system mass of the binary system.

This only holds for radial distances

$$a < r^{\text{max}} = \frac{GM_{\text{sys}}^{\text{min}}}{2c_s^2} = 111 \text{ AU} \left( \frac{M_{\text{sys}}^{\text{min}}}{M_{\odot}} \right) \left( \frac{c_s}{2 \text{ km s}^{-1}} \right)^{-2}, \quad (3.16)$$

between the two stars constituting the binary system because in his derivation Stahler (2010) assumed that interactions with the gas close to the stars themselves can be neglected.

To analyse the effect of the gas-induced orbital decay of binary systems on the period distribution,

C. Korntreff applied Eq. 3.14 to the entire population of a young ONC-like star cluster. Starting from a cluster with the initial conditions given in Sec. 3.2.2, the temporal development of the binary population is followed for different gas density models.

Only when a binary system fulfills the restriction given by Eq. 3.16 is the orbital decay calculated, otherwise the orbit remains unaltered. This means, for example, that for a system mass of  $0.08M_{\odot}$ ,  $1M_{\odot}$ , and  $50M_{\odot}$  the orbital decay is only calculated for binary systems that have separations  $r < 8.88 \text{ AU}$ ,  $r < 111 \text{ AU}$ , and  $r < 5550 \text{ AU}$ , respectively. As in Stahler's modelling all orbits are assumed to be circular.

For gas-induced decay, the gas density distribution in the cluster is of vital importance. Here an isothermal gas density is used that follows the stellar density distribution. To prevent the distribution from diverging at the centre, the density is kept constant at a value  $\rho_{\max}$  inside the cluster core radius  $R_{\text{core}} = 0.2 \text{ pc}$ . Outside this area, the density decreases isothermally. Thus, the isothermal gas density distribution can be described by the equation

$$\rho_{\text{gas}}(r) = \rho_{\max} \begin{cases} 1, & r < R_{\text{core}} \\ (R_{\text{core}}/r)^2, & R_{\text{core}} < r < R_{\text{cluster}}. \end{cases} \quad (3.17)$$

For an isothermal density distribution  $\rho_{\text{gas}}(r) = c_s^2/2\pi G r^2$  (see Binney & Tremaine, 2008, Eq. 4.103), the sound speed is given by

$$c_s = \sqrt{2\pi G \rho_{\text{gas}}(r) r^2}. \quad (3.18)$$

Although the density distribution (Eq. 3.17) is not isothermal over the whole parameter range, the sound speed can be approximated as

$$c_s = \sqrt{2\pi G \rho_{\max} R_{\text{core}}^2}. \quad (3.19)$$

The resulting sound speeds for distributions with  $\rho_{\max} \in [10^4, 10^6] \text{ cm}^{-3}$  lie between the sound speed of an ideal gas at 10K,  $c_s = 0.2 \text{ km s}^{-1}$ , and the observed value in infrared dark clouds (Sridharan *et al.*, 2005)  $c_s = [1.0 - 2.2] \text{ km s}^{-1}$ . In the simulations performed for this study, a cluster density of  $10^5 \text{ cm}^{-3}$  has been applied which corresponds to a sound speed of  $0.49 \text{ km s}^{-1}$ .

If the separation becomes smaller than the radius of both stars  $a < R_{s1} + R_{s2}$  assuming a main-sequence mass-radius relationship (Binney & Merrifield, 1998, p. 110)

$$\left(\frac{R_i}{R_{\odot}}\right) \approx \left(\frac{M_i}{M_{\odot}}\right)^{0.7}, \quad i = s1, s2$$

a binary system is treated as a 'merged' system. This is clearly a strong simplification, because the merging of stars is a far more complex process that depends on a variety of parameters such as the presence of a surrounding disc, the eccentricity of the orbit, mass transfer, and the conditions of the molecular cloud in which the stars are embedded. However, including all these processes was beyond

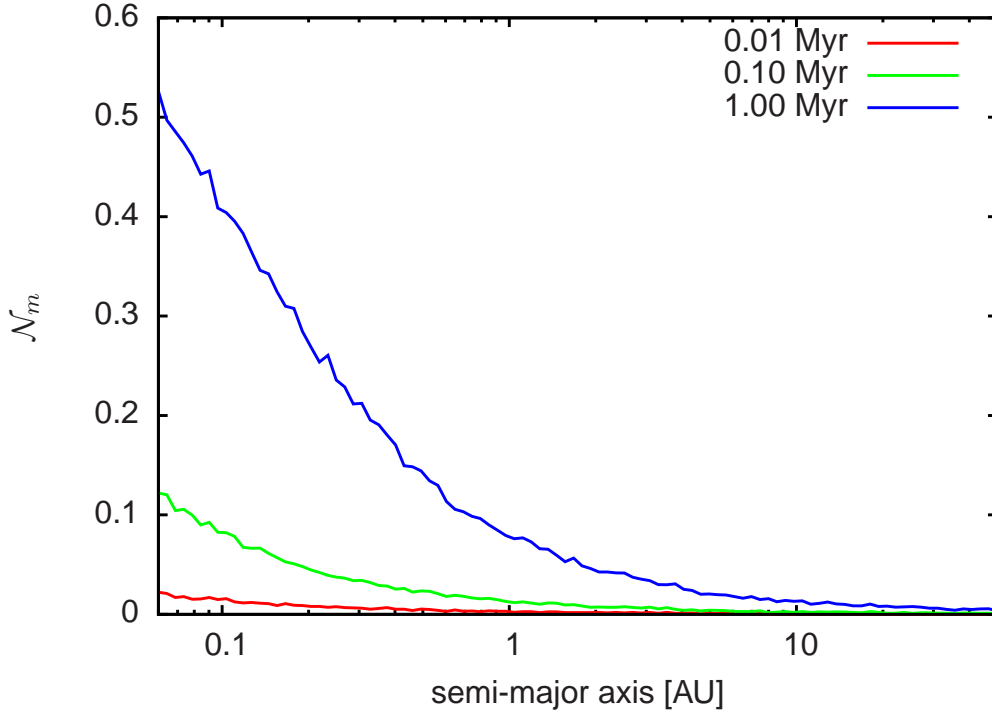


Figure 3.6: The number of merged binaries relative to the initial number of binaries due to gas-induced orbital decay after 0.01 Myr (red line), 0.1 Myr (green line) and 1 Myr (blue line).

the aims of the current study. Here, all processes acting at such small distances were excluded under the assumption that the two stars in such cases might possibly merge.

### 3.3.2 Results orbital decay

Applying the gas-induced orbital decay on the cluster model results in  $\approx 12\%$  of all binaries merging within 1 Myr. It turns out that preferentially tight binaries merge as can be seen in Fig. 3.6. It shows the number of merged binaries  $N_m$  relative to the initial number of binaries  $N_{\text{tot}}$ ,  $\mathcal{N}_m = N_m/N_{\text{tot}}$  as a function of the initial semi-major axis of the merged binary systems. The binaries with small semi-major axes merge to a greater degree than wider binaries. While binaries with initial semi-major axis of 10 AU rarely merge, 40% of all binaries with initial semi-major axis of 0.1 AU coalesce after 1 Myr (solid line).

The overall effect of the gas-induced orbital decay of the binaries in the cluster is to reshape the period distribution by pushing binaries to tighter orbits, which can even lead to the merging of a binary. This can be seen in Fig. 3.7, which shows the relative numbers of binary systems  $\mathcal{N}_b = N_b(t)/N_b(0)$  as a function of the semi-major axis after 0 Myr (thin solid line), 0.01 Myr (red line), 0.1 Myr (green line), and 1 Myr (blue line) for a binary distribution embedded in a  $r^{-2}$  gas density distribution with  $\rho_{\text{max}} = 10^5 \text{ cm}^{-3}$  and a sound speed of  $0.49 \text{ km s}^{-1}$ . Since the orbital decay is more rapid for tighter binaries (see. Eq. 3.15), binaries in the left part of the period semi-major axis distribution are first altered leading to a depopulation of binaries with semi-major axes between 0.02 AU and 1 AU and the

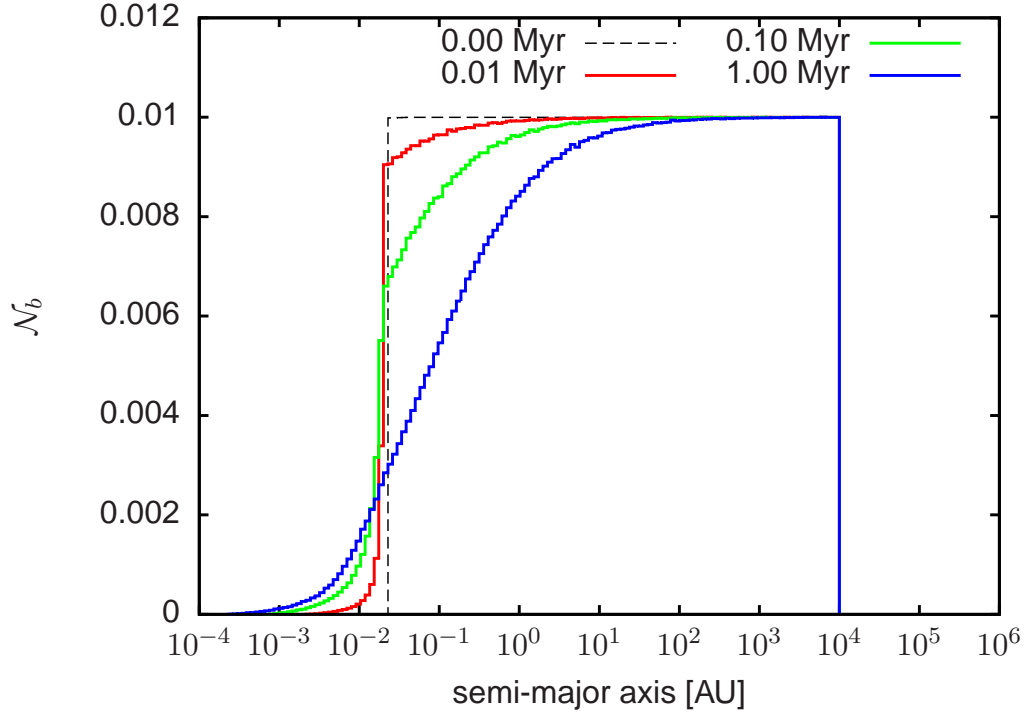


Figure 3.7: Chosen initial semi-major axis distribution (thin solid line) and effect of the gas-induced orbital decay on a semi-major axis distributions embedded in an  $r^{-2}$  gas density distribution with  $\rho_{max} = 10^5 \text{ cm}^{-3}$  and a sound speed of  $0.49 \text{ km s}^{-1}$  after 0.01 Myr (red), 0.1 Myr (green), and 1 Myr (blue).

formation of a tail for semi-major axes shorter than 0.02AU after 0.01Myr. As time proceeds, binaries with even larger orbits are affected until the orbital decay process stops when the gas is expelled from the cluster which here is assumed to happen after 1Myr. At this point, the process of orbital decay alone is responsible for the binary frequency in the cluster declining from its initial value of 100% to 88% by means of the merging of very tight binaries.

### 3.4 Combination and comparison with observations

In reality both processes the dynamical evolution of the clusters and the gas-induced orbital decay of binary naturally take place in such clusters. Therefore, in the following I will describe the combined effect of these processes on the binary population in ONC-like star clusters and how the resulting distributions compare to the observations of the field binary population by Raghavan *et al.* (2010). In order to do so, the resulting semi-major axis distributions have to be converted into period distributions and re-binned in the same way as in Raghavan *et al.* (2010). As their observations were limited to F6 to K3 dwarf stars which roughly corresponds to binary systems with primary masses  $M_{s1} \in [0.5 M_{\odot}, 1.5 M_{\odot}]$ , in the following only binaries with primaries in this mass range will be considered.

Figure 3.8 shows the resulting initial period distributions as thin black lines and the final period



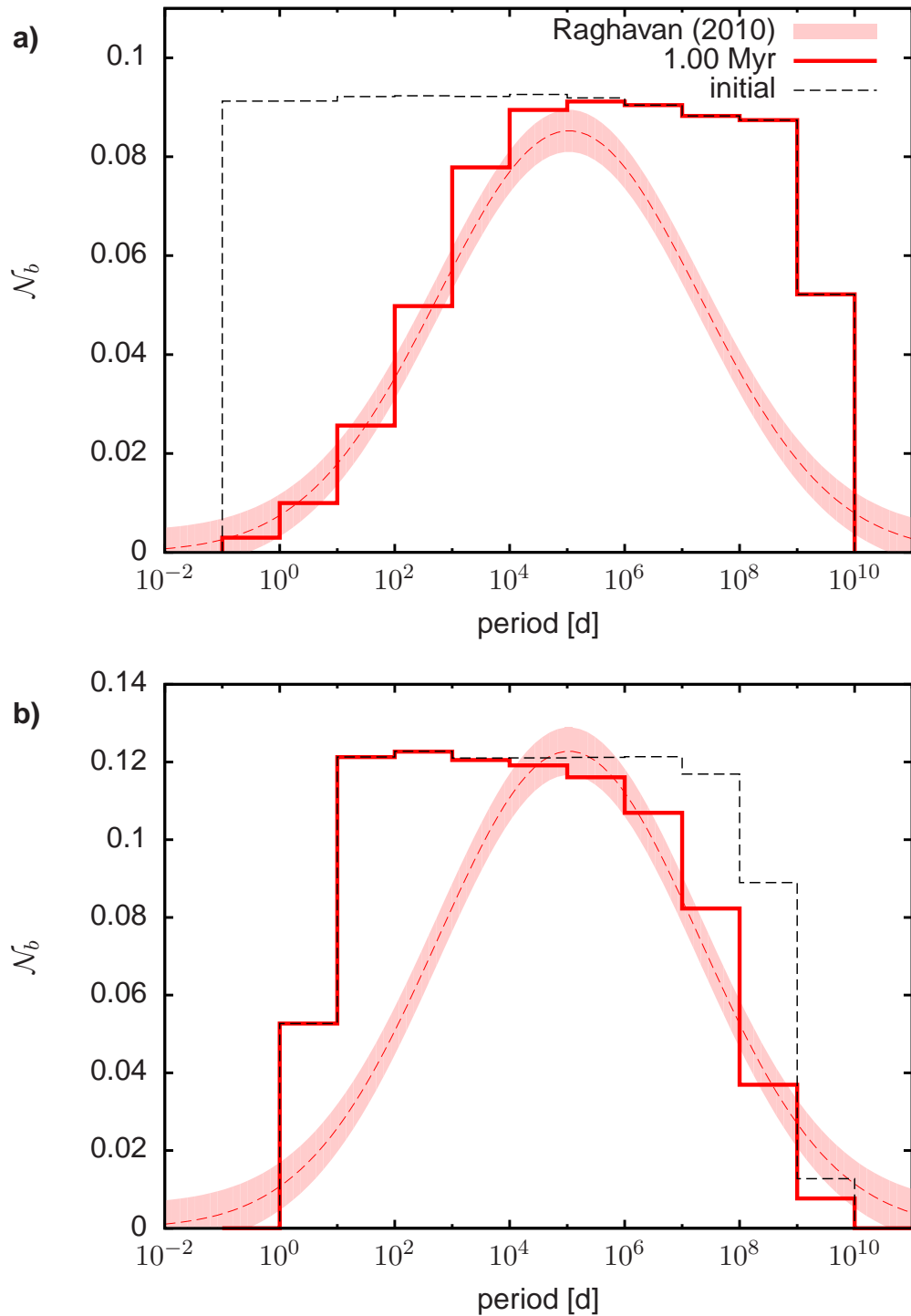


Figure 3.8: a) Chosen birth period distribution (black dashed line) and effect of the gas induced orbital decay after 1 Myr (red line line) compared with the Gaussian fit (red area) to the observations by Raghavan *et al.* (2010). b) Same as in a), with period distribution resulting from the dynamical destruction.

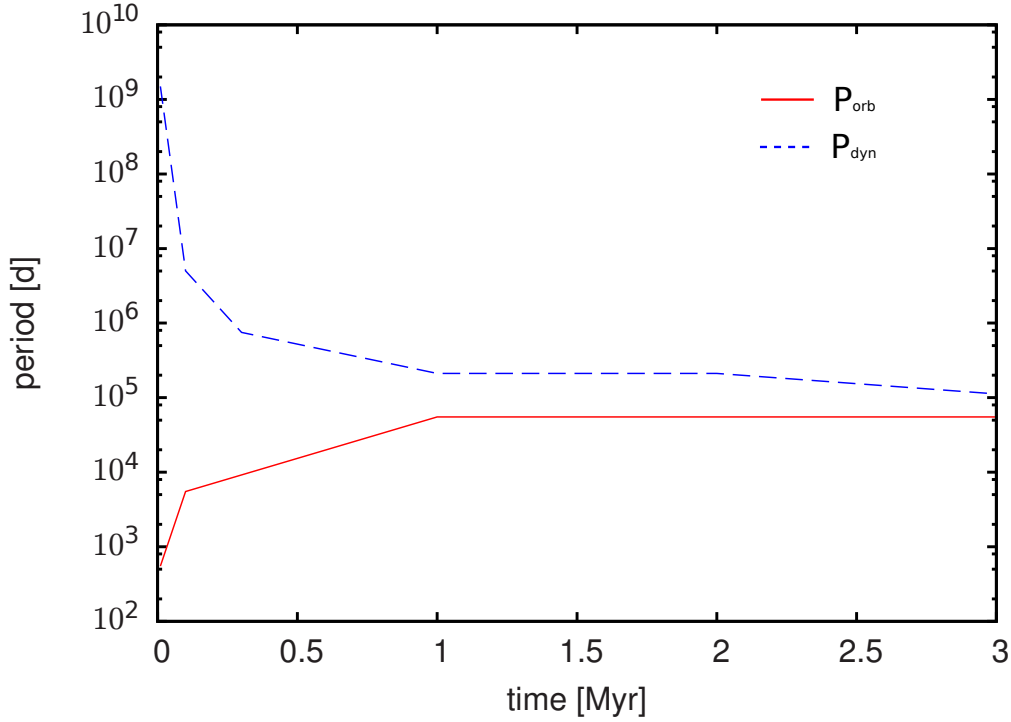


Figure 3.9: Evolution of  $P_{\text{dyn}}$  (upper line) and  $P_{\text{orb}}$  in the first 3 Myr of cluster evolution.

distributions as thick red lines for the process of orbital decay (a) and the process of dynamical destruction (b). In accordance to the results for the semi-major axis distribution the orbital decay (Sec. 3.3.2) reduces the number of short period binaries and the dynamical destruction (Sec. 3.2.3) the number of long period binaries.

The question arises whether there is any region in the period distribution which is significantly affected by both processes? To answer this question the maximum effective period for the orbital decay  $P_{\text{orb}}$  and the minimum effective period for the dynamical destruction  $P_{\text{dyn}}$  at which min. 3% of the binaries are affected by the corresponding processes and are shown in 3.9. As the simulations progresses more binaries are affected by both processes, and both values converge towards their final values of  $P_{\text{orb}} = 5.5 \times 10^4$  days and  $P_{\text{dyn}} = 1.1 \times 10^5$  days. However, during the complete simulations  $P_{\text{orb}}$  is always smaller than  $P_{\text{dyn}}$  which means that although both processes act simultaneously in a cluster no binary in the cluster will be affected by both processes. This implies that the gas-induced orbital decay and the dynamical destruction can be treated separately (see Fig. 3.9) and their outcomes can be combined without any major concerns.

To determine the likelihood that our simulated period distributions correspond to the observed field population,  $\chi^2$ -tests of the simulated and observed period distributions have been performed as described by Press *et al.* (2007)

$$\chi^2 = \sum_{i=1}^N \frac{(R_i - S_i)^2}{R_i + S_i}, \quad (3.20)$$

where  $N$  is the number of bins, and  $R_i$  and  $S_i$  are the two distributions to be tested. This is only

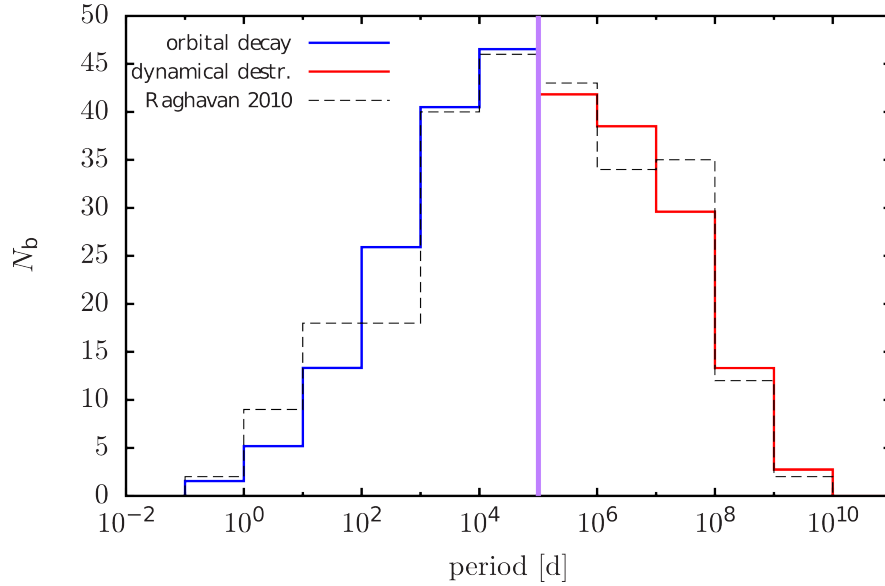


Figure 3.10: Comparison of the period distributions resulting from the gas-induced orbital of embedded binaries (blue line) and the dynamical destruction (red line) with the observations of (dashed line). The simulated period distributions have been combined at  $P = 10^5$  d indicated by the purple, vertical line.

applicable if  $\sum_i R_i = \sum_i S_i$ . To warrant this, the calculated period distributions have been rescaled to the total number of binaries observed by Raghavan *et al.* (2010). Afterwards, the  $\chi^2$ -probability function  $Q(\chi^2|v)$  is used to calculate the probability that both distributions were sampled from the same underlying distribution.

Table 3.1 shows the results of  $\chi^2$ -tests for the Raghavan *et al.* (2010) period distribution and the simulated one. The probability that the initial period distribution from the simulations and the observed period distribution of the field were sampled from the same underlying distribution is obviously negligible (probabilities of  $2.3 \times 10^{-11}$  and  $9.0 \times 10^{-3}$ ). Similarly, only considering the final period distributions after one of the two processes alone acted on the binary population results in (higher, but still) low probabilities. Restricting the  $\chi^2$ -test to the proper period ranges ( $10^{-1} - 10^5$  d for the orbital decay and  $10^5 - 10^{10}$  d for the cluster dynamics) yields much more robust results - both the orbital decay and the cluster dynamics result in  $Q(\chi^2|v)$  values of 67% and 92%, respectively, indicating the extremely good agreement of our simulated period distributions and the observations by Raghavan *et al.* (2010). A superposition of the distribution of periods  $P < 10^5$  d depleted by orbital decay and the distribution of periods  $P > 10^5$  d resulting from the dynamical destruction is shown as a thick solid line in Fig. 3.10. Performing the  $\chi^2$ -test on this complete distribution over the entire period range results in a  $Q(\chi^2|v)$ -value of 94.1%. This clearly demonstrates that together these two processes naturally reshape a log-uniform distribution to a log-normal distribution as observed in the field today, without the need of any other processes that might additionally alter the binary population in star clusters.

The emerging picture can be summarised in the following way (illustrated in Fig. 3.11): binaries

	orbital decay		N-body dynamics	
	complete period range			
	$\chi^2$	$Q(\chi^2 v)$	$\chi^2$	$Q(\chi^2 v)$
initial	71.5	$2.3 \times 10^{-11}$	23.6	0.009
final	36.4	$7.2 \times 10^{-5}$	22.4	0.013
	adopted period ranges			
	$\chi^2$	$Q(\chi^2 v)$	$\chi^2$	$Q(\chi^2 v)$
initial	45.7	$1.1 \times 10^{-8}$	6.6	0.171
final	3.2	0.67	0.9	0.92

Table 3.1:  $\chi^2$ -test results calculated for the initial and final theoretical period distributions and those observed by Raghavan *et al.* (2010). The first four column block shows the results of tests of the complete Raghavan *et al.* (2010) period distribution ranging from  $\times 10^{-1}$  to  $\times 10^{10}$  d. The second four column block shows tests of the left part of the Raghavan *et al.* (2010) period distribution ( $\times 10^{-1} - \times 10^5$  d) for the orbital decay distributions and the right part of the Raghavan *et al.* (2010) period distribution ( $\times 10^{-5} - \times 10^{10}$  d)

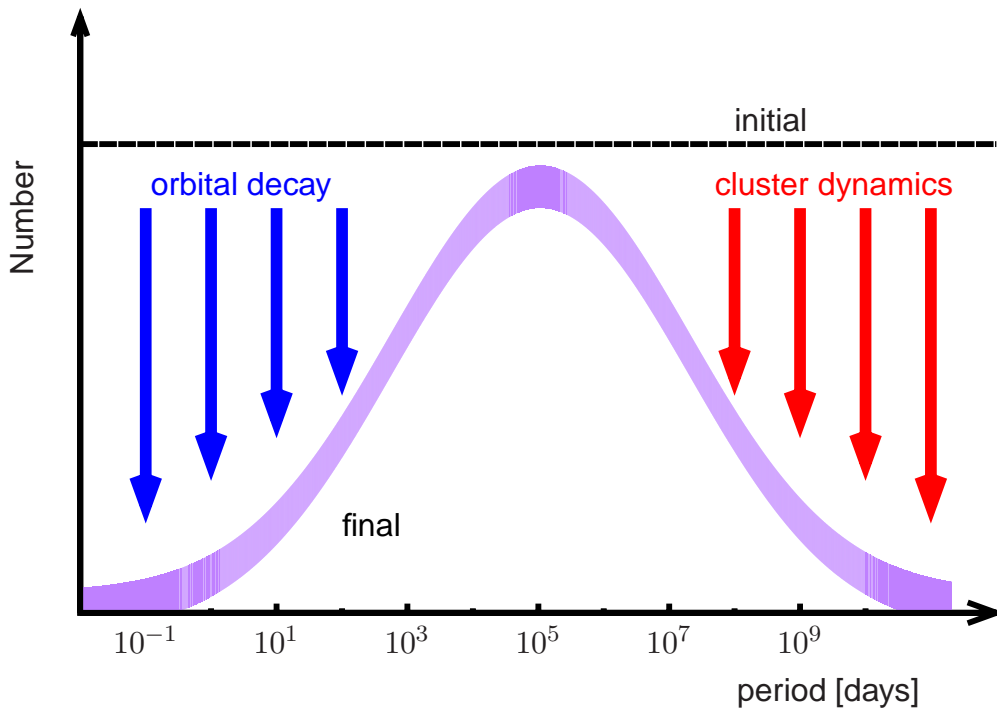


Figure 3.11: Schematic illustration of the two-stage process forming the log-normal field-binary period distribution observed today (grey line) from an initial log-uniform distribution (solid line).

born in dense, embedded clusters with initially log-uniformly period distributions are processed in two ways. As long as the cluster is embedded in its natal gas (about 1 Myr), the orbital decay of the embedded binaries depopulates the left-hand side of the period distribution. The dynamical evolution of the cluster destroys wide binaries, depopulating the right-hand side of the period distribution. The combined effect of these equally important processes is that the final period distribution of the binary population in the star cluster has become log-normal, although it was initially log-uniform.

### 3.5 Summary

In this chapter it was investigated how the binary population in ONC-like star clusters evolves due to dynamical interactions taking place in this type of clusters. The main results can be summarised the following way:

- The normalised number of binaries evolves independently of the initial binary frequency. This is in stark contrast to the evolution of the binary frequency which is commonly used in studies of binary populations. Using instead the number of binaries makes the temporal evolution of the binary population predictable. It is given by

$$N_b(t) = \alpha(t) N_b(0) = (-0.35t^{0.89} + 0.27t + 1) N_b(0). \quad (3.21)$$

In a comparable way, the initial binary frequency in a cluster can be calculated if its current binary frequency is known by

$$b_f(0) = \frac{b_f(t) - \alpha(t) + 1}{\alpha(t)}. \quad (3.22)$$

- Observations show a much higher binary frequency for massive stars than for low-mass stars in the ONC (Köhler *et al.*, 2006). The here presented results show the mass dependence of the binary frequency is most likely the outcome of the dynamical evolution of the clusters with time rather than due to the star formation process. The reason is that binaries with a low-mass primary ( $M_{\text{prim}} < 2M_{\odot}$ ) are much more likely to be destroyed during the cluster evolution ( $\approx 14\%$  within 3Myr) than binaries with a massive primary ( $M_{\text{prim}} > 2M_{\odot}$ ,  $\approx 7\%$  within 3Myr). In addition, the destruction of binaries with a massive primary can free low-mass stars, which again lowers the binary frequency of low-mass stars.
- In collaboration with C. Korntreff (Hövel) it was found that the combination of the dynamical evolution and the gas-induced orbital decay in the embedded phase of clusters results in a binary population that resembles that of the field. Comparison of the simulated period distribution with observations of the field binary population yields a probability of 94.1% that both distributions originate from the same underlying distribution. This means that these two processes are capable to produce a field-like binary population over reasonable time-scales ( $\sim 3\text{Myr}$ ), making the need for other physical processes acting on the binary population unnecessary.



## 4 Density-dependence of binary dynamics

### 4.1 Introduction

In Chapter 3 it was shown, that the evolution of a binary population in ONC-like star clusters is independent from the initial binary frequency of the clusters. This allows to either predict the further evolution of a binary population or to reverse the calculation to obtain the original binary population in such ONC-like star clusters. In the following, I will investigate the evolution of binary populations in star clusters of different initial densities and test if the results obtained for binary populations in ONC-like star clusters can be generalised to clusters with different densities.

### 4.2 Setup

The evolution of density scaled-versions of the ONC-like star clusters from Chap. 3 has been simulated using NBODY6. The number of stellar systems (number of single stars + number of binaries) within the clusters has been chosen to be in the range from 1000 up to 32000 while the stellar density distribution and the size of the clusters have been chosen to be the same as in the standard ONC-model. As the size of the clusters is kept constant, a higher number of systems is equivalent to a denser cluster. So the densities of the here investigated clusters vary between 0.25 and 8 times the density of the original ONC-model clusters studied in Chapter 3. Including a primordial binary population additionally increases the stellar number densities since one binary system consists of two stars. Two initial binary frequencies have been chosen here, 30% and 75%, the densities of the here simulated clusters vary in the range 0.3 to 12 times the standard initial ONC density (see Table 4.1).

In Chap. 3 it was shown, that the primordial binary population in ONC-like star clusters most probably was characterised by a log-uniform period distribution and that is reshaped by dynamical evolution of the clusters and the orbital-decay of embedded binaries to become the log-normal distribution that is observed in the field today (Duquennoy & Mayor, 1991; Raghavan *et al.*, 2010). As here the cluster is modelled without gas, meaning that the orbital decay of embedded binaries is not considered explicitly, the binary population model by Kroupa (1995a) is used to set up the binary population in the clusters. It has a rising period-distribution and can therefore be regarded as being a “pre-evolved” binary population. The other characteristics of the Kroupa (1995a) binary population are the so-called pre-main-sequence eigenevolution, which mimics the early evolution of close binaries while they are still embedded and are random pairing of the binary component masses. This process should not be mistaken with the orbital decay of binary systems that is described in Chap. 3. Although acting at the same stage as the orbital decay and on the same type of binaries, pre-main-

sequence eigenevolution is not based on a physical process but simply changes the parameters of tight binaries generated during the setup to match the observations by Duquennoy & Mayor (1991). By contrast the orbital decay of embedded binaries is the consequence of the torque the surrounding gas exhibits on a binary system and has not been adjusted to give results matching the observations. So, while the pre-main-sequence eigenevolution was constructed to result in a field-like period distribution, the gas-induced orbital decay produces it naturally. The Kroupa (1995a) binary population model is used here, because the dynamical evolution influences only the wide binaries and the gas-induced orbital decay and the pre-main-sequence eigenevolution have no influence on this type of binaries.

Since here a “pre-evolved” binary population model is used here, the initial binary frequency in the clusters is assumed to be 75% reflecting that 25% of all binaries were merged by orbital decay as described in Chap. 3. In addition, a second set of simulations with initially 30% has been studied to test, if the initial binary frequency influences the evolution of the binary population in star clusters with other densities than the ONC.

Table 4.1 summarises the properties of the clusters simulated here and gives the number of simulations evaluated for each density, the initial system and stellar densities ( $\rho_{\text{Trap}}$  and  $\rho_{*,\text{Trap}}$ ) within 0.3pc around the cluster centre, which corresponds to the size of the Trapezium region in the ONC and the overall densities ( $\rho_{\text{tot}}$  and  $\rho_{*,\text{tot}}$ ) for each cluster type.

To improve the statistical significance, multiple realisations of each cluster have been performed and their results have been averaged. The number of realisations has been chosen in such a way that approximately the same total number of stellar systems per cluster type is obtained. Only for clusters with 32000 stellar systems and an initial binary frequency of 75% less simulations could be used for the averaging, as these simulation took very long ( $\approx 80$  hours) and could often not be completed because the conservation of energy could not be ensured (only three out of 16 simulations could be finished). Problems of this kind usually arise in simulations, when several stars interact very strongly with each other and can not be regularized (see Sec. 2.4) because they are too strongly disturbed by the cluster environment.

### 4.3 Evolution of the binary population in dense star clusters

In the following the importance of the stellar density within a cluster for the evolution of a binary population will be investigated. First the binary frequency  $b_f = N_b / (N_s + N_b)$  is studied. It is commonly used by observers to describe the current state of a binary population in a star cluster and is applied to compare the binary populations in different star clusters. Fig. 4.1 shows the evolution of the binary frequency of star clusters with initially 75% binaries as solid lines and the binary frequency of star clusters with initially 30% as dashed lines for clusters of different density.

The reason for the deviations of the initial binary frequency from the intended ones is the same as in Chapter 3. During the cluster set up, the locations of the binary systems are chosen randomly



$N_{\text{sys}}$	$N_{\text{sim}}$	initial $b_f$	$N_{\star}$	$\rho_{\text{Trap}} [10^3 \text{pc}^{-3}]$	$\rho_{\text{tot}} [\text{pc}^{-3}]$	$\rho_{\star, \text{Trap}} [10^3 \text{pc}^{-3}]$	$\rho_{\star, \text{tot}} [\text{pc}^{-3}]$
1000	438	30%	1300	1.3	9.8	1.6	11.7
1000	281	75%	1750	1.3	9.8	1.9	16.0
2000	236	30%	2600	2.7	19.6	3.5	24.2
2000	234	75%	3500	2.7	19.6	4.0	32.9
4000	101	30%	5200	5.3	39.2	7.2	49.4
4000	101	75%	7000	5.3	39.2	8.1	67.2
8000	101	30%	10400	10.5	78.3	14.4	100.0
8000	61	75%	14000	10.5	78.3	16.1	134.0
16000	26	30%	20800	21.1	156.6	29.2	201.0
16000	18	75%	28000	21.1	156.6	32.4	268.0
32000	11	30%	41600	42.0	313.2	57.7	399.0
32000	3	75%	56000	42.0	313.2	65.7	536.0

Table 4.1: Parameters of the density-scaled clusters. The first two densities given are the system density in the innermost 0.3pc representing the size of the Trapezium cluster ( $\rho_{\text{Trap}}$ ) and the overall density of the cluster ( $\rho_{\text{tot}}$ ) which do not change for different initial binary frequencies in a cluster. The second two densities give the corresponding stellar densities in the clusters.

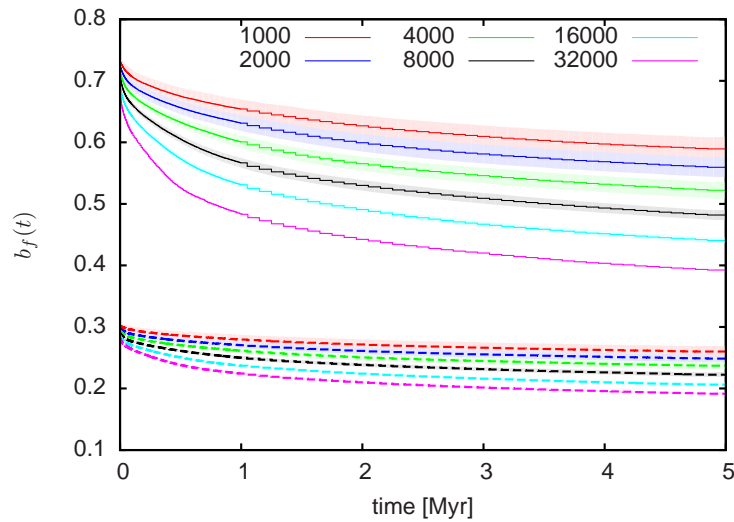


Figure 4.1: Evolution of the binary frequency for clusters with different densities. Solid lines denote clusters with initially 75% binaries while dashed lines denote clusters with initially 30% binaries.

within the cluster independent of the binary separations. This means that if a wide binary is placed in a dense part of the cluster, it is possible that a third star, by chance, is closer to one of the binary components so that these two stars will not be identified as a binary any more (see Sec. 3.2.1 for the definition of binary systems applied here). Since the density in clusters with higher total number of stars is higher than the density in clusters with fewer stars, the probability to destroy wide binaries during the setup is higher in clusters with more stars which is the reason why this clusters also show a higher discrepancy between their measured initial binary frequencies with the intended ones.

During the evolution of the star clusters, the binary frequency decreases in all cases. The change in the binary frequency depends on the initial binary frequency of the clusters and its density. The higher the initial binary frequency of a cluster the larger is the decrease in the binary frequency. For example, the binary frequency of clusters with 1000 stellar systems and initially 30% binaries

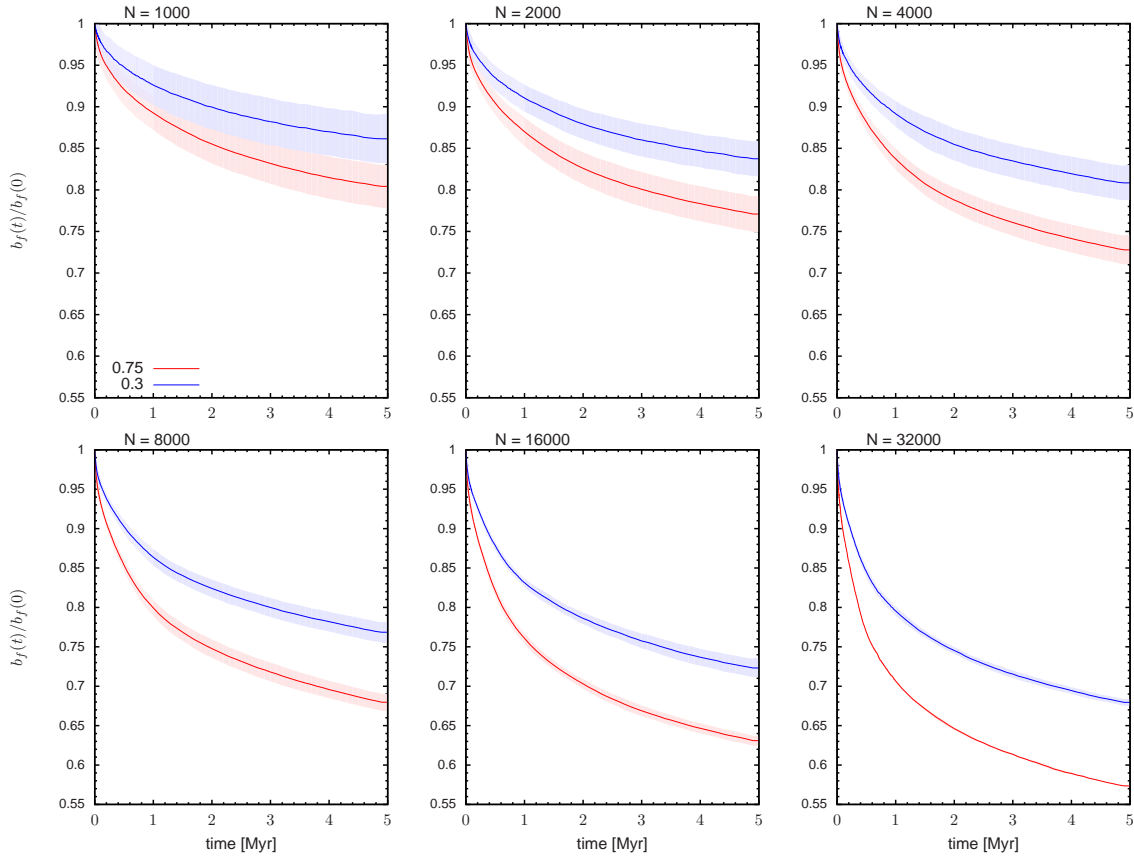


Figure 4.2: Evolution of the normalised binary frequency for clusters with different densities.

decreases by  $\approx 4\%$  while the binary frequency for clusters with the same number of stellar systems but initially 75% binaries lessens by  $\approx 14\%$ . This dependence on the initial binary frequency becomes stronger for higher cluster densities. For instance, the binary frequencies for clusters with 32000 stars drop by  $\approx 9\%$  and  $\approx 29\%$ , respectively.

This discrepancy in the evolution of the binary frequency is also observable in the evolution of the normalised binary frequency  $b_f(t)/b_f(0)$  (Fig.4.2) which allows direct comparison of the evolution of clusters with the same total number of stellar systems but different initial binary frequencies. Also the normalised binary frequency decreases with time and shows a clear dependence on the initial binary frequency in the clusters. The higher the density larger is the fraction of the binary frequency that has been destroyed by the end of the simulations. For instance, the difference of the normalised binary frequency of clusters with initially 1000 stellar systems and initially 30% and 75% binaries is about 6% while for clusters with initially 32000 stellar systems this difference is increased to 10%.

However, in Chap. 3 it was described that the binary frequency in general is not the best measure for the evolution of the binary population as it is influenced by the single star population in the clusters. The normalised number of binaries is a much better measure. Therefore, Fig. 4.3 shows the evolution of the normalized number of binary systems  $\mathcal{N}_b = N_b(t)/N_b(t=0)$  for clusters with the same initial number of stellar systems separately. As in ONC-like star clusters the initial binary frequency has

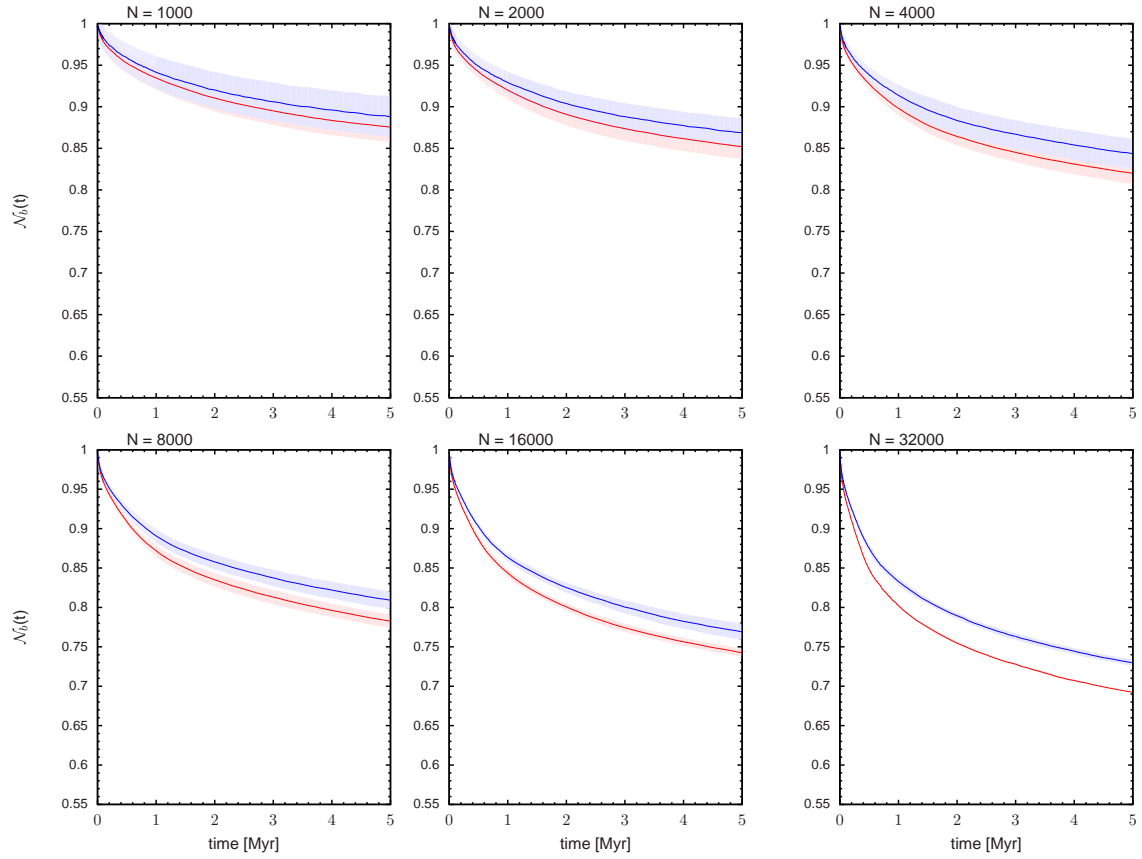


Figure 4.3: Evolution of the normalized number of binaries  $\mathcal{N}_b$  for clusters with different densities.

no significant influence on the evolution of  $\mathcal{N}_b$ . Even for clusters including 32000 stellar systems initially the difference of the relative number of binaries is only  $\approx 4\%$  which is much less than the  $\approx 11\%$  that is found for the evolution of the binary frequency. This supports the claim from Chap. 3 that the evolution of the binary population in a star cluster can be directly predicted for any initial binary frequency.

The values at 5Myr of the normalised binary frequency and of the normalised number of binaries for all clusters can be seen Fig. 4.4a and Fig.4.4b respectively as a function of the initial number of stellar systems in the clusters. Clearly the degree of the decrease of the normalised binary frequency and of the normalized number of binaries strongly depends on the initial number of stellar systems in the cluster. The higher the initial number of stellar systems in the clusters the larger is the decrease of the normalised binary frequency and of the normalised number of binaries. The result of this is that about 16% more binaries get destroyed in the most populated clusters (initially 32000 stellar systems) than in the least populated clusters (initially 1000 stellar systems).

The reason more binaries are destroyed in clusters with high densities is twofold. As here only the pure gravitational interactions between the stellar systems in the clusters are taken into account, binary systems can only be destroyed if they are encountered by a second stellar system (this could be a single star or another binary) that transfers enough energy to the binary to overcome its binding

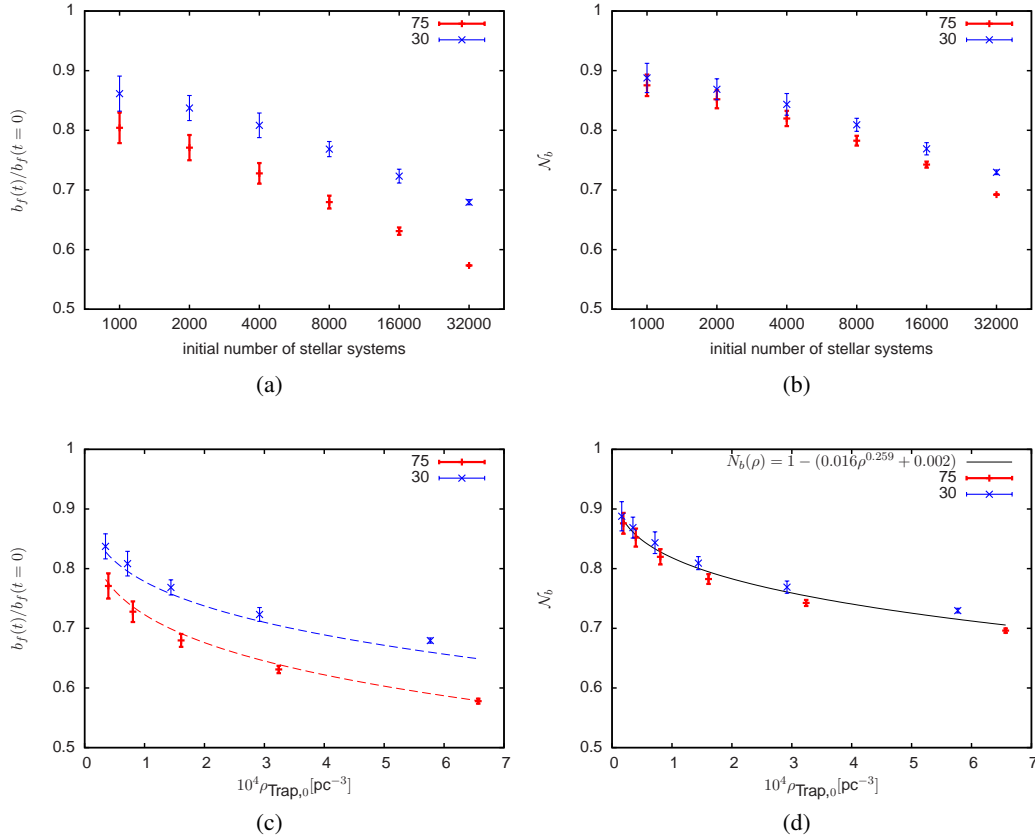


Figure 4.4: Normalized number of binary systems and normalized binary frequency as functions of the initial number of stellar systems (4.4a & 4.4b) and as functions of the initial density within 0.3pc from the cluster centre  $\rho_{\text{Trap}}$  (4.4c & 4.4d) in all simulations after 5Myr.

energy meaning that the encountering stellar system must have a larger kinetic energy than the binding energy of the binary. Here all clusters have been set up to be initially in virial equilibrium so that the mean kinetic energy of stellar systems is higher in clusters with higher number of stellar systems. This is necessary to account for the deeper potential of the clusters. The binding energies of the binaries are not altered between the simulations so that clusters including more stellar systems have a larger fraction of stellar systems, that are capable to destroy binaries. Additionally, the probability for encounters of stellar systems in a star cluster is increasing with the density in the cluster. Both arguments, the increased mean kinetic energy and the increased probability of encounters, explain why more binaries are destroyed in clusters with higher system numbers.

Besides the strong dependence on the initial number of stellar systems in a cluster Fig. 4.4a and Fig. 4.4b show that the evolution of both, the normalised binary frequency and the normalised number of binaries, weakly depend on the initial binary frequency in a cluster. The normalised number of binaries (binary frequency) for the least populated clusters differ by about 1% (8%) while for the most populated clusters they differs by about 4% (11%).

However, this weak dependence on the initial binary frequency for the normalized number of bina-

ries drops if the densities of the clusters are taken into account instead of their membership numbers. Using the initial stellar density in the clusters instead of the initial number of stellar systems (number of single stars + number of binaries) to plot the values after 5Myr of the normalised binary frequency and of the normalised number of binaries yields Fig. 4.4c and Fig. 4.4d. Comparing these with above figures at any given time clearly shows, that the dependence on the initial binary frequency is negligible given the errors. This means there is a unique function of the normalised number of binaries that can be used to calculate the fraction of binaries present after any given time depending on the initial density in the cluster. After 5Myr this function is given by

$$\mathcal{N}_b(\rho) = 1 - (0.016\rho^{0.259} + 0.002), \quad (4.1)$$

which is shown as black line in Fig. 4.4d. The slope of  $\mathcal{N}_b(\rho)$  is highest for small values of  $\rho$  and decreases for increasing densities. This implies that differences in cluster densities become less important for the evolution of their binary populations the higher the density of the clusters are. Hence, predictions for the binary population in starburst clusters like the Arches or Quintuplet cluster can be given. Following the results obtained here, these very dense clusters should have removed almost the same amount of binaries during their evolution as the clusters that initially contained 32000 stellar systems in the here simulated clusters. Therefore, the Arches cluster with an age of about 1Myr should possess 70% and the Quintuplet cluster with its age of about 5Myr should possess about 55% of their initial binary population. For very sparse clusters Eq. 4.1 predicts that the dynamical evolution should have almost no effect on the binary population, which has already been verified with N-body simulations of the sparse Taurus-Auriga star forming region ( $\rho = 1 - 10\text{pc}^{-3}$  Luhman *et al.*, 2009) by Kroupa & Bouvier (2003).

As has been shown in Sec. 3.2.3, the binary frequency in the cluster after 5Myr can be calculated if the initial binary frequency in the cluster is known using

$$b_f(t) = \frac{\mathcal{N}_b(t)}{\frac{1-b_f(0)}{b_f(0)} - \mathcal{N}_b(t) + 2}. \quad (4.2)$$

The resulting curves for initial binary frequencies of 30% and 75% simulated here are shown as dashed lines in Fig. 4.4c. As can be seen each curve matches the simulated normalised binary frequency for its initial binary frequency very well, but significantly deviate from the others. As the evolution of the normalised number of binaries can be given by a single equation (Eq. 4.1), this again shows that while the evolution of the binary population does not depend on the initial binary frequency in a cluster, the binary frequency does. Therefore studies investigating the evolution of binary populations should avoid using the binary frequency but instead use the normalised number of binaries.

Fig. 4.5 shows fits of the form  $f(t) = a t^b + c t + 1$ , which was already used in Chap. 3.2.3 to fit the evolution of the binary population in ONC-like star clusters, to the evolution of the normalised

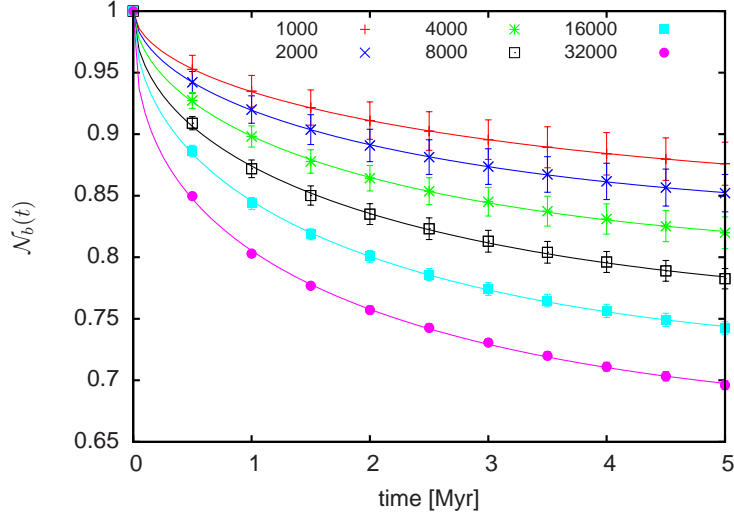


Figure 4.5: Fits of evolution of the normalised number of binaries for all simulated clusters within the first 5 Myr of cluster evolution.

$N_{\text{sys}}$	$a$	$\Delta a$	$b$	$\Delta b$	$c$	$\Delta c$
1000	-0.081	$\pm 0.001$	0.56	$\pm 0.01$	0.015	$\pm 0.001$
2000	-0.104	$\pm 0.002$	0.58	$\pm 0.01$	0.023	$\pm 0.002$
4000	-0.131	$\pm 0.004$	0.57	$\pm 0.02$	0.029	$\pm 0.004$
8000	-0.152	$\pm 0.005$	0.51	$\pm 0.03$	0.026	$\pm 0.006$
16000	-0.186	$\pm 0.004$	0.50	$\pm 0.02$	0.032	$\pm 0.004$
32000	-0.218	$\pm 0.003$	0.41	$\pm 0.02$	0.024	$\pm 0.003$

Table 4.2: Fitting parameters of function  $f(t) = a t^b + c t + 1$  to the evolution of the normalised number of binaries to all star clusters with initially 75% binaries.

number of binaries in all clusters with initially 75% binaries. The parameters resulting from the fitting process are compiled in Tab. 4.2.

#### 4.4 Evolution of the period distribution at different densities

In the previous section it was shown that the evolution of the binary population is independent of the initial binary frequency and does rather depend on the initial stellar density of the cluster. The question is now how the density influences the binary population for a given density range. To answer this the evolution of the period distributions of the binary populations will be investigated in the following. Fig. 4.6 shows the initial binary period distribution in the simulations initially containing 1000 (red lines) and 32000 stellar systems (blue lines) for both initial binary frequencies (30% solid lines, 75% dashed lines). The period distributions of the other clusters with initial densities between these extremes fit within the here shown period distributions and are therefore not shown to simplify the plot.

The initial period distribution does not show any dependence on the initial binary frequency in the cluster. In contrast, the initial period distribution of clusters with different initial numbers of stellar systems show significant differences. Clusters with more stellar systems initially lack binaries with

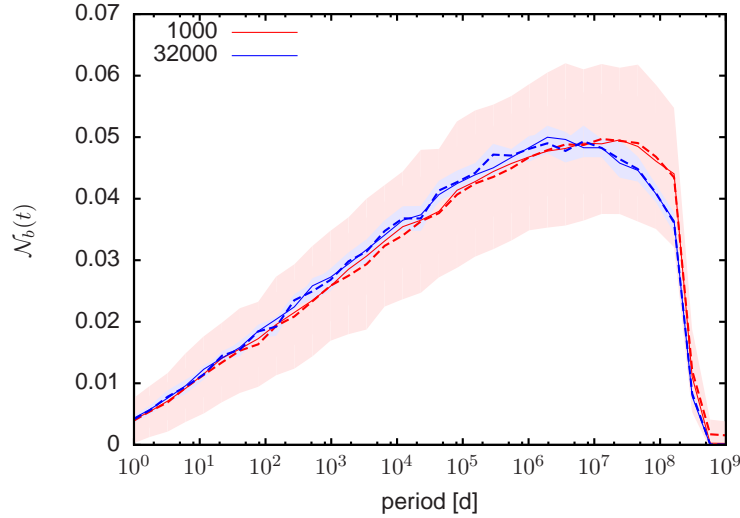


Figure 4.6: Initial normalized period distributions of simulated clusters with initially 1000 and 32000 stellar systems.

periods in the range  $10^7 - 10^8$  d compared to less dense star clusters. The reason for this lack of long-period binaries is that the locations of binaries are chosen randomly within the cluster during the cluster setup. Therefore it is possible for a binary to be sampled into a region, within which the density is so high that the binary is not bound anymore, although it is intended to (see also discussion of Fig. 4.1).

The evolution of the period distribution in the clusters is shown in Fig. 4.7 which displays the period distribution in clusters with initially 1000 (red lines) and 32000 stellar systems (blue lines) after 0.1 Myr (Fig. 4.7a), 1.0 Myr (Fig. 4.7b), 3.0 Myr (Fig. 4.7c), and 5.0 Myr (Fig. 4.7d). Additionally each plot includes the the initial period distributions as dotted lines for comparison. The period distribution of the clusters with different densities after 5 Myr are shown for reference in Fig. A.1 in the Appendix separately.

Clearly, the dynamical evolution of the star clusters has a significant effect on the shape of the period distribution of the binary populations in the clusters. The number of wide binaries decreases continuously with time while the number of short period binaries is not altered at all. The result is that the initially rising period distribution becomes more bell shaped where the actual shape of the distribution depends on the density in the cluster. The higher the density the narrower the distribution becomes.

As can be seen in Fig. 4.7a the dynamical evolution of the star clusters destroys wide binaries directly from the beginning. The destruction of wide binaries proceeds during the complete evolution of the cluster and is more pronounced for clusters with higher densities (see also Fig. 4.3). Binaries can only be destroyed in three- or four-body encounters in which the approaching star(-s) need to provide enough energy to the binary to unbind it. This requires the approaching star to get close to the binary to be capable to interact strongly with the binary (see e.g. Figs. 5-7 in Hut & Bahcall,

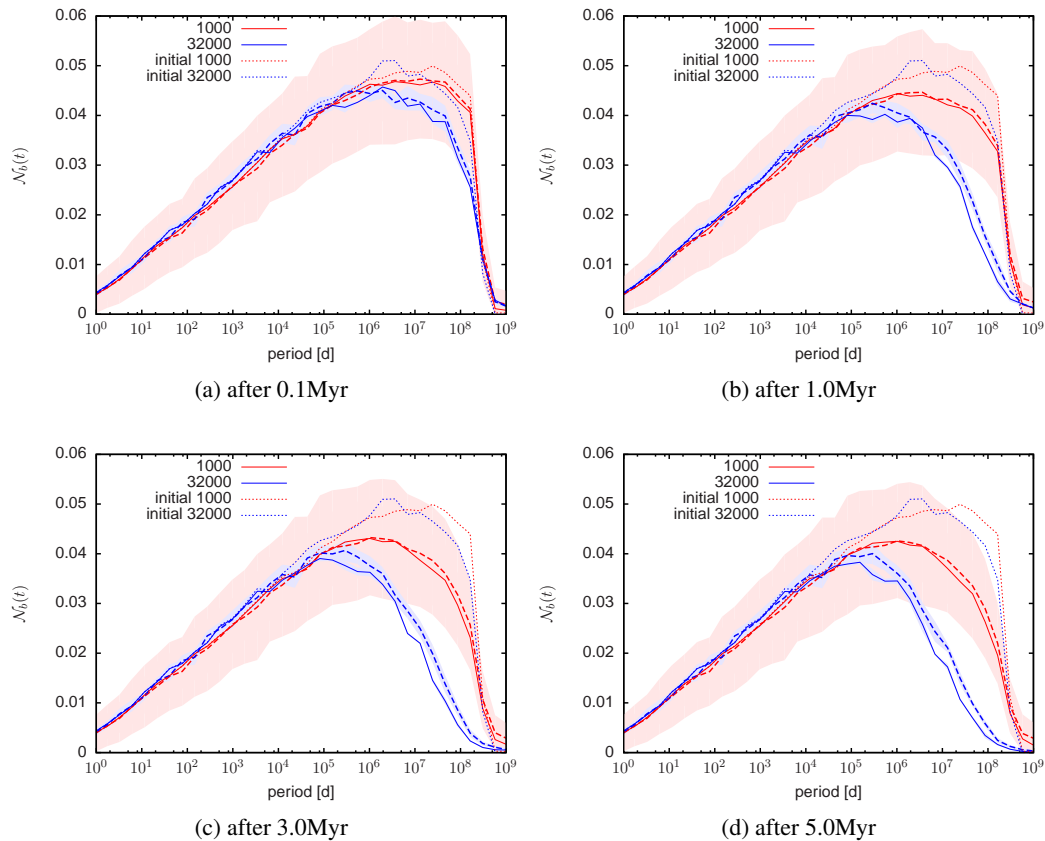


Figure 4.7: Normalized period distributions of star clusters with initially 1000 and 32000 stellar systems and initial binary frequencies 30% (dashed lines) and 75% (solid lines). Dotted lines denote the corresponding initial period distributions.

1983). Since the probability for an encounter with a given periastron separation to occur within a star cluster depends on the density within the cluster (see e.g. Olczak *et al.*, 2010) these encounters take place more often in clusters with higher densities than in clusters with lower densities.

Increasing the density in the clusters does not only destroy more binaries at a given period, but also leads to the destruction of binaries that are unaffected in clusters of lower density. Fig. 4.8 gives the period bins from Fig. 4.7 within which at least 4% of the binaries have been destroyed after 5Myr as a function of the initial cluster density. Clearly the higher the density in a cluster is, the smaller are periods of binaries, that are destroyed during the evolution of the cluster. The reason for this is that not only the mean kinetic energy of the stellar systems (again single stars or binaries) in clusters with higher densities is larger than in clusters with lower kinetic energies but also their maximum kinetic energies. As an encountering stellar system must have a kinetic energy exceeding the binding energy of the binary to destroy it, this explains why binaries with smaller periods are destroyed in clusters with higher densities.

The dependence of the smallest binary period bin affected by the dynamical evolution of the cluster could have serious implications for the results in Sec. 3. There it was assumed that the dynamical



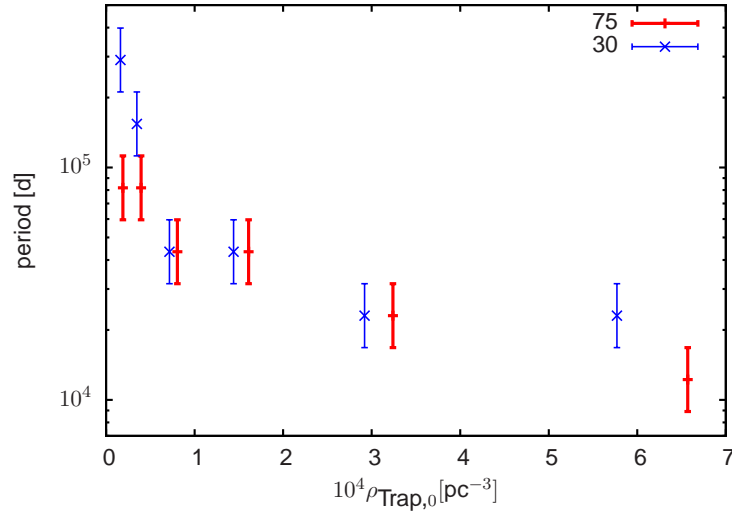


Figure 4.8: Smallest period bin that lost more than 4% of its initial content after 5 Myr. Binaries with periods below this value are not affected by the dynamical evolution of the cluster.

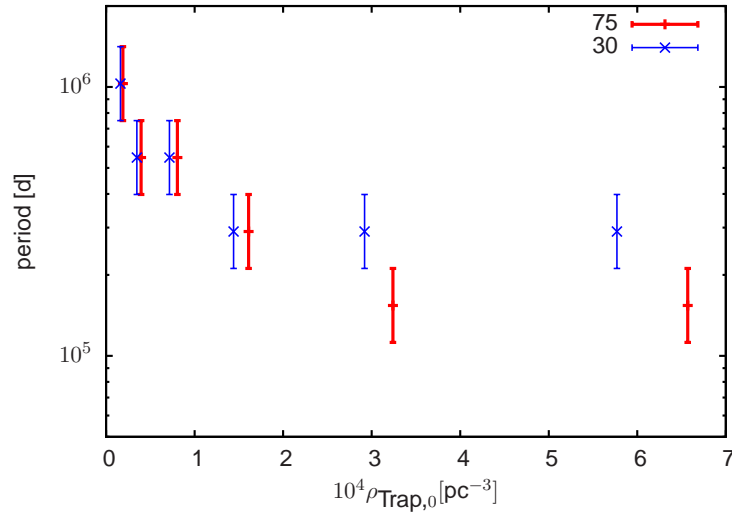


Figure 4.9: Maximum of period distributions after 5 Myr.

evolution of a star cluster and the orbital decay do not influence the same binaries and can therefore be treated separately. Above finding now seems to imply that this assumption does not hold anymore for clusters with high densities. However, the dependence on the cluster density becomes weaker the higher the density in a cluster is just as has been found for the destruction of binaries in Sec. 4.3. Therefore it can be taken to be valid up to central cluster densities of about  $6 \times 10^4 \text{pc}^{-3}$ . For cluster densities above this value, the dynamical evolution of the clusters affects a significant fraction of binaries that are subject to the orbital decay so that in these clusters simulations that treat both processes simultaneously are needed to obtain reasonable results.

The destruction of binaries with ever smaller periods has also an effect on the maximum in the binary period distribution of the clusters in the sense that it is shifted towards smaller periods the

$N_{\text{sys}}$	initial $b_f$	$N_{*,\text{tot}}$	$N_{*,\text{high}}$	$m_{\text{inter}} [M_{\odot}]$	$N_{*,\text{inter}}$	$m_{\text{low}} [M_{\odot}]$	$N_{*,\text{low}}$
1000	0.30	1300	12	5.81	641	0.25	642
1000	0.75	1750	16	6.15	863	0.26	864
2000	0.30	2600	25	5.82	1281	0.25	1281
2000	0.75	3500	34	5.95	1724	0.26	1725
4000	0.30	5200	51	5.85	2548	0.25	2548
4000	0.75	7000	69	5.88	3430	0.26	3430
8000	0.30	10400	102	5.81	5096	0.25	5096
8000	0.75	14000	137	5.96	6814	0.26	6814
16000	0.30	20800	199	5.75	9884	0.25	9884
16000	0.75	28000	263	5.92	13044	0.26	13044
32000	0.30	41600	374	5.87	18532	0.25	18532
32000	0.75	56000	448	6.01	22176	0.26	22176

Table 4.3: Number of high, intermediate and low mass stars in all simulations.

higher the density in a cluster gets. This can be seen better in Fig. 4.9 which shows the location of the maximum of the period distribution of all clusters as a function of the density in the cluster. While the maximum of the period distribution is of the sparsest cluster about  $1 \times 10^6$  d it drops to about  $10^5$  d for clusters with the highest densities. Again, the gradient in the data points in Fig. 4.9 is highest for the clusters in the low density regime while it almost vanishes for higher densities. This implies that the maxima of the period distributions in starburst clusters should be of the same order as in the clusters with the highest densities simulated here.

#### 4.5 Dependence on the primary mass

Observations of binaries not only in the solar neighbourhood (e.g. Duquennoy & Mayor, 1991; Fischer & Marcy, 1992) but also in star clusters (e.g. Köhler *et al.*, 2006) have shown, that stars with higher masses are more often part of binary systems than stars of lower mass. This raises the question if this overabundance of binaries with massive primaries is the result of the evolution of the binary population in its natal environment or if it originates from the star formation process itself.

Fig. 4.10 shows the evolution the normalised number of binaries separately for binaries with a high-mass (red-lines), intermediate-mass (blue-lines) and low-mass primary (green-line) in all simulated clusters. Here high-mass stars are defined as the 1% most massive stars in a cluster, intermediate mass stars the next 49.5% and low mass stars the remaining 49.5% of all stars. Due to the statistical nature of the here simulated clusters, the mass boundaries between these mass regimes vary from simulation to simulation and become larger the higher the density in a cluster is (see Table 4.3, which summarises the number of stars in the corresponding mass regimes and their boundary masses).

Basically, the evolution of the number of binaries in the intermediate and low primary mass regimes proceeds as for the overall binary population. During the evolution of the clusters the number of binaries with an intermediate or low mass primary decreases monotonically whereas the decrease is stronger in clusters with higher densities. The fraction of binaries with a low-mass primary, that is destroyed during the evolution is always higher than the number of binaries with an intermediate-mass primary. This difference becomes larger the larger the density in the clusters is. The reason for this is

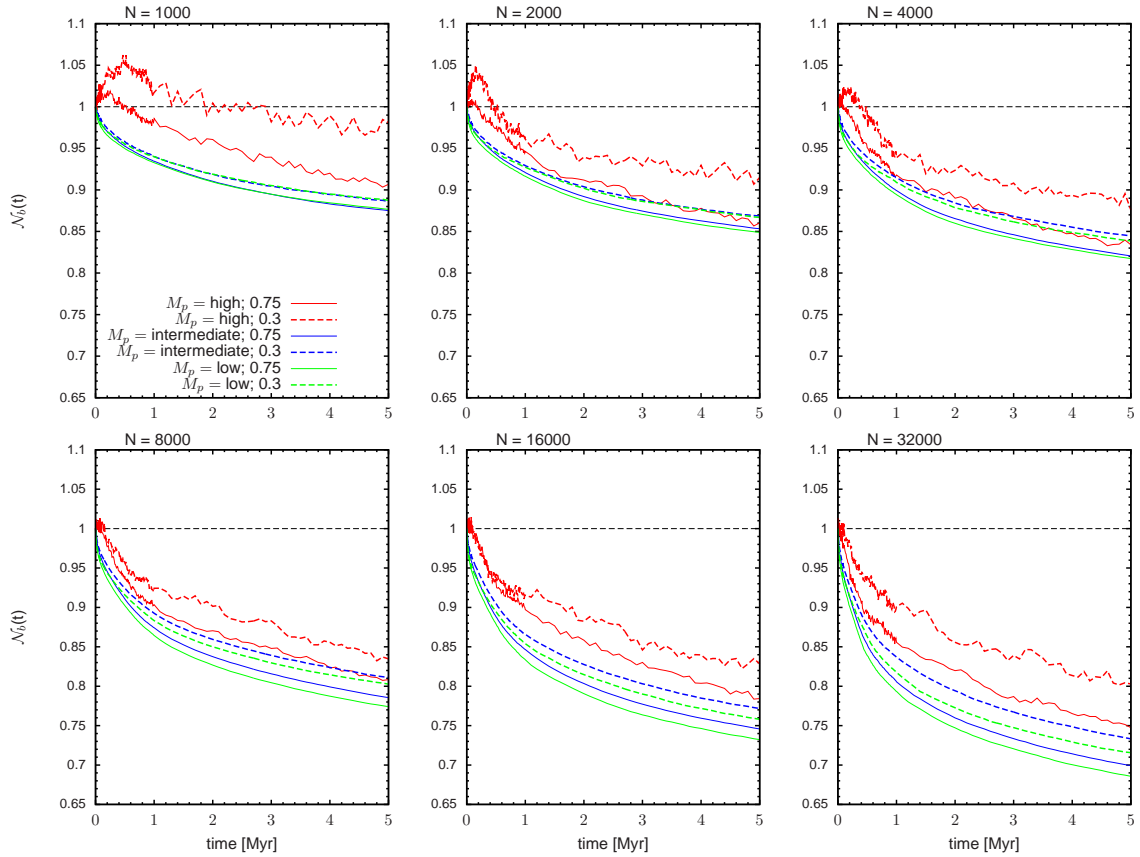


Figure 4.10: Evolution of the normalised number of binaries with high, intermediate and low mass primaries in all simulated star clusters.

that binaries with intermediate mass primaries are in general more massive and are thereby, following Eq. 1.26, more strongly bound than binaries with a low mass primary. As the dynamical evolution of the cluster preferentially destroys weakly bound binaries, this explains the stronger decrease of the number of binaries with a low mass primary.

The number of binaries with a high-mass primary evolves a bit differently from the rest. Instead of directly decreasing after the start of the simulation, the number of binaries with a high-mass primary first increases before they decrease for all simulated cluster densities. The duration of this increase and its amount depends on the density in the cluster. The time the number of binaries with high-mass primaries increases is longer and more pronounced the lower the density of the cluster is. For the sparsest clusters with an initial density of  $1.6 \times 10^3 \text{pc}^{-3}$  (1000 stellar systems with initially 30% binaries) the number of binaries increases for about 0.5Myr by almost 4% while for the densest clusters with densities of  $6.6 \times 10^4 \text{pc}^{-3}$  (32000 stellar systems with initially 75% binaries) it rises for about 0.3Myr by about 1%. For comparison, during the same time the number binaries with an intermediate mass primary drops by about 4% and 14%, respectively.

In contrast to the general result the evolution of binaries with a high-mass binary does not only depend on the density in the cluster but also on the initial binary frequency. In clusters having an

initial binary frequency of 30%, the increase in the number of binaries with a high-mass primary is more pronounced than in clusters with initially 75% binaries. The reason is that in clusters with the higher binary frequencies, the majority of all massive stars are already bound in binary systems and can therefore the number of binaries can not so easily decrease by forming new ones.

The reason that the number of binaries with a massive primary increases is that massive single stars are able to capture other single stars during a three-body encounter thereby forming a new binary star. Analysing the formation of such binaries by studying ONC-like star clusters comparable to the simulations performed here but without a primordial binary population, (Pfalzner & Olczak, 2007) has shown that the probability to capture another single star is only not negligible for the most massive stars in the clusters while stars of lower mass almost never capture another star. This result is confirmed here for clusters with an even wider density range and an additional primordial binary population. However, as has been mentioned before, this process strongly depends on the binary frequency in the clusters and is most effective if no primordial binary stars are present in the simulations.

In contrast to Pfalzner & Olczak (2007), where the binary frequency of the massive stars remains almost constant during the complete evolution of the cluster (see Fig.3 in Pfalzner & Olczak, 2007), the binary frequency of massive stars decreases monotonically after reaching their maximum value in all simulations performed here (Fig. 4.10). The reason the binary frequency decreases here is that while initially the rate the massive stars capture another single star to form a new binary is sufficient to overbalance the number of wide binaries with a massive primary, that is destroyed during the evolution. As the density in the clusters decreases, so does the probability for the massive stars to capture another star. This probably leads to their binary formation rate becoming less than the destruction of binaries by encounters. A second effect stabilising the binary frequency of massive stars in Pfalzner & Olczak (2007) is that all massive stars are placed in the central cluster region to meet the demands due to the observed mass segregation of the ONC Hillenbrand & Hartmann (1998). This implies that the probability to form a binary with two massive components is much higher in the Pfalzner & Olczak (2007) simulations than here, because there the most massive stars are initially always very close while in the simulations that were performed here the most massive stars are distributed over the complete cluster.

The final period distributions of massive, intermediate and low-mass stars are shown in Fig. 4.11 as red, blue, and green lines, respectively. The period distributions of intermediate and low mass stars have a very similar shape in all clusters and reproduce the period distribution of the overall binary population. Due to the destruction of wide binaries, the right hand side of the period distributions is reduced while the left, short-period side is not affected by the evolution of the clusters.

Again the period distributions of the high mass stars represent an exception from this. Especially clusters with initially 30% binaries contain after 5Myr significantly more binaries with high-mass primaries with periods exceeding  $10^8$ d compared to the number of binaries with intermediate and low-mass primaries. These have not been generated during the set up of the simulations and most

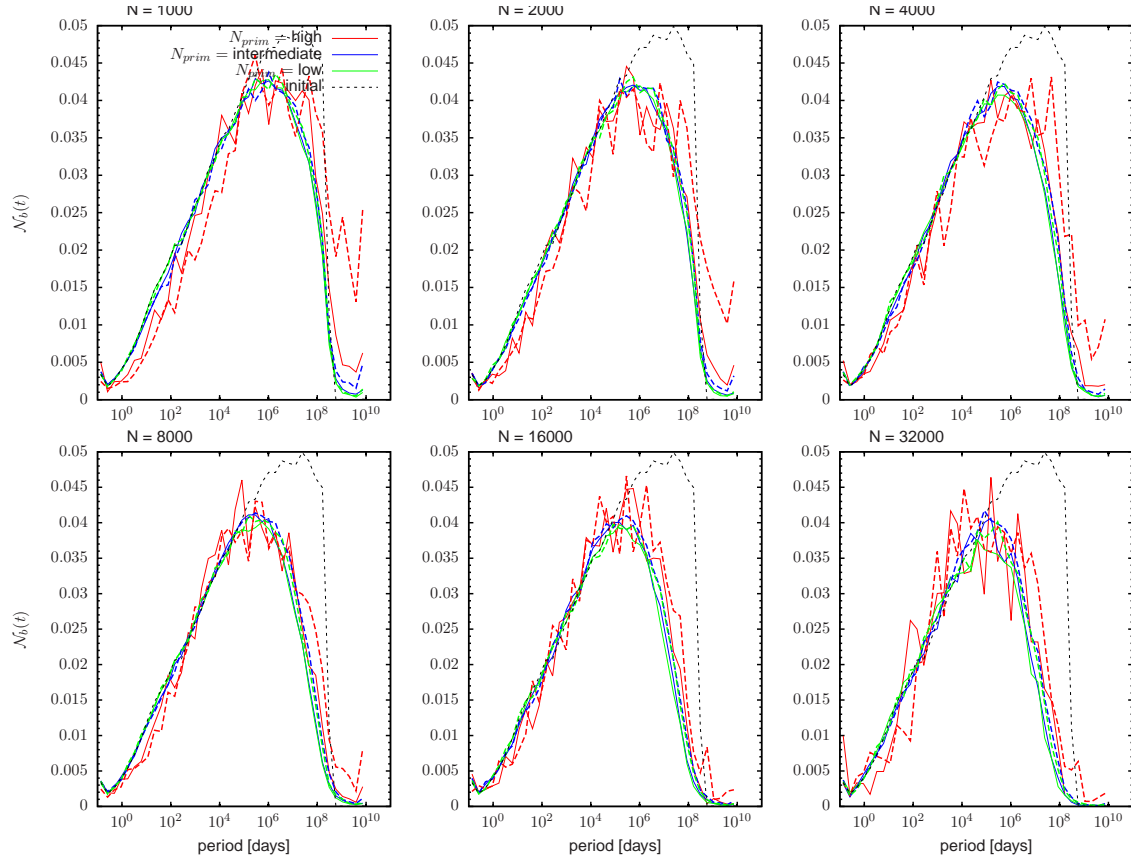


Figure 4.11: Comparison of the period distributions of binaries with high (red), intermediate (blue) and low-mass primaries (green) for all clusters after 5Myr.

therefore have formed during the evolution of the clusters.

#### 4.6 Evolution of the eccentricity and mass-ratio distribution

The following section will describe the evolution of the binary parameters not described so far: the evolution of the eccentricity distribution and the evolution of the mass-ratio distribution.

Fig. 4.12 shows the relative number of binaries at a given eccentricity ( $N_b(ecc, t)/N_b(ecc, 0)$ ) after 5Myr normalized to the initial number of binaries in the respective eccentricity bin. The red-lines give the number of binaries in the clusters with the lowest and the blue-lines the number of binaries in clusters with the highest simulated densities.

Generally, the smaller the eccentricity of a binary the larger is the probability that the binary will survive the dynamical evolution of the cluster. This means that the fraction of binaries with small eccentricities in a cluster increases during the cluster evolution. However, the evolution of the eccentricity distribution shows a clear dependence on the density of the clusters. The higher the density of a cluster, the more eccentric binaries compared to binaries with low eccentricities are destroyed during the evolution. To emphasise this, guiding lines of the form  $f(x) = mx + b$  have been added to Fig. 4.12 as solid red (lowest density clusters) and blue lines (highest density clusters). The slopes of

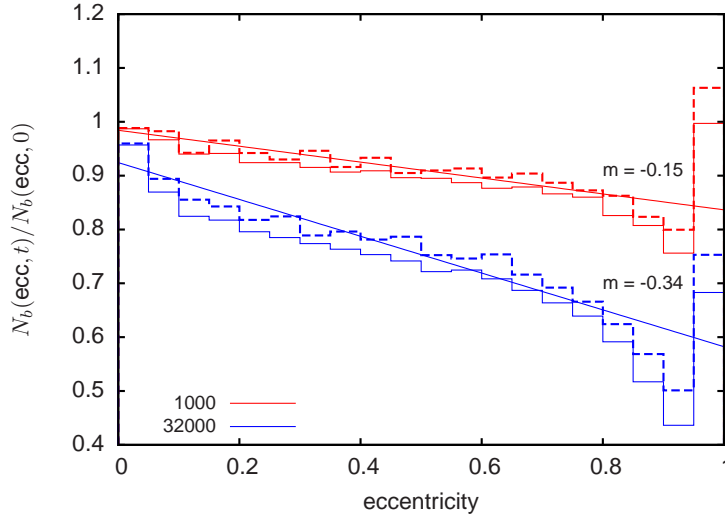


Figure 4.12: Change of the eccentricity distribution of binaries after 5 Myr for clusters with initially 1000 stellar systems (red-lines) and initially 32000 stellar systems. Solid lines denote simulations with initially 30% binaries and dashed lines simulations with initially 75% binaries.

the two lines are  $m_{\text{low}} = -0.15$  and  $m_{\text{high}} = -0.34$ , respectively. The reason for this is that binaries with high eccentricities spend most of the time at wide separations, where they are more vulnerable to encounters with other stars.

The relative number of binaries at a given mass-ratio ( $M_2/M_1$ ) bin ( $N_b(Q, t)/N_b(Q, 0)$ ) after 5 Myr normalized to the initial number of binaries in the respective mass-ratio bin for clusters with the lowest (red-lines) and highest (blue-lines) density clusters is shown in Fig. 4.13. Clearly, the higher the mass-ratio of a binary is, the higher is the probability that the binary survives. As has been found for the eccentricity distribution above, the evolution however depends on the density in the cluster. The higher the density of a cluster is, the more binaries with low mass-ratios are destroyed during the evolution of the cluster. This again is emphasised by the two guiding lines that have been added in Fig. 4.13 which have been obtained by fitting the function  $f(x) = mx + b$  to the data in the mass-ratio range 0 – 0.9. While the slope of the guiding line for the sparsest cluster is only 0.1, the slope of the densest cluster is much higher (0.15) which clearly illustrates that in denser cluster more binaries with low mass-ratios are destroyed.

#### 4.7 Comparison with the observations

The current picture of star formation states that most if not all stars are born in star clusters that mostly dissolve shortly after their formation (see Lada & Lada, 2003, and Chap. 5). This means that the binary population in the solar neighbourhood which represents the best studied binary population today should have originated from these clusters. Both the stellar and gas density in the solar neighbourhood is much too low to significantly alter the properties of the binary population so that its properties must have already been determined in their natal environments, the dense stellar cluster.

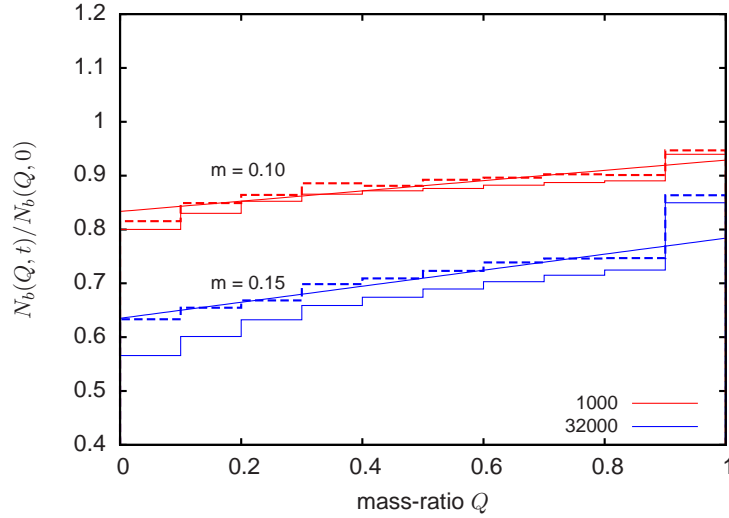


Figure 4.13: Change of the mass-ratio distribution of binaries after 5 Myr for clusters with initially 1000 stellar systems (red-lines) and initially 32000 stellar systems. Solid lines denote simulations with initially 30% binaries and dashed lines simulations with initially 75% binaries.

As has been shown in Sec.4.4 the effect the dynamical evolution of the star clusters has on the binary populations in the star clusters depends on the stellar density in the cluster. This raises the question if clusters of any density contributed to the binary population in the solar neighbourhood or if clusters of a certain density display the dominant source of binaries for the solar neighbourhood.

To compare the period distributions of the simulated binary populations to the observations of Raghavan *et al.* (2010), only binaries with a G-type primary have been taken into account. Additionally, the same binning of the periods as given by Raghavan *et al.* (2010) has been applied which gives the period distributions shown in Fig. 4.14. It displays the period distributions after 5 Myr for all simulated clusters as solid blue (initially 30% binaries) and as solid red (initially 75% binaries) lines. The observations by Raghavan *et al.* (2010) are shown as dashed black lines.

Clearly, the density of the cluster influences how well the distributions match to the observations. Clusters with densities of  $4 \times 10^3 \text{pc}^{-3}$ , corresponding to clusters with 2000 systems and a initial binary frequency of 75%, and lower maintain slightly too many wide binary systems after 5 Myr of evolution, clusters with intermediate densities ( $7 \times 10^3 \text{pc}^{-3} - 2 \times 10^4 \text{pc}^{-3}$ , corresponding to clusters with 4000 - 8000 stellar systems) have almost matching numbers of tight and wide binaries, while clusters with higher densities ( $> 2 \times 10^4 \text{pc}^{-3}$ , corresponding to more than 16000 stellar systems) maintain to few wide binaries compared to the observations. To judge which cluster type matches the observations best in a more objective way,  $\chi^2$  tests were performed using the initial period distributions of all star clusters and the ones after 1 Myr, 3 Myr and 5 Myr. The results of the  $\chi^2$ -tests are summarised in Tab. 4.4 which besides showing the resulting  $\chi^2$  values (third column), gives the corresponding probability, that the tested period distribution and that observed by Raghavan *et al.* (2010) have been drawn from the same underlying distribution (fourth column).

time [Myr]	$N_{\text{sys}}$	$\chi^2$	significance
0.0	1000	11.29	0.335
1.0	1000	6.51	0.771
3.0	1000	4.72	0.909
5.0	1000	4.39	<b>0.928</b>
0.0	2000	11.11	0.349
1.0	2000	5.44	0.860
3.0	2000	4.18	<b>0.939</b>
5.0	2000	4.38	0.929
0.0	4000	10.91	0.364
1.0	4000	4.61	<b>0.916</b>
3.0	4000	4.71	0.910
5.0	4000	6.00	0.815
0.0	8000	10.27	0.417
1.0	8000	4.37	<b>0.929</b>
3.0	8000	6.79	0.745
5.0	8000	9.47	0.488
0.0	16000	9.73	0.464
1.0	16000	5.41	<b>0.862</b>
3.0	16000	10.97	0.360
5.0	16000	15.11	0.151
0.0	32000	9.36	0.498
1.0	32000	7.47	<b>0.680</b>
3.0	32000	16.22	0.107
5.0	32000	21.80	0.017

Table 4.4:  $\chi^2$  Test results for several pairs of distributions. The test boundaries reach from  $10^{-1}$  –  $10^{10}$ d.

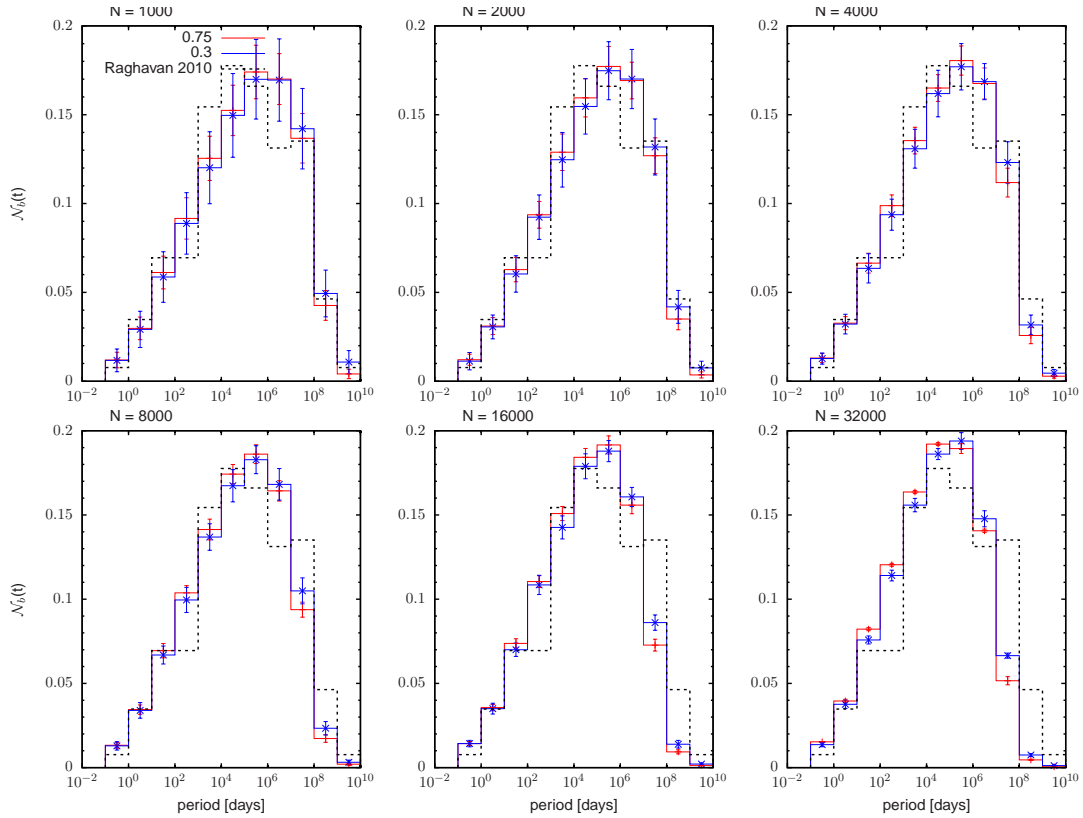


Figure 4.14: Comparison of the period distribution of G-type stars in the different clusters with the observations by Raghavan *et al.* (2010).



For all simulated star clusters, the initial and the observed period distributions are very different from each other as pointed out by the very large  $\chi^2$  values. As the evolution of the cluster proceeds, the probability that the simulated and observed period distribution are equal grows in all clusters. The best conformity of 93.9% is found in star clusters with initially 2000 stellar system. However, all clusters with initially 1000 – 8000 stellar systems result in comparable best conformity probabilities and on the densest clusters with more than 16000 stellar systems yield probabilities that are well below 90% ( 86.2% and 68% for clusters with 16000 and 32000 stellar systems, respectively).

The time, the conformity of the simulated period distributions in a cluster match best to the observed period distribution of the field depends on the density of the cluster. While in clusters with low densities (1000 – 2000 stellar systems) the best conformity is found towards the end of the simulations and might even improve afterwards, intermediate (4000 – 8000 stellar systems) and high-density (> 16000 stellar systems) clusters match the observations best at much earlier times and the earlier, the higher the density of the cluster is. The reason the conformity of the simulated and observed period distributions set in later the lower the density in a cluster is that the rate at which binaries are destroyed in star cluster due to three-body interactions depends on the density in the clusters as more three-body interactions take place in denser clusters than in less dense clusters when compared over the same time spans. In low density clusters, this rate is so low, that the towards the end of the simulation, the destruction of binaries still goes on improving the conformity of simulations and observations. In contrast in high density clusters, already after very short times to many binaries are destroyed to lead to a good conformity between the simulated and observed period distributions. Additionally, as has been shown in Fig. 4.8, the higher the density in a cluster is, the tighter are binaries that can be destroyed during the evolution of the cluster. This leads to a wrong shape of the resulting period distribution as it can also be seen in Fig. 4.14.

Although the  $\chi^2$  test are a good way to determine conformity between the simulated and observed period distribution, it alone does not mean that the simulated binary population and the observed one are the same. The additional parameter that has to match is the binary frequency. The binary frequencies resulting from the simulations at the instant of best conformity are 54.6% (1000), 70% (2000), 67% (4000), 68.9% (8000), 65.9% (16000), and 61.1% (32000). As can be seen, the binary frequencies in all star clusters at the instant of best conformity are, despite the simulations with 1000 stellar systems, always larger than the observed binary frequency of G-type stars of 58% Raghavan *et al.* (2010). This means, that the initial binary frequency of 75% of all stars chosen here to reproduce the field binary population is probably to higher and in reality is a bit lower around 65 – 60%. This however also indicates, as the gas-induced orbital decay is capable to merge about 10 – 15% of all binaries, that not all stars are born in a binary system, but about one fourth of all stars are born as single stars.

## 4.8 Summary

In this chapter the influence of the stellar density in a star cluster on the evolution of a primordial binary population has been investigated. The aim was to test whether the independence of the evolution of the binary population on the initial binary frequency for ONC-like clusters, still holds in star clusters with smaller and higher densities. A extensive set of simulations of clusters with densities in the range from 0.25 – 8 times the density of the ONC (central densities  $\rho = 1.6 \times 10^3 \text{pc}^{-3}$ ) - ( $\rho = 6.6 \times 10^4 \text{pc}^{-3}$ ) have been performed starting with initial binary frequency of 30% and 75%.

It was found that:

- The evolution of the binary population remains independent of the initial binary frequency for cluster of an given densities. This allows predict the evolution of binary population in star clusters with arbitrary densities without the need of further costly Nbody-simulations. In addition it allows to determine the initial binary frequency from the current observed binary frequency in a cluster.
- The higher the density in a cluster the tighter are binaries that are affected by the dynamical evolution. As a result the peak period in the period distribution decreases with increasing density. For example, while in the sparsest clusters simulated binaries periods down to  $\approx 2 \times 10^5 \text{d}$  are destroyed, in the densest clusters binaries with periods down to  $\approx 9 \times 10^3 \text{d}$  are destroyed. The maxima of the period distributions in this two clusters change from  $\approx 7 \times 10^5 \text{d}$  in the sparsest to  $\approx 1 \times 10^5 \text{d}$  in the densest cluster.
- The evolution of binaries with a high mass primary differs from the evolution of intermediate and low-mass binaries in the sense that in contrast to these two, the evolution of binaries with a high mass primaries show a dependence on the initial binary frequency. For clusters with low initial binary frequencies, the binary frequency of high-mass stars always decreases slower than for clusters with higher initial binary frequencies and even increases for clusters with central densities below  $\approx 7 \times 10^3 \text{pc}^{-3}$  due to the formation of new binaries.
- The higher the density in a cluster the more binaries with low-mass ratios and high eccentricities are destroyed during the evolution of the cluster.
- The higher the density in a cluster the shorter the binary population is allowed to be exposed to the dynamical evolution of the clusters if the binary population shall resemble the binary population in the field. For example while the period distributions of the sparsest cluster match the observations best after 5Myr, the best accordance for the densest star clusters already occurs after less than 1Myr.
- There seems to be a density limit ( $\approx 3 \times 10^4 \text{pc}^{-3}$ ) were the effect of increasing the cluster density does not lead to significantly more binaries being destroyed. This means that in dense star clusters, almost the same amount of binaries is destroyed and almost the same binaries are affected by the dynamical evolution.

## 5 Binary populations in supervirial clusters

### 5.1 Introduction

The current picture of star formation says that most stars do not form in isolation but are born in star clusters (e.g. Lada & Lada, 2003). Fig. 5.1a summarises observations of the densities of young, massive ( $> 10^3 M_{\odot}$ ) star clusters in the Milky Way as a function of cluster age. Clearly the observed cluster densities at any cluster age cover a wide range of possible values in the range from  $0.01 M_{\odot}\text{pc}^{-3}$  to  $10^5 M_{\odot}\text{pc}^{-3}$ . At the same time they also vary in size from  $\approx 0.1$  pc up to few ten pc. These findings lead to the assumption that star clusters form over a wide range of initial densities, extents and masses.

However, a careful reinvestigation of the observations of star clusters in the Milky way by Pfalzner (2009) has however shown, that the variety of observed cluster densities does not originate from an initial spread in the cluster densities but arises from two different cluster types. Fig. 5.1b shows the observed cluster densities from Fig. 5.1a as a function of the cluster size. The age of the star clusters is color-coded in the data points with red points representing the youngest clusters (age  $< 4$  Myr), green points clusters with intermediate ages ( $4 \text{ Myr} < \text{age} < 10 \text{ Myr}$ ) and blue points the oldest clusters (age  $> 10$  Myr).

Displaying clusters in this way reveals two distinct evolutionary tracks star clusters can follow during their evolution. Clusters following the first evolutionary track start at very high densities of about  $10^6 M_{\odot}\text{pc}^{-3}$  and radii of about 0.1 pc and evolve to smaller densities of about  $10^2 M_{\odot}\text{pc}^{-3}$  and radii of a few pc and are called **starburst clusters**. The evolution of clusters on the other track starts at densities below  $10^2 M_{\odot}\text{pc}^{-3}$  and radii of several pc and develops to densities well below  $1 M_{\odot}\text{pc}^{-3}$  and radii of several ten pc. These clusters are called **leaky clusters**.

The evolution of both, starburst and leaky clusters is therefore characterised by an immense expansion of the clusters that is accompanied by a decrease of the cluster density over the first 20 Myr at least. Several processes are known to cause an expansion of star clusters such as the instantaneous loss of gas that has not been used to form stars, the mass loss due to stellar-evolution, the stripping of loosely-bound stars from cluster by the tidal field of the Milky way, etc.. The latter two processes are unlikely to cause the expansion seen in Fig. 5.1b because they act on timescales much larger than 20 Myr.

Pfalzner & Kaczmarek (in preparation) studied if the gas expulsion can explain the observed expansion of the leaky star clusters and performed simulations of star clusters consisting of 30000 single-stars in a King-model cluster with an initial half-mass radius of 1 pc and star formation efficiencies in the range from 10 % - 100 %. Fig. 5.2 shows their comparison of the simulated evolution of the

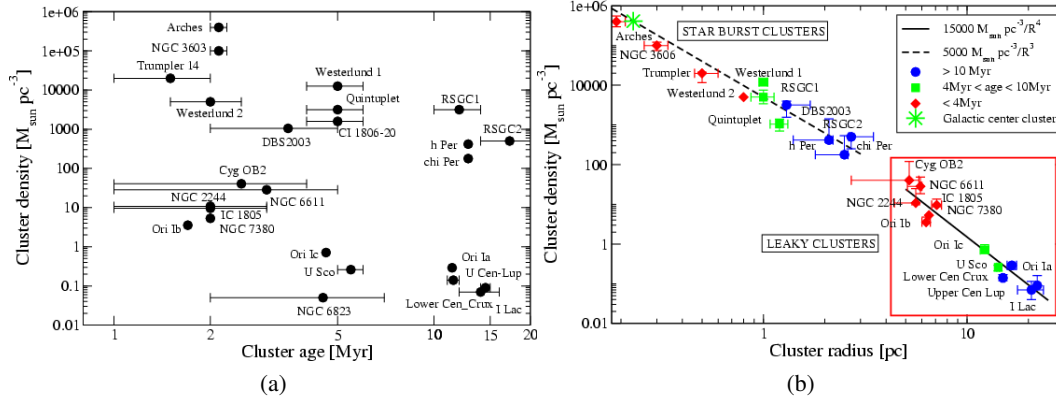


Figure 5.1: Observed cluster density as function of the cluster radius for clusters more massive than  $10^3 M_{\odot}$ . Taken from Pfalzner (2009).

half-mass radius as it would be measured by an observer of the model-clusters with star formation efficiencies of 20 % – 40 % with the observations from Fig. 5.1b. The evolution of the model clusters with a star formation efficiency of 30 % match the evolution of the observed leaky clusters quite well while the evolution of the clusters with slightly higher and lower star formation efficiencies differ significantly from the observations. As also observations of embedded clusters (e.g. Kroupa *et al.*, 2001; Baumgardt & Kroupa, 2007; Lada & Kylafis, 1999; Elmegreen *et al.*, 2000) have shown, that star clusters have to form with star formation efficiencies of about 30 % (see Sec. 1.4) this implies that leaky star clusters indeed undergo instantaneous gas loss where they lose 70 % of their mass on very short time scales.

The clusters investigated in Pfalzner & Kaczmarek (in preparation) initially only contained single stars. Since a primordial binary population in these clusters can be expected to influence the evolution of the clusters, I will investigate the evolution of leaky clusters undergoing instantaneous gas expulsion which already obtain a binary population directly from the beginning. The main focus will lie on the evolution of the clusters in the density - radius plot (Fig. 5.2) and on the evolution of the binary population itself.

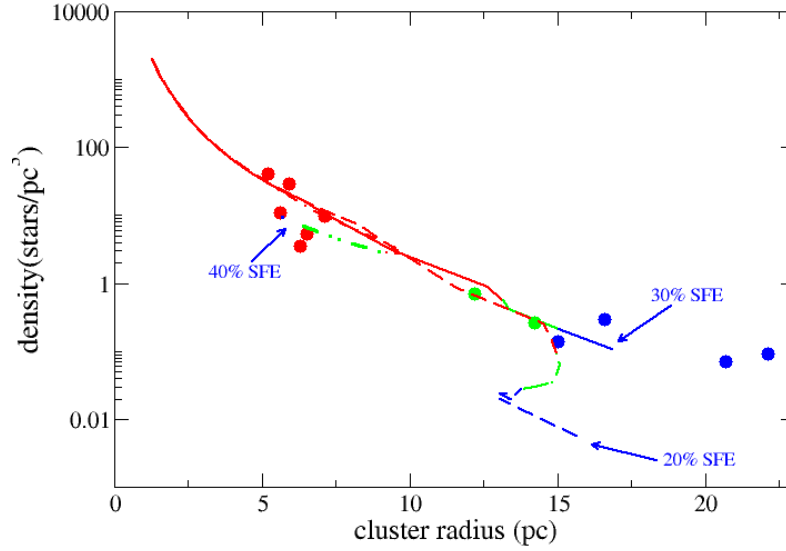


Figure 5.2: Evolution of simulated "leaky" clusters compared to observations. Taken from Pfalzner & Kaczmarek (in preparation).

## 5.2 General evolution of star clusters after gas expulsion

Before investigating the specific evolution of massive star clusters after gas expulsion as observed in the cluster sequences (Fig. 5.1b), the influence of instantaneous mass loss on the energetics of the clusters are described here, as they mainly determine the evolution of the cluster. The energy of a star cluster *before* gas expulsion with a arbitrary virial ratio  $Q_0 = T/|V|$  is given by

$$E = \frac{1}{2}M_0v^2 - \frac{GM_0^2}{2R_0} = Q_0M_0v_{\text{eq}}^2 - \frac{GM_0^2}{2R_0} = \frac{GM_0^2}{2R_0}(Q_0 - 1), \quad (5.1)$$

where  $M_0 = M_{\text{stars}}(0) + M_{\text{gas}}(0)$  is the total mass of the star cluster,  $v^2 = 2Q_0v_{\text{eq}}^2$  is the velocity dispersion of the star cluster,  $v_{\text{eq}}^2 = |V|/M_0 = GM_0/2R_0$  is the velocity dispersion of the star cluster if in virial equilibrium  $Q = 0.5$  and  $R_0$  is the "effective" or "average radius" of the cluster (see Sec. 1.4). Clusters with virial ratios less than unity are bound systems ( $E < 0$ ) while clusters with larger virial ratios are unbound ( $E > 0$ ).

Assuming instantaneous gas loss both the velocity of the stars and the effective radius of the cluster, will not be able to immediately adjust to the new overall potential so that the energy of the star cluster *after* the gas expulsion is given by

$$E = \frac{1}{2}\varepsilon M_0v^2 - \frac{G\varepsilon^2 M_0^2}{2R_0} = Q_0\varepsilon M_0v_{\text{eq}}^2 - \frac{G\varepsilon^2 M_0^2}{2R_0} = \frac{G\varepsilon M_0^2}{2R_0}(Q_0 - \varepsilon), \quad (5.2)$$

where the star formation efficiency  $\varepsilon = M_{\text{stars}}/M_0$  is the fraction of the total cluster mass, that has

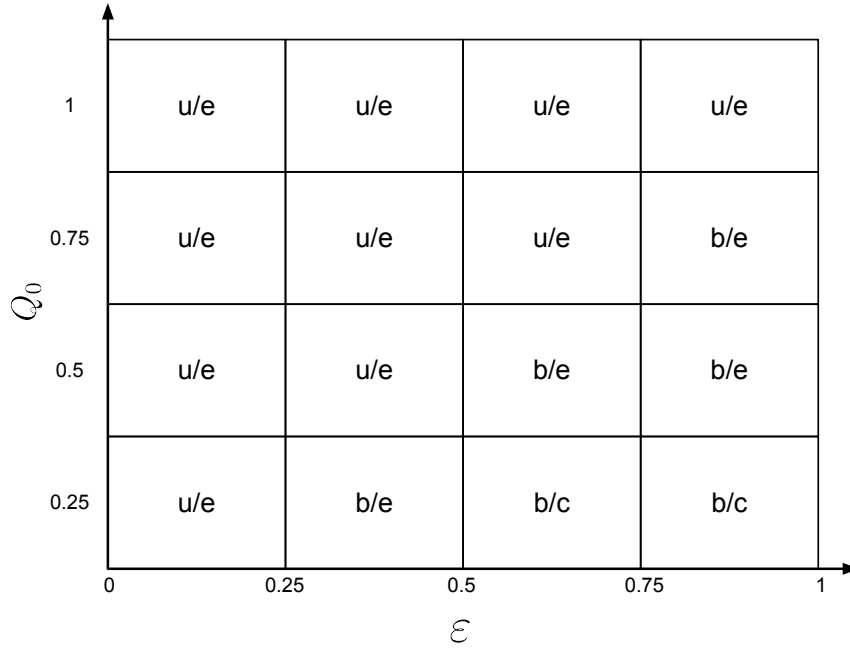


Figure 5.3: The outcome states of an equilibrium star clusters directly after gas expulsion. Each box represent the outcomes for cluster with  $\epsilon$  in the given range for the given virial ratio before gas expulsion  $Q_0$ . b and u represent bound and unbound clusters and e and c represent expanding and contracting clusters.

been converted into stars. Therefore the total energy of a star cluster after it has lost it's natal gas will always be lower than it's energy before the mass loss. This loss of energy can even lead to star clusters becoming unbound, that have been bound before the gas was removed if their  $\epsilon$  is smaller than the virial ratio of the cluster before the gas expulsion.

The virial ratio after gas expulsion of a cluster with virial ratio  $Q_0$  is given by ( $T = \epsilon T_0$ ,  $V = \epsilon^2 V_0$ )

$$Q = \frac{Q_0}{\epsilon}, \quad (5.3)$$

which means that the virial ratio of any cluster independent of it's virial state before gas expulsion will increase due to gas expulsion. This means that clusters will either begin to expand if their virial ratio exceeds the equilibrium value of 0.5 or they will contract less fast than before gas expulsion. In fact clusters that are contracting before gas expulsion might even begin to expand if their  $\epsilon$  is less than half the virial ratio of the cluster before gas expulsion ( $\epsilon < 2Q_0$ ).

Fig. 5.3 gives a schematic representation of the outcome directly after gas expulsion in dependence of the  $\epsilon$  of the clusters and their virial ratio before the gas removal ( $Q_0$ ) for clusters, that are in virial equilibrium before the gas expulsion. For clusters to remain bound after the gas expulsion, the  $\epsilon$  in the cluster has to be rather high. For a contracting cluster, the star formation efficiency has to be even higher while simultaneously the virial ratio before the gas expulsion has to be very small.

The further evolution of the clusters is then given by the virial ratio of the clusters. If the clusters

are in a supervirial state ( $Q > 0.5$ ), the clusters will expand as their potentials are not capable to confine the clusters to their present sizes. Due to this expansion the potential energy of the clusters decreases even further as the separations of the stars inside the clusters increase. At the same time the kinetic energy of the clusters will decrease by the same amount as the cluster potential energy to preserve the total energy of the clusters. The result is that the virial ratio of the clusters does not grow as fast as expected from the changes in the potential alone or decrease with time finally resulting in a cluster in virial equilibrium, if the cluster is bound after the gas expulsion. In contrast to that, the evolution of subvirial ( $Q < 0.5$ ) clusters will be characterised by an contraction which simultaneously rises the cluster potential and cluster kinetic energy. During this contraction the virial ratio of the clusters will rise so that the clusters end up in virial equilibrium.

This opposite influences of the changes of the potential and kinetic energy on the virial ratio make it difficult to predict the evolution of the virial ratio and therefore the evolution of the complete clusters at first glance. However, it turns out that the overall effect of the cluster expansion on the dynamical evolution of the clusters can be described with the help of the total energy of the cluster if the relation  $T = E + V$  is used to remove the dependency of the virial ratio on the kinetic energy of the cluster:

$$Q = \frac{T}{V} = \frac{E}{V} + 1. \quad (5.4)$$

Now introducing the potential energy of the star clusters as  $V = G \sum_{i \neq j=1}^N m_i m_j / |\mathbf{r}_i - \mathbf{r}_j| = k\bar{R}^{-1}$  where  $k$  is a constant comprising the masses of the clusters and structural parameters of the cluster in Eq. 5.4 gives

$$Q = \frac{E\bar{R}}{k} + 1. \quad (5.5)$$

Eq. 5.5 shows that the virial ratios of unbound clusters ( $E > 0$ ) will increase with time without any boundary due to the expansion of the cluster. In contrast, the virial ratios of bound clusters will evolve towards the equilibrium value of 0.5. This means that the expansion velocity of clusters that start to expand after they lost their gas will decrease with time until the expansion stops, while clusters that start contracting will also stop their contraction after some time.

As soon as the clusters have reached the virial equilibrium no further expansion or contraction is to be expected due to the energetics of the clusters. However, other processes than the energetics of the cluster are capable to cause the clusters to evolve and some of them will be investigated in the forthcoming sections.

### 5.3 Simulation setup

The scope of this section is to investigate, how a primordial binary population alters the evolution of leaky star clusters undergoing instantaneous gas expulsion. For this purpose a comprehensive set of simulations of massive clusters has been performed with  $\varepsilon$  in the range from 10% – 100%. Here, only

the evolution of the clusters after the gas expulsion will be studied so that the initial time step in the simulations describes the instant, at which the gas is removed from the cluster. As the clusters are supposed to be in virial equilibrium before the gas loss, they should expand from the beginning and evolve as described in Sec. 5.2.

The cluster model used for this simulations is based on observations of the ONC, a typical gas-embedded star cluster which is assumed to be a precursor of leaky-clusters. Hillenbrand & Hartmann (1998) have determined the density profile to be a King-model cluster with a central potential of  $W_0 = 9$  corresponding to an concentration  $c \approx 2$  (see Sec. 1.1.2). However, in contrast to the model by Hillenbrand & Hartmann (1998) which predicts a half-mass radius of 0.8 pc, the initial half-mass radius of the here simulated clusters has been set to 1.3 pc since the ONC is most probably still forming stars and has not reached its final size. Accordingly it can be expected that the total stellar mass of the ONC at the instant of gas expulsion from when on it will be classified as leaky-star cluster has to be much higher as is observed in the ONC today ( $4500M_\odot$ ). Indeed, closer inspection of the cluster masses used to generate Fig. 5.1b implies, that the total stellar mass of the star cluster must have been of the order of about  $20000M_\odot$ . Here, all clusters have been set up with initial total masses of about  $17600M_\odot$  corresponding to 30000 stars if there masses have been sampled from Kroupa (2002) IMF.

Star clusters with different mass functions have been set up to be able to point out, which effect binaries really have on the evolution of leaky-star clusters undergoing instantaneous gas loss. First, clusters only containing stars with a single mass have been simulated and will be called single-mass clusters from now on. Their evolution is least complicated by encounter driven processes (see Sec. 1.2) so that their evolution should follow the predictions from Sec. 5.2 best. Next simulations of star clusters containing stars with masses sampled from the Kroupa (2002) were performed (IMF clusters) which should be influenced stronger by encounters. Finally clusters including a primordial binary population (binary clusters) were simulated since their evolution is to be investigated here.

While it is straight-forward to set up star clusters with single-mass stars or stars drawn from the Kroupa (2002) IMF, setting up a primordial binary population for leaky-star clusters requires additional considerations. As has been shown in Chap. 3 and Chap. 4 both the dynamical evolution of star clusters and the interactions of the binaries with the surrounding gas heavily change the properties of the binary population in these star clusters. Here the embedded phase of the star clusters is not simulated implying that the initial state of the here simulated clusters displays an already evolved state. This means that it is not possible to simply use either the Kouwenhoven *et al.* (2007) binary population model nor the Kroupa (1995a) as these represent the primordial state of the binary populations before they have been processed by the cluster environment. However, as has been shown in both Chapters the dynamics of the cluster and the binary-gas interactions alter the binary population on very short timescales ( $< 3$  Myr, see Sec. 4.7), that they should resemble the binary population as it is observed in the solar neighbourhood when the gas expulsion sets in. Therefore, the here used initial binary population model is based on the observation of the binary population in the solar neigh-



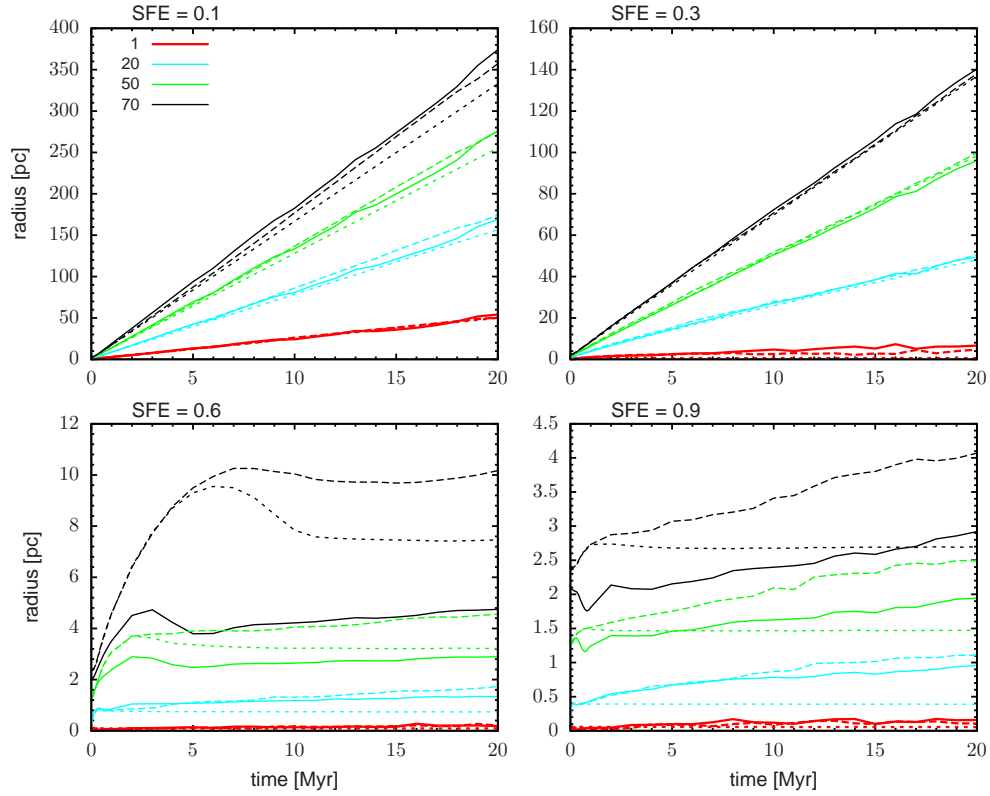


Figure 5.4: Evolution of the Lagrangian radii of star clusters with  $\epsilon = 0.1, 0.3, 0.6$  and  $\epsilon = 0.9$ . For reference the evolution of all simulated clusters is shown in Fig. B.1 in the appendix. Short dashed lines show the evolution of single-mass star clusters, long dashed lines the evolution of star clusters consisting of single stars drawn from the Kroupa (2002) IMF and solid lines the evolution of star cluster set up with a primordial binary population.

bourhood (Duquennoy & Mayor, 1991; Raghavan *et al.*, 2010) and is characterised by a log-normal period distribution with  $\overline{\log P} = 4.8$  and  $\sigma_{\log P} = 2.3$ , a thermal eccentricity distribution and randomly paired binary component masses.

All clusters have been simulated for 20 Myr after which all clusters have completed their reaction on the instantaneous gas loss. To improve the statistical significance of the results, 15 realisations of each cluster model have been simulated and analysed, before their results have been averaged and shown here.

#### 5.4 Evolution of the star clusters

A convenient way to describe the structural evolution of star clusters is to follow the evolution of the Lagrangian radii of the cluster. A Lagrangian radius of a cluster gives the radius within which a certain fraction of the total cluster mass can be found. Fig. 5.4 shows the evolution of the Lagrangian radii including 1%, 30%, 50% and 70% of the total cluster mass for single-mass (short-dashed lines), IMF (long-dashed lines) and binary clusters (solid lines) with  $\epsilon = 0.1, 0.3, 0.6$  and  $0.9$ . The evolution of the other clusters show do not any additional insights and are therefore shown in the Appendix B.1.

Note that the y-ranges in the different plots have not been kept constant, but have been varied between clusters with different  $\varepsilon$  so that the complete evolution of each cluster is displayed.

The evolution of the unbound star clusters ( $\varepsilon < 0.5$ ) proceed as expected. Due to the decrease of the cluster potential, all Lagrangian radii of these clusters increase directly after the mass loss (at  $t = 0$ ) and do not show any signs of stopping the expansion during the here simulated time.

In general, the expansion velocities are highest for the binary clusters, followed by the IMF clusters, and the single-mass clusters expand slowest. However, the differences in the expansion velocities between the different cluster types are only very small. The velocities, with which the Lagrangian radii expand, depend more strongly on the  $\varepsilon$  of the cluster, and on the mass fraction the Lagrangian radii includes. The lower the  $\varepsilon$  and the larger the mass fraction of the Lagrangian radius the higher is the expansion velocity of the corresponding Lagrangian radius. The reason is that star clusters with lower  $\varepsilon$  are more out of virial equilibrium. Since here all clusters have been set up to initially contain the same mass in stars, this means that the mean kinetic energy and thus the mean velocities of the stars in the clusters with lower  $\varepsilon$  are higher than in clusters with higher  $\varepsilon$ . Smaller Lagrangian radii expand slower than larger radii, because the cluster potential is deeper in the cluster centre. Since the initial velocities of the stars in the clusters are sampled independently from their location this means that the fraction of kinetic energy of stars in the cluster centre available for the expansion is smaller than for stars in the outskirts of the clusters.

The initial evolution of the Lagrangian radii of both - bound single-mass and bound IMF clusters ( $\varepsilon > 0.5$ ) proceeds as predicted in Sec. 5.2. Due to the instantaneous mass loss and the associated decrease of the overall cluster potential the Lagrangian radii of all clusters expand initially. In contrast to the unbound clusters ( $\varepsilon < 0.5$ ), the expansion velocities of the bound star clusters decrease with time as the clusters approach the virial equilibrium.

The evolution of the bound binary clusters (solid lines) shows remarkable differences to that of these star clusters. The expansion velocities of the Lagrangian radii of the of bound binary star clusters are in general much lower than that of the corresponding single-mass and IMF clusters. Again, as has been found for the unbound clusters, the expansion velocity of a cluster decreases the higher the  $\varepsilon$  of a cluster is. However, this time the decrease of the expansion velocity causes star clusters with  $\varepsilon$  above 0.9 not to expand initially, but to collapse.

The reason for both, the much lower expansion velocities and the initial contraction, is that in contrast to the single-mass and IMF clusters, the clusters including a primordial binary population may not only cool (lower their kinetic energies) by expanding as described in Sec. 5.2, but also through the destruction of wide binaries during three-body interactions. During such a three-body encounter, the intruding star transfers some of its kinetic energy to the binary rising the binding energy of the binary. This causes the binary to become wider or even become unbound, if the binding energy gets positive. The effect of these interactions on the star cluster is to cool it down because it lowers the kinetic energy of all three stars.

The here used initial binary population contains a significant number of wide binaries (periods

$\gtrsim 10^4$ d) that are susceptible to the destruction during three-body interactions so that all binary clusters independent of their  $\varepsilon$  are able to cool down by destroying the wide binaries. However, the efficiency with which wide binaries are destroyed during the cluster evolution depends on the  $\varepsilon$  in the cluster (see Sec. 5.5). While clusters with  $\varepsilon = 1.0$  destroy about 23% of their initial binaries within 20Myr, clusters with  $\varepsilon = 0.1$  only destroy about 3% of their initial binaries during the same time. The reason for this is, as will be explained in Sec. 5.5 in more detail, that the number of encounters capable to destroy binaries in star clusters reduces significantly in star clusters with low  $\varepsilon$  as the stellar densities in these clusters decrease.

However, as will also be shown in Sec. 5.5, binaries are not only destroyed in star clusters, but can also form through three-body interactions. During such an interaction, the cluster is heated as the kinetic energy of the star not being bound in the newly formed binary and of the binary is increased by the amount of binding energy needed to form the binary. As the formation of binaries is more effective the smaller the  $\varepsilon$  of a cluster is (see Sec. 5.5) this explains the slightly increased expansion velocities of binary star clusters with  $\varepsilon < 0.4$  when compared to the corresponding single-mass and IMF clusters.

The evolution of the star clusters after this initial expansion phase can not be explained by the cluster energetics alone which predicts that the clusters should stop their expansion and pass over to a steady state. What happens instead depends on the mass function. After they have reached the virial equilibrium the Lagrangian radii of single-mass star clusters shrink a bit and become constant in the end (see also Goodwin & Bastian, 2006). Also the Lagrangian radii of the IMF-clusters show such a rebound. However, the higher the  $\varepsilon$  of a star cluster the less obvious the rebound becomes as the Lagrangian radii of the IMF-clusters do not stay constant after the rebound, but increase further but at slower velocities than before the rebound.

Binary clusters that expand after the gas expulsion (basically clusters with  $\varepsilon$  less than 0.8) evolve comparable to the IMF-clusters. However, the time of the rebound and the expansion at this point are smaller than for the corresponding IMF clusters. After the rebound the expansion of the IMF and binary clusters is marginally the same. Binary clusters with  $\varepsilon$  exceeding 0.8 also show a rebound, however this time in the other direction. After reaching their maximal concentration, the Lagrangian radii of these clusters reexpand again before a second, “normal” rebound happens after which the clusters expand like the clusters with lower  $\varepsilon$ .

The rebound after the initial expansion of the clusters is explained by the decreasing influence of stars leaving the clusters. As these stars move away from the clusters, their gravitational attraction to stars remaining in the bound star cluster decreases and finally become negligible compared to the gravitational attraction within the cluster.

The reason star clusters set up with an IMF do not stop their expansion is that due to the mass spectrum of stars in the clusters, gravitational interactions of the stars in the clusters become more important. As described in more detail in Sec. 1.2.5 encounters in star clusters are capable to unbind stars by either ejecting them in a strong single encounter or evaporating them in several weak encounters.

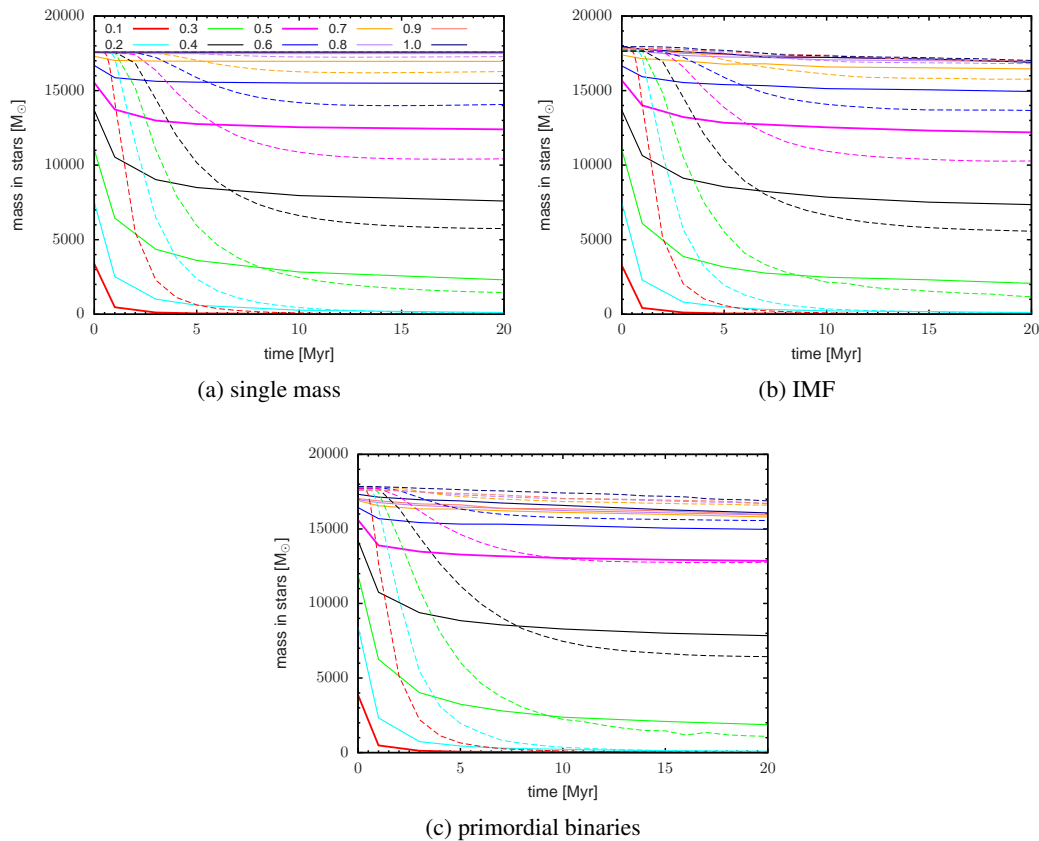


Figure 5.5: Evolution of the mass of stars bound (solid lines) and stars associated (dashed lines) to star clusters with different  $\epsilon$ . Shown are the evolutions of clusters consisting of single-mass stars and clusters with stars sampled from the Kroupa (2002) IMF.

Determining the escape rates from star clusters set up with single-mass stars and stars sampled from an IMF Henon (1969) shows, that introducing a mass spectrum into the calculations, the timescales to dissolve a cluster only due to gravitational interactions inside the clusters is significantly reduced.

Up to now the evolution of all stars bound to the star cluster before the gas expulsion has been investigated. However, due to the drop in the cluster potential caused by the removal of the gas, a certain fraction of the stars in the clusters will become unbound. While determining the bound stellar mass of star cluster is achieved straight-forwardly in numerical simulations, this is much more complicated when observing real star clusters because there it is not possible to calculate the energies of the stars in the cluster as usually the 3D-positions and 3D-velocities and the stellar masses are not known accurately enough. What is done instead is to estimate the cluster mass from the total luminosity within a certain cut-off radius around the cluster centre and multiplying it with a appropriate mass-to-light ratio. However, this mass estimate does not give the bound mass of the star cluster but the mass of stars that are associated to the star cluster.

Fig. 5.5 shows the evolution of the mass of stars bound to a star cluster for all simulated  $\epsilon$  for the single-mass, IMF and binary clusters separately. For all three cluster types the initial stellar mass

bound to the star clusters varies between clusters with different  $\epsilon$ . The higher the  $\epsilon$  the higher is stellar mass that is bound to the cluster. For example the bound stellar mass of clusters with an  $\epsilon$  of 50% is reduced by about 12% independent of the mass function while in star clusters with an  $\epsilon$  of 30% about 37% of the stellar mass becomes unbound for the single-mass and IMF clusters. The fraction of the stellar mass becoming unbound for binary clusters is with about 33% a little lower. The reason is that due to the sudden drop of the cluster potential the escape velocity  $v_{\text{esc}}(r) = \sqrt{2\Phi(r)}$  in the star cluster reduces significantly while the velocity distribution of the stars has no time to adopt to the new cluster potential. This means that stars with velocities exceeding the escape velocity of the cluster after the mass loss become instantaneously unbound. This process can be regarded as a special form of violent relaxation (Lynden-Bell, 1967) which denotes the change of stellar energies in star clusters due to temporal changes in the cluster potential.

Fig. 5.5 shows, that the decrease of bound stellar mass continues for another 5 Myr after the gas expulsion in all star clusters. The result of this second decrease is that the star clusters with  $\epsilon < 0.2$  almost loose all their stellar mass and can be considered as being completely dissolved. Star clusters with  $\epsilon > 0.2$  keep a significant fraction of their initial bound stellar and can be considered as having survived the gas expulsion, although also this clusters can loose significant fractions of their stellar content. For example clusters with  $\epsilon = 0.3$  loose about 80% (70%) of the total stellar mass the cluster had directly before (after) the gas expulsion while clusters with  $\epsilon = 0.5$  loose about 29% (18%).

The reason for the decrease of the bound mass after the gas expulsion is that although the total energy of all stars in the simulation does not change after the gas has been removed, the potential of the cluster does. The cluster potential after the gas expulsion is generated by the bound and unbound stars. Directly after the gas loss, the unbound stars still reside at their positions inside the clusters they had directly before the gas expulsion occurred. As the unbound stars depart from the cluster, their influence on the star cluster potential decreases which in turn again lowers the potential of the cluster (now meaning the collection of stars that are gravitationally bound) and its escape velocity. This means that stars with velocities just below the escape velocity after the gas expulsion also become unbound and depart from the cluster which again leads to an decrease of the cluster potential and the bound stellar mass.

The rate with which the bound stellar mass of the clusters decreases is highest at the instant of the gas expulsion and becomes less during the following evolution. One reason for this is that the largest fraction of the mass bound to the cluster is removed during the instantaneous gas expulsion. For example the star clusters with  $\epsilon = 0.1$  simulated here with their initial stellar mass of about  $17000M_{\odot}$  loose about  $153000M_{\odot}$  during the gas expulsion while in the following evolution only the remaining  $17.000M_{\odot}$  are removed. The second reason is that while the gas expulsion is assumed to be so fast, that the cluster has no time to adjust to the new potential, the gradual loss of stars during the following cluster evolution is much slower. The clusters response to the mass loss is to expand (see Sec. 5.2) and thereby a decrease in the average kinetic energy of the stars in the clusters. This means that less stars will become unbound due to the decrease in the cluster potential which in the end leads to an

reduction of the mass loss rate.

Above considerations imply that the decrease of the bound mass of a cluster is a self-feeding process. The removal of unbound stars lowers the potential of the cluster which again unbinds stars which leave the cluster and so on. However, during this process the star cluster adapts to the new conditions by expanding as described in Sec. 5.2. This means that with each step in this iterative process less stars get unbound until the point where the removal of a single unbound star is insufficient to lower the potential of the cluster that much that another star becomes unbound. In the here simulated clusters, this happens after about 5 Myr and later the larger the  $\varepsilon$  of a cluster is.

The evolution of the bound mass of clusters with  $\varepsilon$  less than 0.8 does not depend on the mass function. In contrast, the evolution of star clusters with higher  $\varepsilon$  differs between the clusters with different mass functions. For example, while the bound mass of single-mass clusters with  $\varepsilon$  1.0 remain constant during the whole simulation time (the change is smaller than 0.1%, the mass bound to IMF and binary clusters drops by 5% and 10%, respectively. Again, the reason for this is that encounters are more probable to remove stars from a cluster set up with stars drawn from an IMF than in single-mass clusters (see discussion of Lagrangian radii).

Fig. 5.5 shows the evolution of the mass of stars that are at a given time found within 20 pc from the cluster centre which mimics the luminosity mass estimate from observations and will from now on be called the associated mass of the cluster. Initially the associated mass is the same for all star clusters, independent of the  $\varepsilon$  because all clusters initially fit with the here applied cut-off radius. After about 1 Myr the associated mass of star clusters with  $\varepsilon = 0.1$  begins to vanish and is completely removed within the next 10 Myr. The associated masses of the other clusters start to decrease later and is less pronounced the higher the  $\varepsilon$  of the cluster is. The reason is that the expansion velocity of star clusters with smaller  $\varepsilon$  is higher than for clusters with higher  $\varepsilon$ . As all cluster have been set up with the same size, star clusters with smaller  $\varepsilon$  expand faster beyond the 20 pc cut-off radius.

The bound mass of the star clusters is initially always lower than the associated mass but as the clusters begin to expand beyond the 20 pc cut-off radius, the associated mass approaches the bound mass of the cluster and after 5 to 10 Myr, depending on the  $\varepsilon$  of the cluster the bound mass becomes larger than the associated mass. Directly after the gas expulsion the clusters have sizes well below the 20 pc cut-off radius so that the associated mass corresponds to the total stellar mass before the gas expulsion. At the same time a certain fraction of the stellar population in the clusters has, however, already become unbound from the cluster and begins to depart from the cluster.

During the next Myr the clusters expand due to the mass loss and more stars become unbound from the clusters. However, as the sizes of the clusters are still below the 20 pc cut-off radius the associated mass does not change at all. After 1 Myr the star clusters with the lowest  $\varepsilon$  begin to grow beyond the 20 pc cut-off and start to loose their associated mass and are followed by the other clusters afterwards. At this time, the rate the clusters unbind stars has already decreased significantly so that the decrease of the associated mass proceeds faster than the decrease of the bound mass.

After about 5 Myr only the evaporation and ejection of stars drives the loss of the bound mass

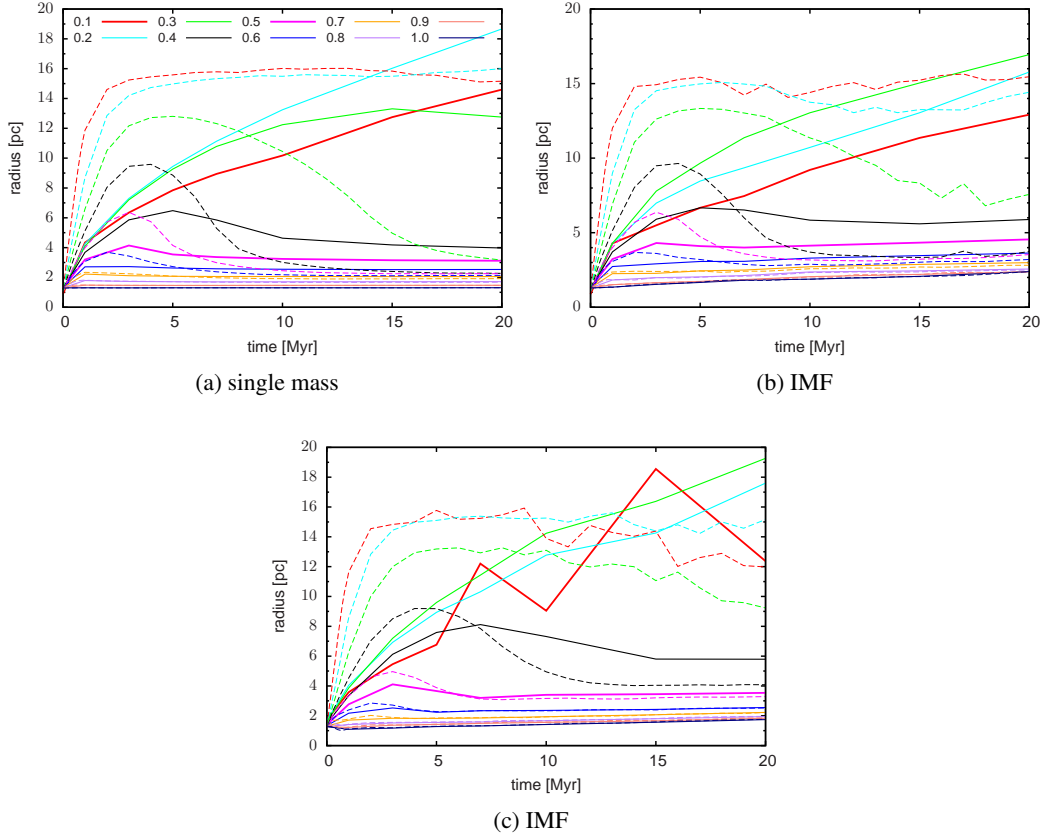


Figure 5.6: Evolution of the half-mass radius of stars bound (solid lines) and stars associated (dashed lines) to star clusters with different  $\varepsilon$ . Shown are the evolutions of clusters consisting of single-mass stars and clusters with stars sampled from the Kroupa (2002) IMF.

which is much slower than the decrease of the associated mass. At this time the rate of the decrease of the associated mass has also reduced noticeably because at this instant the decrease of the associated mass is driven by stars with velocities much lower than after 1 Myr when the fastest stars passed the 20 pc cut-off. However, the mass loss rate remains being faster than for the bound mass. This results in the associated mass of the clusters being smaller than the bound mass which also means that the bound clusters have grown beyond the 20 pc cut-off radius.

After about 15 Myr the evolution of the associated mass begins to be determined by the evaporation and ejection of stars from the cluster because all high-velocity stars have at this instant left the clusters. As from this point on both the bound and the associated masses of the clusters are determined by the same process, their evolutionary rates become the same. This means that the difference in the bound and associated mass of the clusters do not change any more after this point in their evolution.

Fig. 5.6 shows the evolution of the half-mass radii of stars bound to the star clusters (solid lines) and stars that are associated to the clusters (dashed lines) for the simulated single-mass, IMF and binary clusters. The large scatter of star clusters with small  $\varepsilon$  especially for the binary cluster is due to the small numbers of stars remaining bound to the cluster (see Fig. 5.5c).

The half mass radius of the bound stars directly after the gas loss is smaller than the initial half mass radius of the complete clusters and differs more, the smaller the  $\epsilon$  of the cluster is. For example bound stars in clusters with a  $\epsilon = 0.1$  have an initial half-mass radius of 0.9 pc while bound stars in clusters with an  $\epsilon = 1.0$  (clusters that do not loose any mass initially) have an initial half-mass radius of 1.3 pc. The dependence of the initial half-mass radius on the  $\epsilon$  is explained by the preferential loss of stars at the cluster outskirts during the instantaneous gas loss. The result of this is that the remaining bound stars are more concentrated towards the cluster which expresses itself in a smaller half-mass radius.

The evolution of the half-mass radius, which corresponds to the 50% Lagrangian radius, of the bound stars basically proceeds as has already been shown for the Lagrangian radii of all cluster stars. Due to the initial mass loss the bound clusters (from here on meaning the agglomerate of bound stars) expand. During this first expansion phase, the single-mass and IMF clusters expand with almost the speeds while the expansion velocities of the binary clusters is always slower. The reason for that is that the binary clusters do not only cool by their expansion, but also can cool by the destruction of wide binaries so that the expansion of the clusters is decelerated faster than in the other clusters. This even leads to binary clusters with  $\epsilon = 0.9$  and  $\epsilon = 1.0$  to contract initially before they start to expand due to the ejection and evaporation of stars.

Depending on the  $\epsilon$  of and the mass-function used to setup the clusters, the clusters undergo a rebound after which their radii expand much slower than before due to the ejection and evaporation of stars or continues to expand without any boundary. In general, the rebound occurs for clusters with  $\epsilon > 0.3$  with the exception of single-mass clusters with  $\epsilon = 0.3$ . The instant the rebound of the bound clusters starts is about the same for the single-mass, IMF and binary clusters but binary clusters with  $\epsilon = 0.4$  where the rebound is delayed by about 2Myr. As a result, the half-mass radii of binary clusters with  $\epsilon = 0.4$  exceed that of the single-mass and IMF clusters and remains so till the end of the simulation.

The half-mass radii of all clusters with  $\epsilon \leq 0.3$  (except the single-mass clusters with  $\epsilon = 0.3$ ) do not show any signs to stop their expansion implying that these clusters will completely disperse. In fact, as Fig. 5.5 has already shown, at the end of the simulations these star clusters contain any a minor fraction of the stellar mass, they possessed in the beginning

The evolution of the half-mass radii of the associated clusters (from here on meaning the agglomerate of stars that can be found within 20 pc from the cluster centre) proceed similar to the evolution of the half mass radius of the bound clusters. However, particularly for clusters with low  $\epsilon$  differences occur which have serious implications for the later discussion of the evolution of leaky-clusters in general.

The initial expansion of the associated clusters proceeds faster than for the bound clusters independent of the cluster type. The lower the  $\epsilon$  of a cluster is, the larger is the difference in the expansion velocity. The result of this is that independent from the  $\epsilon$  of the clusters and its cluster type the half-mass radii of the associated stars is larger than the half-mass radius of the corresponding bound



stars. In contrast to the bound clusters, where only clusters with  $\varepsilon > 0.3$  stopped their expansion, all associated clusters cease their expansion after about 4 – 5 Myr. Afterwards, the half-mass radius of clusters shrink and becomes smaller than the half-mass radius of the bound clusters during the following evolution if their with  $\varepsilon \geq 0.3$ . Like for the bound clusters, the time of the rebound and its extent depend on the cluster model, so that the binary clusters recollapse latest and the smallest degree. Instead of recollapsing, the half-mass radius of clusters with  $\varepsilon < 0.3$  become constant at a value of about 15 pc which is caused by the cut-off radius of 20 pc used here to determine associated stars.

The reason that the associated clusters initially expand faster than the bound clusters is that they do not only contain the slow bound stars, but also the fast unbound stars that reside within the 20 pc radius applied here to determine associated stars. Initially, all stars fulfil this requirement and are therefore marked as being associated to the cluster (see also Fig. 5.5a). As both the bound and unbound stars have been part of the cluster before the cluster lost its gas, their average distances to the cluster are comparable. During the following evolution of the clusters, the average distance of the unbound stars becomes much larger than the average distance of the bound stars because the unbound stars will leave the cluster on radial tracks while the bound stars will stay inside the bound cluster. The result of this is that the half-mass radius, which corresponds to the average distance of stars to the cluster centre in the single mass case, of the associated cluster is larger than that of the bound cluster alone because the unbound stars enlarge it.

However, during the evolution of the clusters, not all stars necessarily stay within the 20 pc cut-off radius. As has been shown in Fig. 5.5a, significant numbers of stars pass the cut-off radius in single-mass clusters with  $\varepsilon$  as high as 0.8. This means that in these clusters, the importance of the unbound stars decreases with time. As a result, the half-mass radius of the associated clusters decreases towards the half-mass radius of the bound clusters which itself decreases if the cluster is bound (solid lines in Fig. 5.6a). As the fastest unbound stars leave the detection area before the bound clusters have finished their expansion, this explains why the half-mass radii of the associated clusters rebounds stronger and earlier than the half-mass radii of the bound clusters.

During the evolution of the cluster not only unbound stars may move the 20 pc cut-off radius, but also bound stars can find themselves outside the detection area if the cluster as a whole grows enough. The result of this is that the associated clusters not only become less massive than their bound counterparts (see Fig. 5.5a) but also smaller than these which is reflected by the half-mass radius of the associated clusters with  $\varepsilon \geq 0.3$  becoming smaller than that of the bound cluster.

#### 5.4.1 Comparison with observations

The previous section covered the evolution of massive star clusters undergoing instantaneous gas expulsion. What remains to be done is a comparison between the simulated clusters and the observations of leaky star clusters to see if the simulated clusters evolve similarly as the observed clusters. For this purpose the data used in Pfalzner (2009) to produce Fig. 5.1b will be used (see Tab. 5.1). This data

Table 5.1: Properties of clusters and associations more massive than  $10^3 M_{\odot}$  in the Galaxy.

Identification	Distance [pc]	Age [Myr]	$\log(M_c)$ [ $M_{\odot}$ ]	size [pc]	$\log(\rho_c)$ [ $M_{\odot} \text{ pc}^{-3}$ ]
CYg OB2 <sup>1</sup>	$1.74^{+0.2}_{-0.5}$	1–4	4.4	$5.2^{+0.06}_{-2.5}$	$1.61^{+0.02}_{0.4}$
NGC 6611 <sup>1</sup>	$1.995^{+0.01}_{-0.25}$	1–5	4.4	$5.9^{+0.1}_{-0.8}$	$1.45^{+0.22}_{0.11}$
NGC 2244 <sup>1</sup>	$1.88_{-0.4}$	1–3	3.9	$5.6_{-1.2}$	$1.03^{+0.33}$
IC 1805 <sup>1</sup>	$2.34^{+0.1}_{-0.1}$	1–3	4.2	$7.1^{+0.3}_{-0.3}$	$0.98^{+0.03}$
Ori Ib <sup>1</sup>	$0.363^{+0.2}_{-0.2}$	1.7	3.6	$6.3^{+0.3}_{-0.3}$	$0.55^{+0.11}_{-0.02}$
NGC 7380 <sup>1</sup>	3.73	2	3.8	6.5	0.72
Ori Ic <sup>1</sup>	$0.398^{+0.2}_{-0.2}$	4.6	3.8	$12.5^{+0.6}_{-0.6}$	$-0.15^{+0.12}_{-0.01}$
Ori Ia <sup>1</sup>	$0.380^{+0.2}_{-0.2}$	11.4	3.7	$16.6^{+0.9}_{-0.9}$	$-0.54^{+0.05}_{-0.09}$
U Sco <sup>1</sup>	$0.144^{+0.003}_{-0.003}$	5–6	3.5	$14.2^{+0.2}_{-0.2}$	$-0.59^{+0.06}_{-0.01}$
Lower Cen-Crux <sup>1</sup>	$0.116^{+0.002}_{-0.002}$	11–12	3.3	$15.0^{+0.3}_{-0.3}$	$-0.85^{+0.05}_{-0.01}$
Upper Cen-Lup2 <sup>1</sup>	$0.142^{+0.002}_{-0.002}$	14–15	3.6	$22.1^{+0.4}_{-0.4}$	$-1.05^{+0.01}_{-0.01}$
I Lac 2 <sup>1</sup>	$0.368^{+0.06}$	12–16	3.4	$20.7^{+3}_{-3}$	$-1.15^{+0.2}_{-0.17}$

<sup>1</sup>Wolff *et al.* (2007), and references therein. Taken from Pfalzner (2009).

set is based on the observation by Wolff *et al.* (2007) of young (age < 20 Myr) star clusters and can be regarded as being self-consistent in the sense, that all cluster parameters have been determined with the same methods, excluding that additional errors due to the usage of different observational methods is introduced into the data.

Here the problem arises, that observers are not capable to distinguish between bound and unbound stars in a star cluster and have to define a cut-off radius within which all stars are treated as being associated to the cluster (see also discussion to Fig. 5.5 and Fig. 5.6). As has also been shown there, the ratio of unbound and bound stars inside the clusters shifts towards bound stars, as more and more fast moving unbound stars Leave the cluster. This means that after some time, only bound stars remain within the cluster so that an observer to is able to distinguish the cluster masses and sizes correctly making the use an cut-off radius dispensable from this point on and the real, bound clusters can be observed by the observers.

The observations shown in Fig. 5.1b also were subject to this restrictions so that also the simulated clusters have to be treated in the same way if they shall be compared with the observations. For this reason, from now on all cluster masses and sizes shown here will be initially be determined from all stars associated to the clusters (stars within 20 pc from the cluster centre). As soon as the mass of bound stars exceeds the mass of the associated stars, the cluster masses and sizes will be determined from the bound stars alone. So from now on “cluster” denotes either the agglomeration of stars associated to the cluster if their mass exceeds the mass of the bound stars or the bound stars alone otherwise. The transition between these two definitions occurs after about 5 – 20 Myr depending on the  $\varepsilon$  of the cluster and is determined from Fig. 5.5.

To determine the size of their observed clusters Wolff *et al.* (2007) measured the average distance of

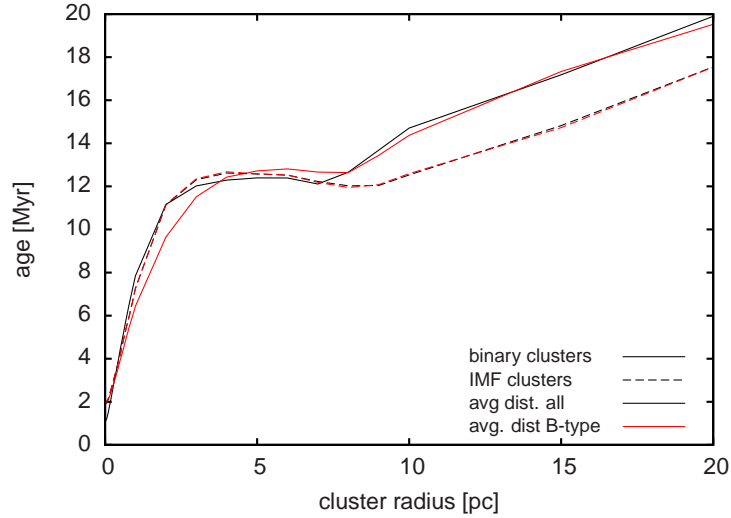


Figure 5.7: Cluster sizes as function of the cluster age for IMF (dashed lines) and binary (solid lines) clusters. Cluster sizes have been determined either by calculating the average distance of all stars to the cluster centre (black lines) or of the B-type stars only (red lines).

all B-type in the cluster to the cluster centre. Here, the average distance of all stars to the cluster centre has been used because in the single-mass clusters, this definition of the cluster size is not applicable as no B-type stars are present in these clusters. However, as is shown in Fig. 5.7 the so determined cluster size does not differ significantly from the cluster size determined by the average distance of the B-type stars to the cluster centre. Future studies of the evolution of leaky clusters should however use the cluster size given by the B-type stars especially if some sort of primordial mass segregation is included into the simulations. In this case the relatively massive B-type stars would be expected to reside closer to the cluster centre than the average cluster star, therefore resulting in smaller cluster sizes.

Fig. 5.8 shows the evolution of the so determined cluster masses, sizes and the resulting density as a function of the cluster size. This unusual form to show the evolution of star clusters has been chosen to first allow direct comparison to the observations and to be able to see, if the simulated clusters follow the evolutionary track, that is suggested by Fig. 5.1b. First the results for clusters with  $\epsilon = 0.3$  will be shown and the effect of lowering or rising the  $\epsilon$  will be investigated afterwards (see Fig. 5.10). Previous theoretical and observational studies (Kroupa *et al.*, 2001; Baumgardt & Kroupa, 2007; Lada & Kylafis, 1999; Elmegreen *et al.*, 2000) have shown that the usual star formation efficiency in giant molecular clouds is about 30%. So, if the observed clusters also have undergone instantaneous gas expulsion, it can be expected that the cluster masses and sizes of the simulated and the observed should be very similar.

Fig. 5.8 I) shows the evolution of the cluster radius of single-mass, IMF and binary clusters with time. In addition, the evolutionary tracks have been coloured in the same way as in Fig. 5.1b so that all data points with ages below 4 Myr are coloured red, data points between 4 Myr and 10 Myr

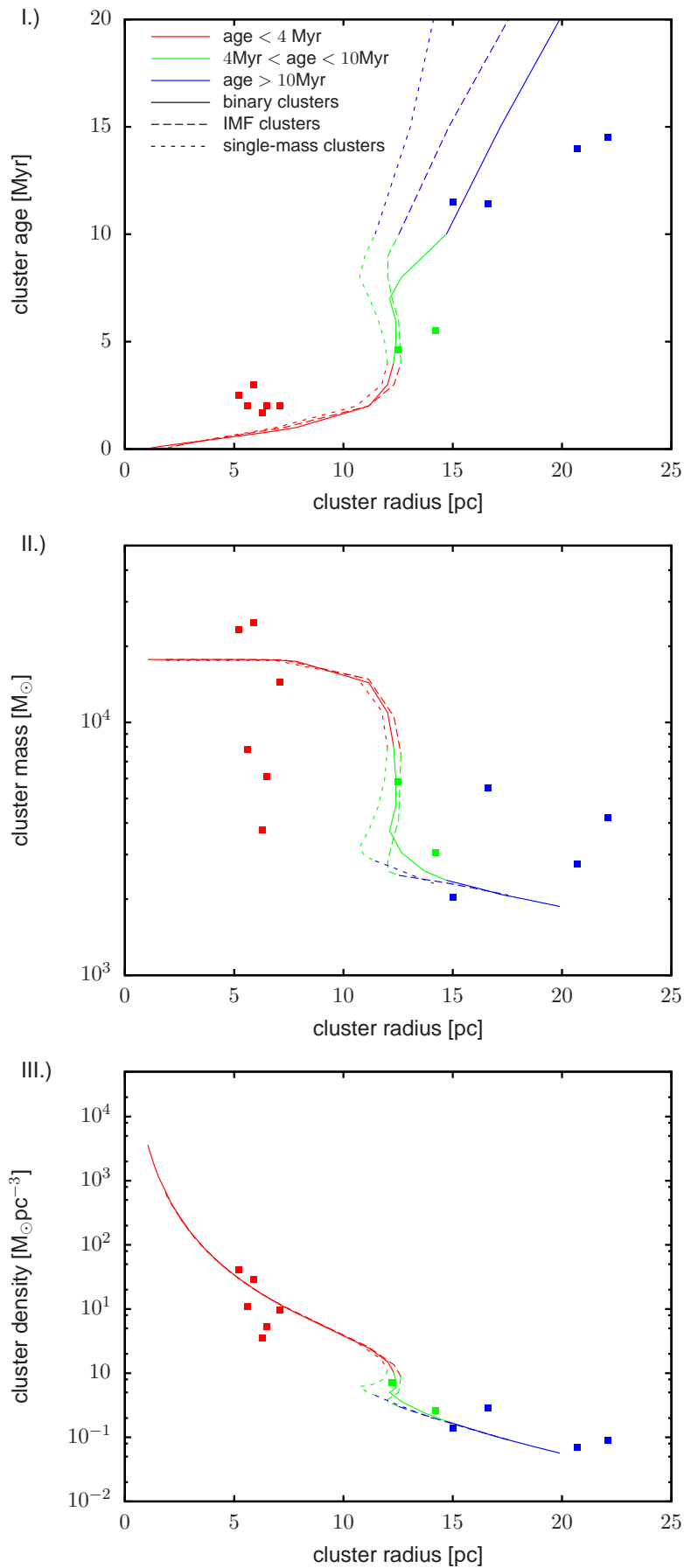


Figure 5.8: Cluster age vs cluster radius (I), cluster mass vs cluster radius (II) and cluster density vs cluster radius (III) plots for single-mass (short dashed lines), IMF (long dashed lines) and binary clusters (solid lines) for star clusters with  $\epsilon$  of 0.3. Data points represent clusters from Tab. 5.1 taken from Pfalzner (2009).

are coloured green and data points older than 10 Myr are coloured blue. As will be shown in the following, this colours chosen by Pfalzner (2009) match rather nicely the three evolutionary phases of star clusters after instantaneous gas expulsion.

The first evolutionary phase of leaky star clusters after instantaneous gas expulsion is characterised by the expansion of the clusters. During this time, the clusters are a mixture of bound and unbound stars and are initially about 3 times smaller than the sizes of the youngest observed star clusters which have sizes of about 5 pc. However, due to the rapid expansion caused by the gas expulsion at  $t = 0$ , the simulated clusters grow larger than the observed star clusters within less than 2 Myr, which corresponds to the observed age of the youngest clusters in Fig. 5.1b.

The second evolutionary phase starts after about 4 Myr, when the simulated clusters begin to grow beyond the 20 pc cut-off radius and begin to be dominated by the bound stars. During this transitional phase the expansion of the cluster slows significantly down. After about 5 Myr, the single, IMF and binary clusters stop their expansion after which for the first time notable differences in the sizes of single-mass, IMF and binary cluster become apparent. While at this time all clusters have expanded to a size of  $\approx 12$  pc which fits the observed size of NGC 7380, the smaller of the two observed cluster in this time regime, the single-mass and IMF clusters begin to shrink afterwards by almost 2 pc over the next 4 Myr while the binary clusters do not shrink significantly. The result of that is that mutual difference between the sizes of single-mass and binary stays almost the same while the binary clusters begin to grow larger than the single-mass and IMF clusters.

During the third and last evolutionary phase the clusters are dominated by the bound stars and therefore expand due to the loss of stars through the ejection and evaporation of stars in stellar encounters. In contrast to the second evolutionary phase, which started at about the same time for all clusters, the binary clusters enter the third evolutionary phase after about 7 Myr while the single-mass and IMF clusters enter it about 1 Myr later. From this point on the expansion of the IMF clusters proceed faster than for the single-mass clusters so that the difference between their sizes increases with time. The expansion of the binary clusters is also driven by encounters so that their expansion velocity is very similar to that of the IMF clusters. The result is that the difference between the IMF and binary cluster sizes remains almost constant during the rest of the simulation. During the final phase of the cluster evolution, the sizes of the binary clusters match the observations best, as they are largest throughout this phase. However, even the binary clusters fail to explain the sizes of the oldest clusters in the sample (Upper Cen-Lup2 and I Lac 2), which at an age of about 14 – 15 Myr have sizes of about 22 pc at while the binary clusters only have sizes of about 17 pc. Possible explanations for this deviations are incorrect determinations of either the cluster size or age during the observations or that other physical processes not included into this study enlarged the clusters further than the gas expulsion is capable of alone.

Fig. 5.8 II) shows the evolution of the stellar mass of the clusters as a function of the cluster size. In addition, the cluster age is colour-coded in the same way as in Fig. 5.8 I) so that a direct comparison between these to is possible. All clusters start with an initial mass of about  $17000 M_{\odot}$  and sizes of

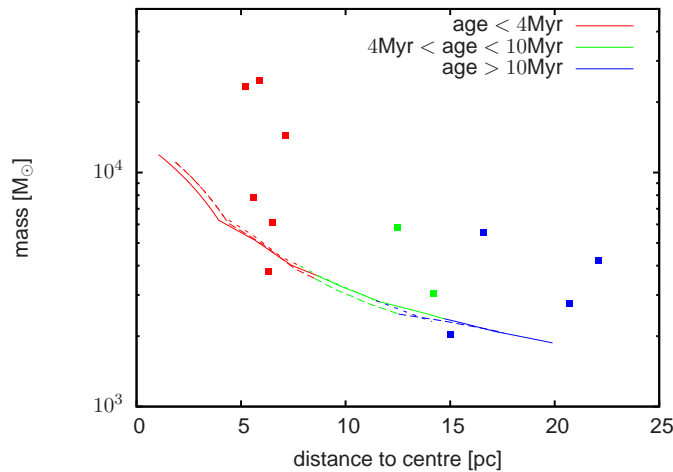


Figure 5.9: Cluster mass vs. cluster radius for single-mass (short dashed line), IMF (dashed line) and binary clusters (solid line) with  $\epsilon = 0.3$ . Only bound stars have been used to generate this figure.

about 2 pc. During the next 3 Myr their masses do not change at all, while over the same time span the cluster sizes increase to about 7 pc so that the simulated cluster sizes and masses fit well to the three observed massive clusters with ages less than 4 Myr (Cyg OB2, NGC 6611 and IC 1805). However, the simulations are not capable to explain the lighter clusters in the sample (NGC 2244, NGC 7380 and Ori Ib). This could mean that either these lower mass clusters already formed with mass lower than assumed in the simulations and do therefore not belong to the type of leaky-clusters investigated here. Alternatively, these clusters could have lost much of their mass due to an another process than the gas expulsion (this seems improbable since such a process must have had only changed the cluster mass and not the cluster radius which is actually not possible) or that the observations were not able to determine the complete mass of the clusters.

However, an additional explanation for the light clusters is possible, if the observations somehow only considered the bound stars in the clusters. In this case the simulations are also able to explain the low mass clusters. This is shown in Fig. 5.9 which shows the same as Fig. 5.8 II) but only for the stars bound to the cluster. By just considering the bound stars of a cluster, its mass after 2 Myr is decreased by almost one order of magnitude in the mass range of the low mass clusters NGC 2244, NGC 7380 and Ori Ib. Since the clusters start to be dominated by the bound stars in the second evolutionary phase, the evolution of the clusters shown in Fig. 5.9 matches the observations well. However, as all data observations should have been performed self-consistently by Wolff *et al.* (2007), it seems improbable that the lower mass clusters only contain bound stars.

As soon as the clusters reach a size of about 6 pc they begin to loose mass as the fastest moving stars pass the 20 pc cut-off and are no more counted as being associated to the cluster. During the following evolutionary phase, the mass loss accelerates while at the same time the expansion of the clusters slows down. The result is that the clusters enter a phase in their evolution, in which they loose a major fraction of their mass (about 85% of their stellar mass before the gas loss) but remain at the

same size (binary clusters) or even shrink if they undergo a rebound (single-mass and IMF clusters). The mass and sizes of all simulated clusters in this evolutionary phase fit to the observed values of Ori Ic, the younger of the two intermediate age clusters observed by Wolff *et al.* (2007). In contrast the size and mass of U Sco, the older of the two intermediate aged clusters, can only be explained if the cluster had a primordial binary population, as the single-mass and IMF clusters fail to evolve to sizes comparable to U Sco within the lifetime of the cluster.

After this transitional phase which is characterised by decreasing cluster masses but constant cluster sizes, the clusters begin to expand again. At this time, the clusters are made up by bound stars only and loose mass through ejection and evaporation due to stellar encounters in the clusters. As these processes are less efficient than the mass loss due to the instantaneous gas expulsion, the rate at which mass is lost from the system is much lower than before and is similar for IMF and binary clusters. The simulated cluster sizes and masses are in accordance with observations of the oldest clusters, although the observed cluster masses and sizes are in general a bit larger than is found from the simulations. However, the results obtained from the binary clusters, again, yield the best agreement with the observations as their sizes fit the observations best.

Finally, Fig. 5.8 III) shows the cluster density as a function of the cluster size, where the colour, again, gives the age of the clusters. All clusters start their evolution with very high densities of about  $5 \times 10^3 \text{ M}_{\odot} \text{pc}^{-3}$  which decrease by about four orders of magnitude during the first 4 Myr of their evolution due to the cluster expansion (Fig. 5.8 I) and the loss of stars (Fig. 5.8 II). During the second evolutionary phase, the decrease of the cluster density slows down as at this time, the expansion of the clusters ceases (binary clusters) or inverts to a recontraction (single-mass and IMF clusters). However, as at this time the clusters are still loosing mass, the curve of the density plot for the single-mass and IMF clusters features a characteristic semi-circle shape, signalling a decrease in density rather than an increase (see Fig. 5.8 III). After this transitional phase has been completed, the clusters expand again, which exposes in a further decrease of the cluster density during the rest of the simulations. As now both, the expansion and the mass loss of the clusters, proceed much slower than before, the decrease of the density is also much slower so that the density of the clusters reduces only by one order of magnitude during the final 10 Myr of the simulations.

During the whole evolution the cluster densities of the binary clusters match the observations best, although the differences between the single-mass and IMF clusters and the observations only become noticeable during and after the transitional phase of the clusters. However, in comparison to the cluster mass vs. cluster size plot (Fig. 5.8 II) the differences between the observations and calculations are less pronounced making the cluster mass vs. size plot the better plot to decide which cluster model describes the evolution of the leaky clusters best.

The influence of the star formation efficiency on the evolution of star clusters after instantaneous gas loss is examined in Fig. 5.10 which shows the same sequence of plots as Fig. 5.8, but this time for clusters with  $\epsilon = 0.2$  (Figs. 5.10a) and  $\epsilon = 0.4$  (Figs. 5.10b). The trends obtained from Fig. 5.10 are directly applicable to cluster with the other  $\epsilon$  making it unnecessary to show their evolution here.

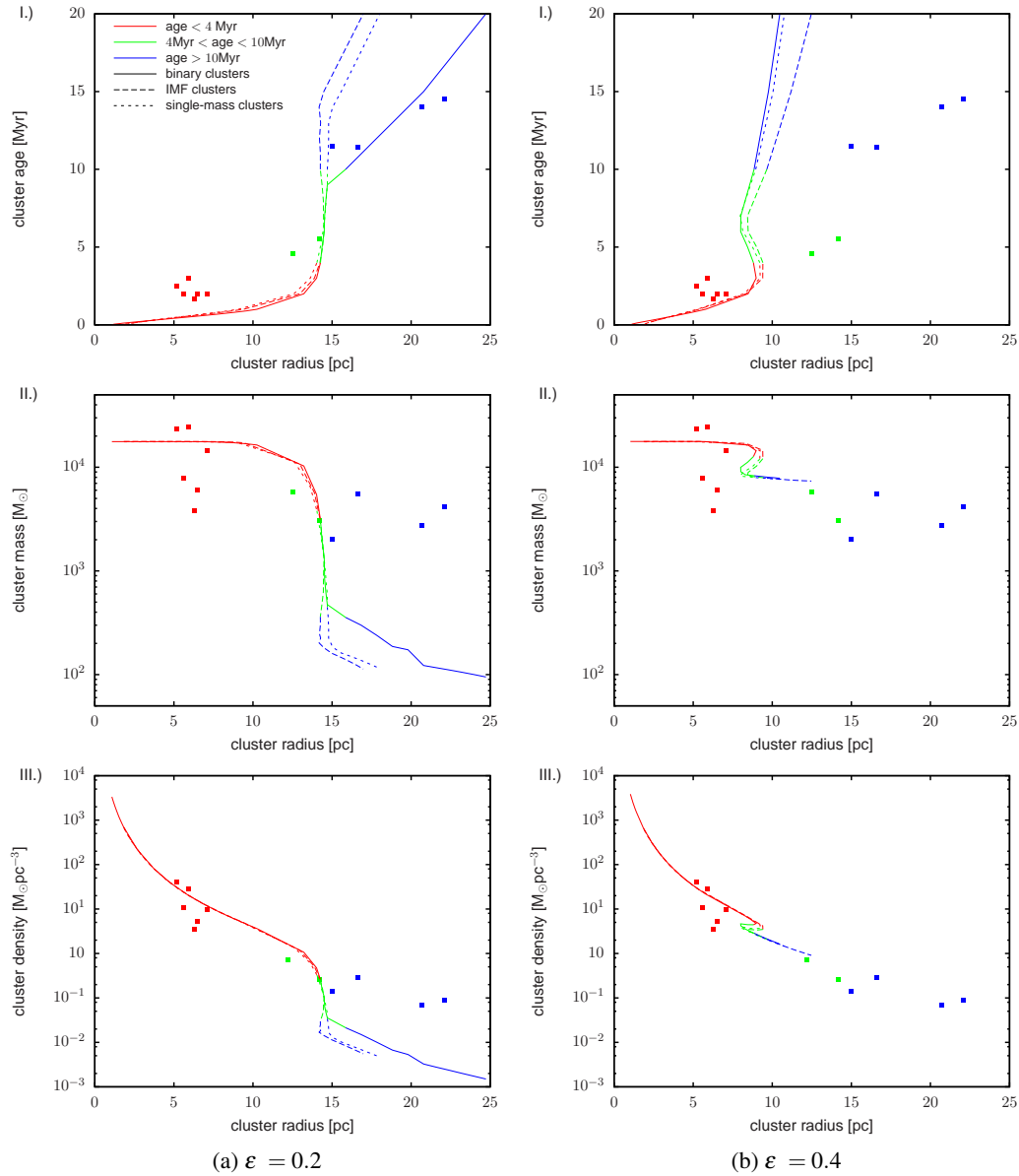


Figure 5.10: Cluster age vs cluster radius (I), cluster mass vs cluster radius (II) and cluster density vs cluster radius (III) plots for single-mass (short dashed lines), IMF (long dashed lines) and binary clusters (solid lines) for star clusters with  $\epsilon$  of 0.2 and 0.4. Data points represent clusters from Tab. 5.1 taken from Pfalzner (2009).

However, for completeness their plots are given in the Appendix (Fig. B.1).

Lowering the  $\epsilon$  in star clusters (Fig. 5.10a I) causes the cluster expansion to proceed faster (see also Fig. 5.6). As a result, the sizes of the single-mass, IMF and binary clusters with  $\epsilon = 0.2$  are significantly larger than the observed sizes of the young clusters in the sample, making them less promising candidates for being the observed leaky clusters. However, their larger sizes make them fit better to the observed cluster sizes of the older clusters. This even leads to the single-mass and IMF clusters having comparable sizes to Ori Ia and Lower Cen-Crux and the binary clusters having sizes



that match all observations.

Although these results for the cluster sizes might imply that the observed clusters might have had  $\epsilon$  of 0.2 instead of 0.3, the mass-size (Fig. 5.10a II) and the density-size plot (Fig. 5.10a III) for these clusters exclude this alternative. While during the first evolutionary phase the masses of the star clusters with  $\epsilon = 0.2$  are in accordance with the masses of the youngest observed clusters (remember, here the cluster mass is initially given by the mass of the associated stars and becomes the bound mass as soon it exceeds the associated mass) the cluster masses and therefore the cluster densities in the middle and last evolutionary phase decrease so much, that the simulated and observed values differ by more than a magnitude, showing that these can be regarded as being totally different.

Increasing the  $\epsilon$  to 0.4 in the clusters also doesn't lead to a better correspondence between the simulations and observations. To make this clear Fig. 5.10b I) shows the evolution of the cluster size with time for star clusters with  $\epsilon = 0.4$ . In comparison to star clusters with  $\epsilon = 0.3$ , the expansion of the clusters proceeds much slower and to a lower degree. As a result, the simulated cluster sizes match the sizes of the youngest observed clusters quite well, but do not even get near the sizes of clusters with ages exceeding 4 Myr (see Fig. 5.10b I). To make it even worse, the masses and densities of the clusters with  $\epsilon = 0.4$  are significantly larger than is observed for all clusters older than 4 Myr, although initially their masses are comparable to the observed young clusters. Combining these two shortcomings, which become even more extreme for star clusters with even higher than 0.4 implies, that it can be excluded that the leaky star clusters from Fig. 5.1b had  $\epsilon \geq 0.4$ .

## 5.5 Binary populations in star clusters undergoing instantaneous gas expulsion

In the following the evolution of the binary population itself during after the gas expulsion will be studied here.

Fig. 5.11 shows the evolution of the number of binaries of the binary clusters for all simulated  $\epsilon$ . Here the absolute instead of the normalised numbers used in Chap. 3 and Chap. 4 are shown because all simulations have been set up with the same number of binaries which allows direct comparison of the binary populations between the different clusters.

Similar to the results in Chap. 3 and Chap. 4 the number of binaries in clusters losing no mass ( $\epsilon = 1.0$ ) decreases significantly during the evolution of the clusters from initially  $\approx 9700$  to  $\approx 7600$  binaries, corresponding to a relative loss of about 21% after 20 Myr.

Star clusters that lose mass during the instantaneous gas expulsion ( $\epsilon < 1$ ) do not lose the same amount of binaries during the evolution, but the less the lower the  $\epsilon$  is. For example, while clusters with  $\epsilon = 0.9$  still lose about 19% of their binaries, clusters with  $\epsilon = 0.5$  only lose 6%. For very low  $\epsilon$  ( $\epsilon < 0.4$ ) even an increase of the number of binaries during the evolution of the clusters can happen.

These findings can be explained by the finding in Chap. 4, that the more binaries are destroyed, the higher the stellar density in a cluster. Here all clusters are set up with the same stellar density,

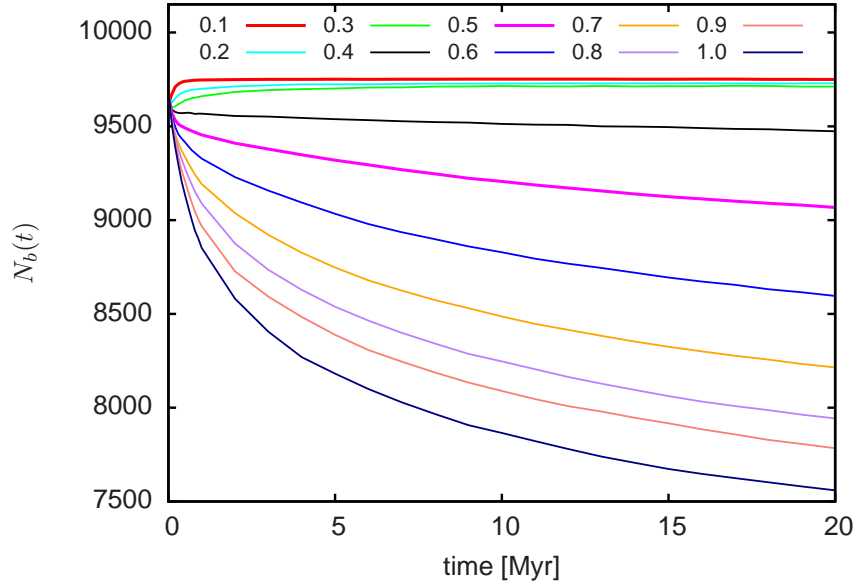


Figure 5.11: Evolution of the number of binary systems in binary clusters with all  $\epsilon$ .

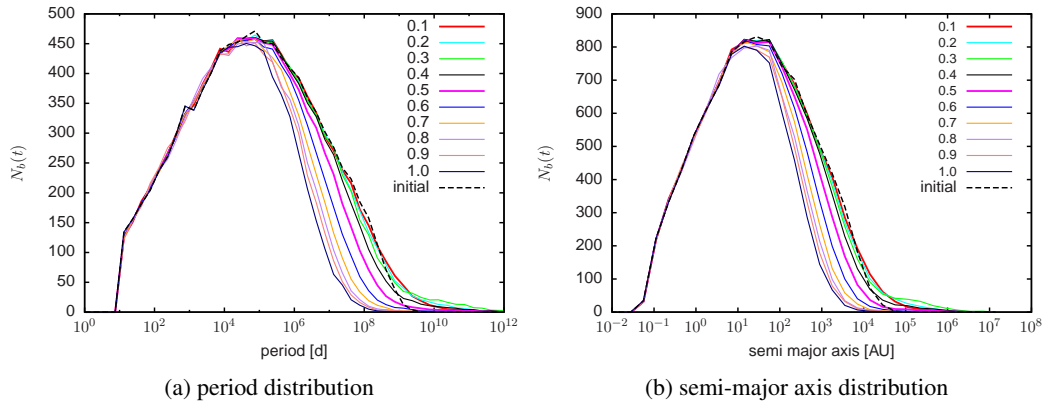


Figure 5.12: Period and semi-major axis distributions in binary clusters after 20 Myr for star clusters with all simulated  $\epsilon$ .

however, due to the expansion caused by the instantaneous gas expulsion, the densities in the clusters decrease (see Fig. 5.8 III) which means that more binaries can survive the dynamical evolution. As the decrease in the stellar density is more pronounced and happens faster the smaller the  $\epsilon$  clusters with smaller  $\epsilon$  also lose less of their binaries after the instantaneous gas expulsion.

The impact on the period distributions of the binary populations is shown in Fig. 5.12 which shows the period and semi-major axis distributions of all simulated binary clusters after 20 Myr plus the initial period distribution of the  $\epsilon = 1.0$  clusters for reference. The dynamical evolution of the clusters only affects wide binaries with periods exceeding  $10^5$  d and leaves binaries with shorter periods completely unaffected independent of the  $\epsilon$  of the cluster.

This cut-off is independent of the  $\epsilon$  of the cluster, however, what clearly depends on the  $\epsilon$  of the

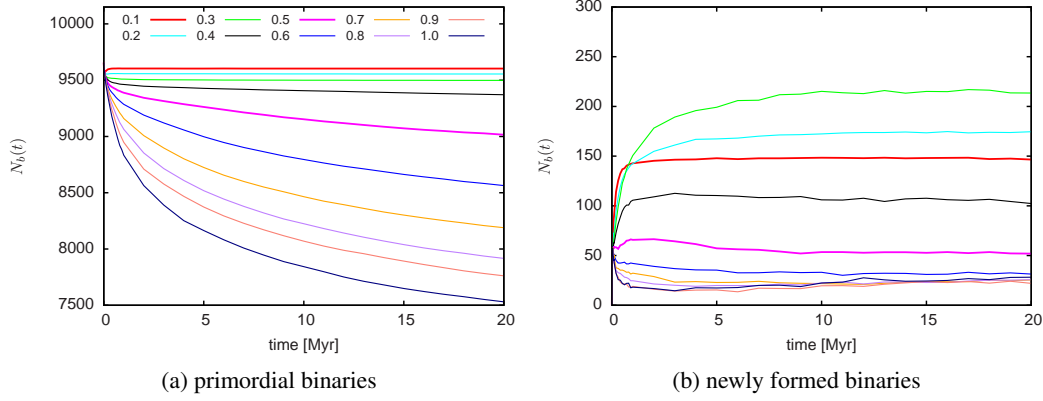


Figure 5.13: Evolution of the number of primordial binary systems and newly formed binary systems in binary clusters with all  $\epsilon$ .

cluster is the amount of binaries at a given period bin that is destroyed during the evolution of the cluster. The higher the  $\epsilon$  of a cluster the higher is the amount of binaries being destroyed. This leads to a deficit of very wide binaries ( $a > 100\text{AU}$ ;  $P > 10^6\text{d}$ ) for clusters with  $\epsilon > 0.6$  in comparison to the initial distribution of periods. For clusters with small  $\epsilon$  the exact opposite happens meaning that while their final and initial period distributions are almost indistinguishable up to periods about  $10^9\text{d}$  ( $10^4\text{AU}$ ), their final period distributions of these star clusters contain much more binaries with periods exceeding  $10^9\text{d}$  than have been present in the beginning.

This findings imply that during the evolution of the clusters considerable numbers of very wide binaries are formed. Newly formed binaries are not directly distinguishable in Fig. 5.11 and Fig. 5.12 and might therefore require to rethink the conclusions on the evolution of binaries in star clusters undergoing instantaneous gas loss. To solve this problem Fig. 5.13 shows the evolution of the number of primordial binaries and the number of newly formed binaries separately. Here a binary is denoted as being primordial, if it has already been detected in the initial time step of the simulation. All binaries that are detected later and do not have a counterpart in the first time step are therefore treated as being newly formed.

The evolution of the number of primordial binaries proceeds as expected and is very similar to the evolution shown in Fig. 5.11. The lower the  $\epsilon$  of the cluster the lower is the fraction of binaries that is destroyed during the evolution of the clusters. This leads to less than 0.5% of all primordial binaries being destroyed in clusters with  $\epsilon < 0.4$  compared to 22% in the  $\epsilon = 1.0$  case. The reason the evolution of the primordial binary population and the overall binary population are so similar is that the primordial binaries dominate the overall binary population by number. Although their number reduces during the evolution of the clusters, there are always minimum 40-times more primordial binaries in the clusters than newly-formed ones.

Basically, the trend for the number of newly formed binaries is a continuation of the trend observed for the primordial binaries. The number of newly formed binaries increases the lower the  $\epsilon$  of the

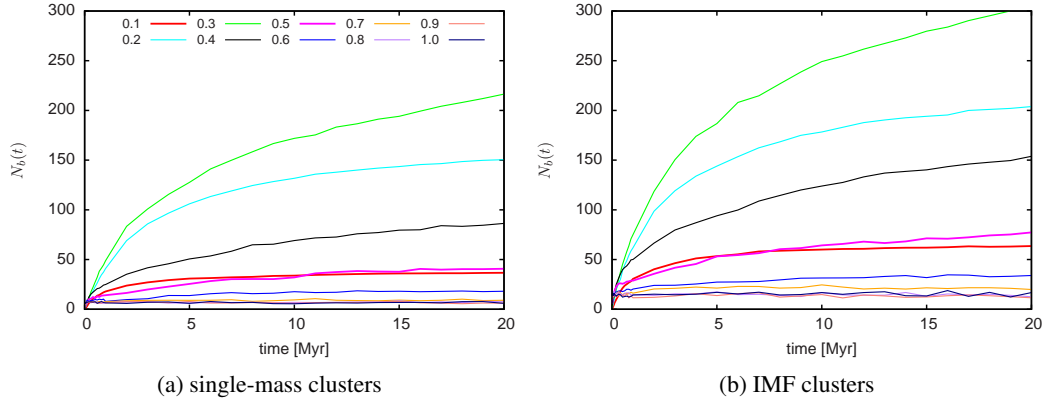


Figure 5.14: Evolution of the number of newly formed binaries in single-mass and IMF clusters for all  $\epsilon$ .

cluster is. However, the formation of new binaries is most effective in clusters with  $\epsilon = 0.3$  and becomes less effective for clusters with smaller  $\epsilon$ . Three different formation mechanisms for the newly formed binaries are possible. i) the binary forms during a usual three-body interaction. During such an interaction, three unbound stars interact gravitationally, leaving behind a bound binary system and a single star. As during this process part of the binding energy of the binary is transferred to the single star, this process heats the cluster. The formation of binaries during three-body interactions requires three stars to be very close in phase space, so that it is most effective in high density regions. However, as the resulting binaries usually are only weakly bound, they are very prone to interactions with other stars in their surroundings so that most of the newly formed binaries will be destroyed shortly after they formed, unless they travel into lower density regions, where such interactions are less probable. ii) the binaries form by chance during the dissolution of the clusters. This process has been introduced by Kouwenhoven *et al.* (2010) and relies on two stars becoming bound, because they are ejected from a cluster into the same direction with almost the same velocities. iii) the binary isn't a real new binary, but is an primordial one that has not been detected in the first time step in the simulations. This can happen if, for example, the secondary star of a wide binary is not the nearest neighbour of the primary so that these two stars are not even considered as binary candidate (see Sec. 3.2.1 to see how binaries are defined here). However, as these two stars are physically bound, they will both travel in the same direction while the third, disturbing star, will most likely depart from the primary star. As a result, the two stars are now recognised as being a “new” binary. This process is most likely to occur in low density regions and is therefore more effective in clusters with low  $\epsilon$ .

The first two formation scenarios do not require a primordial binary population and should therefore also work in the single-mass and IMF clusters. To verify this Fig. 5.14 shows the evolution of the number of newly formed binaries in these clusters. As expected also here binaries are formed during the cluster evolution. However, the number of binaries actually formed depends on the cluster type that is used. In general, most binaries are formed in IMF clusters, followed by the binary and single-

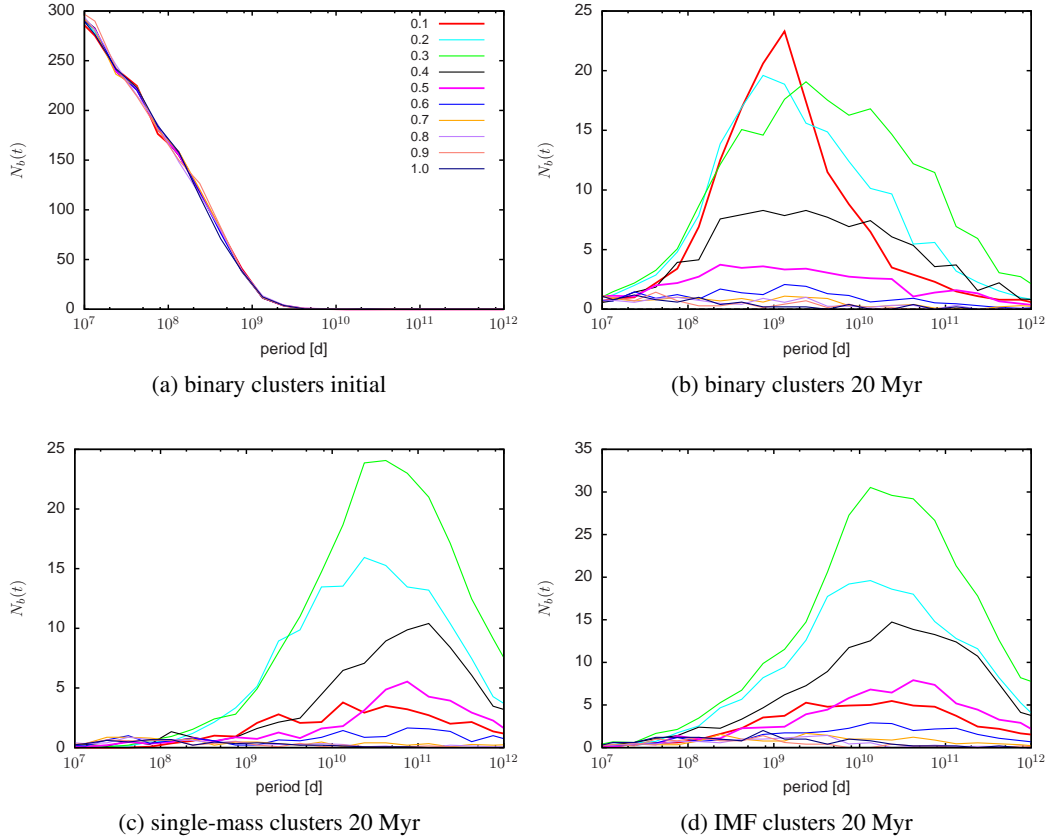


Figure 5.15: Initial period distribution and period distribution of newly formed stars after 20 Myr for binary clusters with all  $\epsilon$ .

mass clusters. The reason for this is that in star clusters consisting of stars with a mass spectrum stellar encounters become more important than in single mass clusters (see also discussion to Fig. 5.4). The reason less binaries are formed into the binary clusters is that in these clusters many stars are already bound in binaries meaning that they are not free to participate in a new one. This does not mean that these stars are not able to form other, higher-order, bound systems like triples or quadruples. However, as here no explicit search for such systems has been taken out, no statements of their evolution can be given here.

Although the evolution of the number of newly formed binaries in single-mass, IMF and binary clusters is very similar for clusters with the same  $\epsilon$  on major exception exists for cluster with  $\epsilon = 0.1$ . While the number of newly formed binaries in the single-mass and IMF clusters with  $\epsilon = 0.1$  is about the same number as for clusters with  $\epsilon = 0.5$ , the number of newly formed binaries in binary clusters with  $\epsilon = 0.1$  is even higher than the number of new binaries in binary clusters with  $\epsilon = 0.4$ . The reason for this is the third formation mechanism mentioned above. A significant fraction of the binaries marked as being formed in the binary clusters are not really formed during the evolution of the clusters, but are initially not detected by the code and therefore treated as being formed during the evolution.

This explanation is strengthened by the period distribution of the newly formed binaries which is shown in Fig. 5.15 for all simulated single-mass, IMF and binary clusters in the restricted period range from  $10^7 - 10^{12}$ d. For reference the initial period distribution of the primordial binaries in the binary clusters is shown over the same period range. While the period distributions of the single-mass and IMF clusters are very similar, the period distribution of the newly formed binaries in the binary clusters shows remarkable differences. So do the single-mas and IMF clusters form binaries with periods exceeding  $10^7$ d, however only very few binaries have such low period so that the majority of the new binaries in these clusters have periods  $> 10^8$ d and have their maximum around  $2 \times 10^{10}$ d. In contrast to that the period distribution of the newly formed binaries in the binary clusters is peaked at a period of about  $10^9$ d and consists of many more binaries with periods in the  $10^7 - 10^{10}$ d period range. Since these binaries are not formed in such high numbers in the corresponding single-mass and IMF clusters, this implies that these binaries didn't actually form during the evolution of the cluster, but haven't just been marked as being primordial because they haven't been found in the initial time step. This means that the number of newly formed binaries in the binary clusters given in Fig. 5.13 most likely overvalues the real number of binaries formed during the evolution, especially for clusters with  $\varepsilon = 0.1$ . However, this does not interfere with the conclusions drawn so far as this simply means, that the binary formation in the binary clusters is even more ineffective as has been stated before.

Fig. 5.16 shows the primary mass distribution of the newly formed binaries after 20 Myr in single-mass, IMF and binary clusters separately. As reference for an primary mass distribution for an randomly-paired binary population, the initial primary mass distribution of the primordial binaries in the binary cluster is shown additionally. The first thing to mention is that the primary mass distribution of the single-mass clusters does not show any features, as the clusters only consist of stars with the same mass. The primary mass distribution of the newly formed binaries in the binary clusters is very similar to the primary mass distribution of the primordial binaries, again showing that part of the newly formed binaries in the binary clusters are not really new ones, but haven't not be recognised as being primordial as they have not been found in the first time step.

The primary mass distribution of the newly formed binaries in the IMF clusters does not suffer from this and shows remarkable differences to the primary mass distribution of the randomly paired binaries Fig. 5.16a. While in both populations binaries with primaries over the entire mass range are present, the newly formed binaries on average have higher primary masses than the randomly paired ones, which manifests itself in the shape of the primary mass distribution. While for the randomly paired binaries the primary mass distribution is raising for small primary masses until it reaches its maximum around  $0.6M_{\odot}$  and sharply declines afterwards as it is predetermined by the Kroupa (2002) IMF, the primary mass distribution of the newly formed binaries does not decrease after reaching its maximum but forms a broad peak up to masses of about  $10M_{\odot}$ , after which the number of binaries decreases. This finding implies, that the formation of the new binaries is not a totally stochastic process, but prefers stars with high masses. Both, the formation of binaries during a three-body interaction and by chance during the cluster dissolution also predict such a dependence on

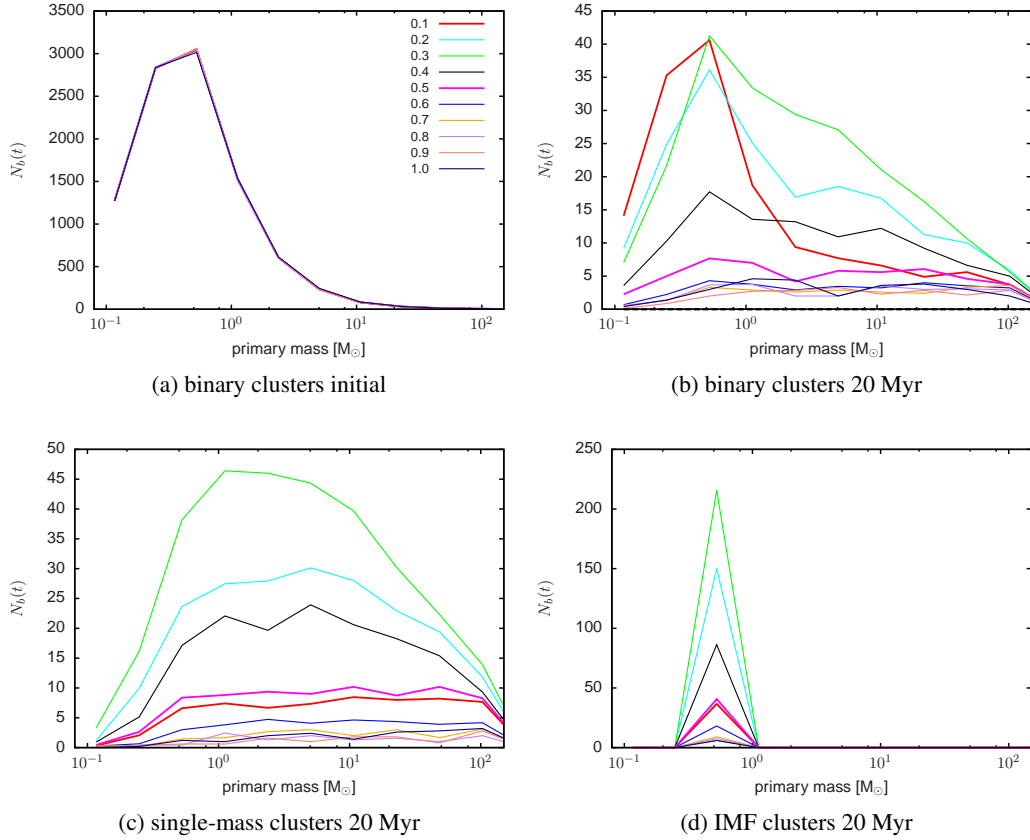


Figure 5.16: Initial primary mass distribution and primary mass distribution of newly formed stars after 20 Myr for binary clusters with all  $\epsilon$ .

the primary mass, as higher mass stars have a higher probability to experience a three-body interaction and higher mass stars allow higher velocities of the secondary star if both have to be bound.

Fig. 5.17 shows the mass ratio distribution resulting from the single-mass, IMF and binary clusters after 20 Myr plus the initial mass ratio distribution of the primordial binaries in the binary clusters. Again, the mass ratio distribution of the single-mass clusters does not provide much information, as all binaries in these clusters naturally have mass ratios of one. The mass ratio distributions of IMF and binary clusters show clearly, that the newly formed binaries preferentially have small mass ratios  $\rightarrow 0$ , meaning that the secondary stars in the newly formed binaries are usually much lighter than the primary. This is in complete opposition to what is found for binaries that are randomly paired as there, all mass ratios appear. The reason the secondary stars in the newly formed binaries are light is that the energy needed to be removed from two stars to bind them is much lower for an unequal-mass binary compared to an equal-mass binary with the same primary mass, as the unequal-mass binary as a whole is much lighter than the equal-mass binary. The increased number of binaries with higher mass ratios in the binary clusters is again explained by binaries, that haven't been marked as being primordial although they are initially bound.

Finally Fig. 5.18 shows the eccentricity distributions of the newly formed binaries in single-mass,

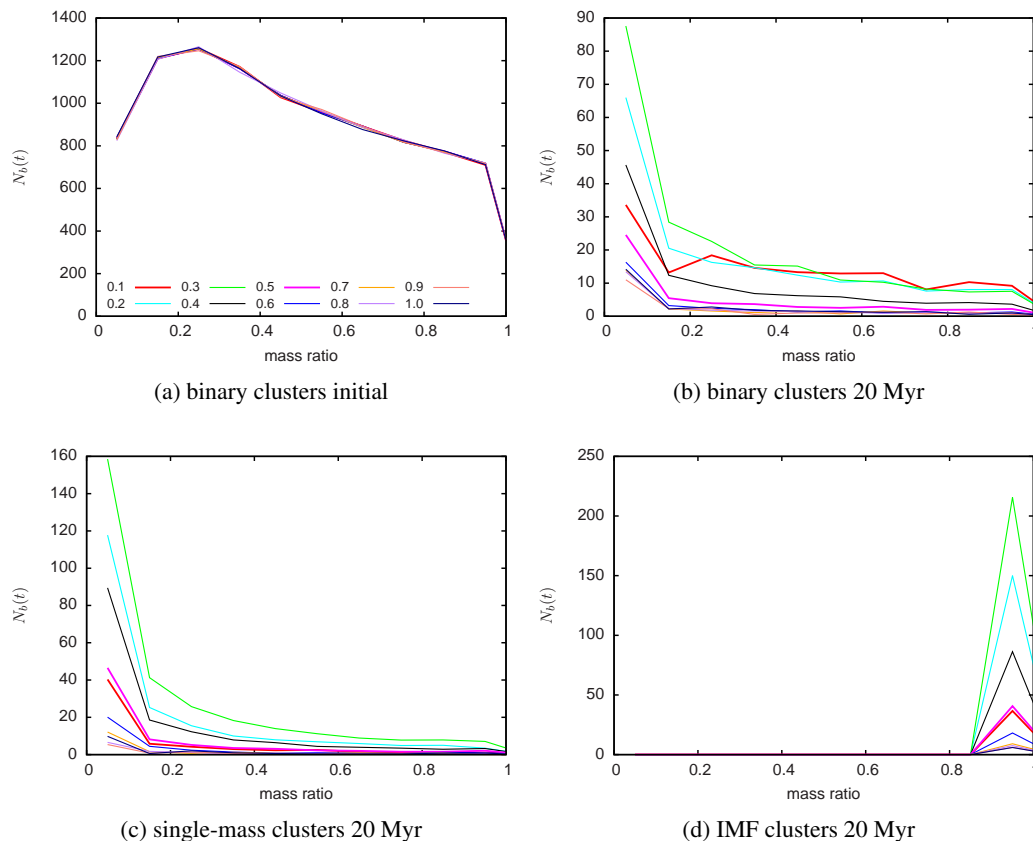


Figure 5.17: Initial mass ratio distribution and mass ratio distribution of newly formed stars after 20 Myr for binary clusters with all  $\epsilon$ .

IMF and binary clusters after 20 Myr plus the initial eccentricity distribution of the primordial binaries in the binary clusters. Clearly, the eccentricity distributions of the newly formed binary in all clusters are very similar and correspond to the thermal eccentricity distribution which was also used to set up the primordial binary population in the binary clusters.

## 5.6 Summary

In this chapter it was investigated how the binary population evolves if the cluster is not in dynamical equilibrium but expands rapidly at the end of the star formation process due to instantaneous gas expulsion.

The simulations have been performed for massive clusters ( $\approx 18000M_{\odot}$ ) that loose their remnant gas at  $t = 0$  with star formation efficiencies varying between 0.1 – 1.0. Both cases, where i) all stars are initially single or ii) a binary population is present at the beginning of the simulation have been investigated.

- The general reaction of the star clusters to the instantaneous gas expulsion is a expansion which is accompanied by loss of stars. A relatively good agreement between the simulations and the



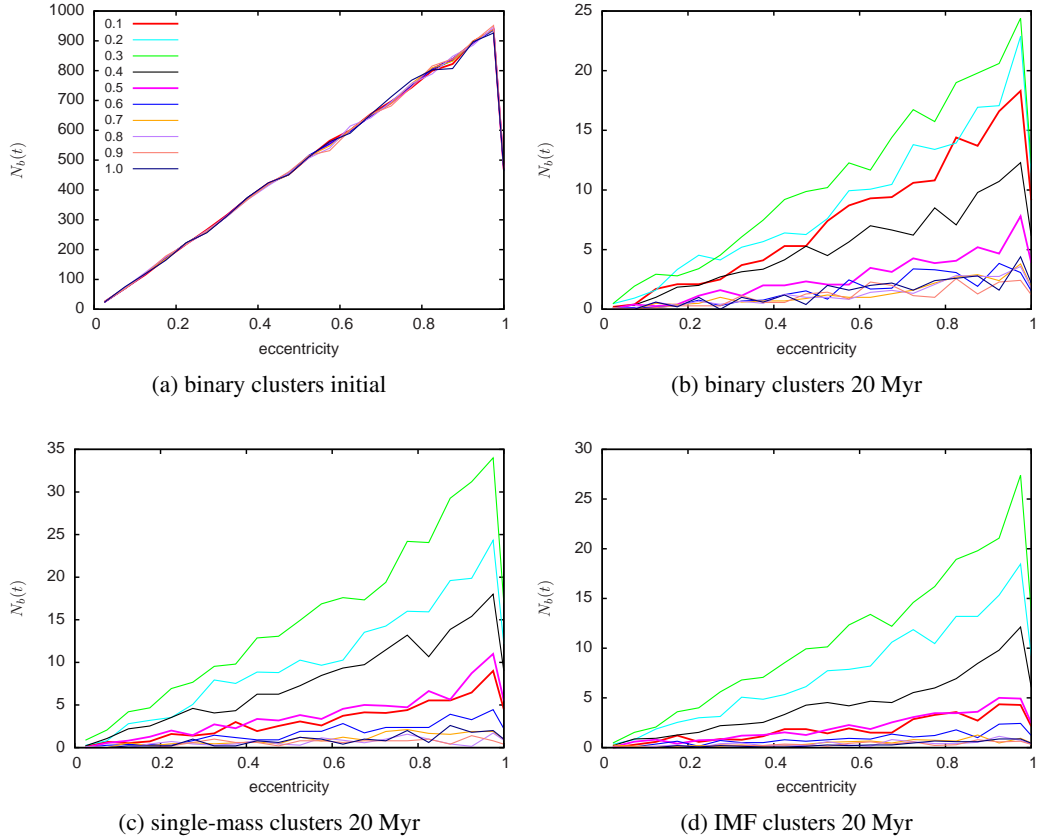


Figure 5.18: Initial eccentricity distribution and eccentricity distribution of newly formed stars after 20 Myr for binary clusters with all  $\epsilon$ .

observed cluster sequence for leaky clusters was found for single-star clusters with  $\epsilon = 0.3$ . However, the simulated cluster sizes at the end of the simulations are smaller than is observed (Pfalzner & Kaczmarek, in preparation).

- Performing the simulations including primordial binaries, the clusters expand faster and to a larger degree ( $\approx 17\text{pc}$  after 20Myr in the single star case,  $\approx 20\text{pc}$  in simulations including binaries) while losing the same amount of mass as the single star clusters - so the observed cluster sequence is now perfectly matched. The tight binaries act as additional energy sources in the clusters. However, as the binaries slowly provide the energy to the clusters, they are able to react on this energy growth by adiabatic expansion that proceeds without any further loss of stars. So binaries contribute noticeably to the expansion of massive clusters.
- The evolution of the properties of the binary populations in expanding star clusters differs significantly from star clusters in virial equilibrium. With decreasing  $\epsilon$  equivalent to a more prominent and faster cluster expansion, less binaries are destroyed due to the rapid decrease in stellar density. So more binaries can survive the dynamical evolution of the clusters.
- In addition, in expanding clusters significant numbers of new binaries are formed. So for clus-

ters with  $\varepsilon < 0.3$  more binaries are present after 20Myr of cluster evolution than in the beginning of the simulations. However, almost all newly formed binaries are wider than  $P > 10^9$ d. This means that they do not really replace binaries that are destroyed during the embedded phase of the cluster. As a result the shape of the evolved binary population in expanding clusters differs from that in clusters in virial equilibrium.

## 6 Discussion

In this thesis it was shown, that the natal environment has serious influence on the evolution of binary populations. An extensive set of numerical simulations of binary populations in star clusters have been performed. However, they are subject to certain limitations due to the here applied assumptions. In the following the most serious limitations and their influence on the results will be discussed.

The first assumption is the star cluster model used to set up the simulations. In Chap. 3 and Chap. 4 the ONC cluster model described by Olczak *et al.* (2006) was used. The reason for choosing this model is that the early evolution of the cluster was investigated and this model has proven to evolve during the assumed lifetime of ONC (= 1Myr) to agree well with the ONC as it is observed today. However, this does not mean, that star clusters have to necessarily form in this way. For example, instead of the here modelled primordial mass segregation, the cluster model could initially be in a subvirial state which still could lead to the same degree of mass segregation as it is observed today in the ONC (e.g. Allison *et al.*, 2009; Olczak *et al.*, 2011). Although changes in the initial star cluster model could have serious influence on the absolute numbers of binaries being destroyed, the main result, the independence of the evolution of the binary population on the initial binary frequency of the clusters should not change. This means that the shape of the evolutionary function  $N_b(t)$  might be slightly different for a given star cluster model. However, it will remain being the same for a given star cluster model if the initial binary frequency is change.

A related assumption is the presumed synchronism of star formation. Currently, it is open if all stars form during a single, short star formation event (e.g. Jeffries *et al.*, 2011) or if the stars form over longer timescales (e.g. Huff & Stahler, 2006; Reggiani *et al.*, 2011). If the star formation, and therefore also the binary formation, would proceed over longer timescales, this would mean that stars stars to interact with each other, while at the same time stars are still formed. In this situation less binaries would be destroyed in the beginning of the evolution of the clusters because the stellar density in the clusters initially would be much lower than in clusters, in which all stars form at the same time. Also it could be expected that more wide binaries should survive the dynamical evolution of the clusters as they keep being formed during the complete evolution of the clusters and therefore could make up for binaries that have already been destroyed. However, this should again not alter the independence of the evolution of the binary frequency on the initial binary frequency but only change the shape of the evolutionary function  $N_b(t)$ .

In Chap. 3 and Chap. 4 the clusters in the simulations did not include gas although they treat the earliest phases of the cluster evolution. Inclusion of the gas would result in a larger velocity dispersion in the cluster which probably would result in more binaries being destroyed. However, as a higher velocity dispersion also means that the duration of the interactions between the stars is shorter this

might cancel out the before mentioned effect.

The gas component also play a major role in the gas induced orbital decay of embedded binaries. During the calculations of the gas-induced orbital decay, which were performed by C. Korntreff, the locations of the binaries within the clusters have been assumed to be constant throughout the calculations so that the gaseous density around them remains constant, too. However, in real star clusters the stars/binaries constantly travel inside the cluster, meaning that the binaries are not always embedded in gas with the same density. Since the trajectories of the stars in the cluster are very chaotic due to the dynamical evolution of the clusters it is difficult to estimate which influence this assumption has on the evolution of the binary population. C. Korntreff is currently working on introducing the gas induced orbital decay of binaries in the NBODY6 simulation code so that this could be answered in the near future.

A related question, that could be answered by this calculations is how the newly formed single stars, that arise through merging stars due to the gas induced orbital decay, will evolve inside the cluster. As these stars are mostly formed in the cluster centre and more massive than the average stars, it can be expected, that they will capture another single star in their surroundings to form new binaries (see also Sec. 4.5 and Pfalzner & Olczak, 2007). These newly formed binaries again could merge into even more massive stars, if enough gas is still remaining in the clusters so that the gas induced orbital decay is effective.

The assumption of instantaneous gas expulsion (Chap. 5) has to be tested. If the gas expulsion does not proceed instantaneously, the expansion of the clusters is much slower and less significant than shown in Chap. 5. This means that more binaries would be destroyed in clusters with low  $\epsilon$  and that probably fewer wide binaries are formed. However, the good agreement between the evolution of the simulated and observed clusters, strongly suggests the gas expulsion has to be very fast as no other process has been shown to cause such a serious expansion of the clusters.

In addition the choice of the primordial binary population and its placement inside the cluster requires discussion. In Chap. 3 and Chap. 5, placing binaries randomly inside the clusters independent of their period leads to the “destruction” of wide binaries that were incidentally placed in the central, denser part of the cluster. However, it seems likely that binaries form with periods that depend on the local density so that wide binaries should only form in the sparse cluster outskirts. This would mean that the evolution of the binary population should depend less strongly on the dynamical evolution of the clusters because the binaries that are capable to be destroyed during a three-body interaction reside in areas of the cluster where only few three-body interaction take place. Also this would not change the major results of this thesis that the evolution of the normalised number of binaries in star clusters does not depend on the initial binary frequency.

## 7 Summary and Conclusions

In this thesis it was investigated how primordial binary populations are affected by their natal environments - namely young, dense star clusters. For this purpose extensive sets of numerical Nbody simulations of binary populations in various kinds of star cluster environments have been performed. First the evolution of binaries in model clusters representing the well known, very young Orion Nebula Cluster (ONC) has been investigated. Afterwards simulations of density-scaled ONC-like clusters have been modelled and it was tested if the conclusions drawn in the first part of the thesis also hold true in clusters with other densities than the ONC. Finally, the evolution of binaries in massive leaky star clusters (Pfalzner, 2009) undergoing instantaneous gas expulsion has been studied.

The main results are the following:

- The evolution of the normalised number of binaries in ONC-like star clusters does not depend on the initial binary frequency. This allows to predict the evolution of the binary population in ONC-like star clusters without the need of costly Nbody simulations or the determination of the initial binary frequency in star clusters if the current binary frequency and age of the cluster are known.
- The increased binary frequency of massive stars observed in the ONC is a natural result of the dynamical evolution of the clusters due to lower destruction rates of binaries with a high mass primary compared to binaries with a low-mass primary.
- The combination of the dynamical evolution with the gas-induced orbital decay of embedded binaries (Stahler, 2010, and the Diploma thesis by C.Korntreff formerly Hövel) can reshape an initially log-uniform period distribution of binaries to the log-normal period distribution of the field binary population.
- The evolution of the normalised number of binaries remains being independent of the initial binary frequency in clusters with arbitrary densities.
- Over a wide stellar density range it holds, that the more and tighter binaries are destroyed the higher the density in a cluster. However, this holds only to a density limit of about  $3 \times 10^4 \text{pc}^{-3}$  above which the environment does not destroy significantly more binaries.
- The general reaction of star clusters on instantaneous gas loss is an expansion accompanied by a loss of stars. The evolution of clusters with a star formation efficiency  $\epsilon = 0.3$  agrees reasonably well with the observed leaky cluster sequence. However, at ages  $> 10\text{Myr}$  the simulated clusters are smaller than the observed ones.

- Including a primordial binary population leads to an increased cluster expansion so that a perfect match between the evolution of the simulated and observed clusters is now found.
- The number of binaries being destroyed in star clusters after instantaneous gas expulsion depends on the star formation efficiency  $\epsilon$  of the cluster and is the lower, the lower the  $\epsilon$  is as these expand fastest.
- However, the evolution of the leaky star clusters undergoing instantaneous gas loss does not only destroy binaries, but also leads to the formation of new ones. The lower the  $\epsilon$  in a cluster the higher is the number of binaries being formed. However, these binaries are generally very wide  $P > 10^9$ d so that they do not really replace binaries that have been destroyed during the embedded phase of the clusters.

The here obtained results have not only serious implications on how the field binary population is generated but has as well far reaching consequences for the formation of the primordial binary population. The prevailing picture of binary formation assumes, that only very few close binaries are formed during the star formation process. The here proposed picture of the origin of the properties of the field star population, has the consequence that the star formation process would have to produce more close binaries than so far expected. If this is the case than it would be more likely that disc fragmentation is the dominant binary formation mechanism, since in this process binaries naturally form closer to the primary star than in the core fragmentation scenario.

The here found similarity between the field binary population as it is observed in the solar neighbourhood with that the in ONC-like cluster environments processed binary populations imply, that the ONC might represent a prototype of a star forming region in the solar neighbourhood. However, more massive/dense star clusters than the ONC are potentially more important towards the galactic centre and in the spiral arms because they can withstand better the strong tidal field encountered there. The result would be that the field binary population towards the galactic centre could lack wide binaries compared to the binary population in the solar neighbourhood.

The similarity of the period distribution of observed and simulated binary populations could, however, also be explained by the observed binary population being a mixture of the binaries originating from clusters of different densities. This could be achieved in two different ways. First, if the time over which the cluster environment is processing the binary population is the same for all clusters, the lower density clusters have to replace the wide binaries that are destroyed in the denser clusters and are therefore missing in the overall period distribution. This would imply that the total number of stars that are created in sparse clusters is similar to the number of stars generated in dense clusters. This means that sparse clusters, which contain much less stars than dense clusters, have to be much more common than dense clusters.

The second way the field population could emerge from clusters with different densities requires less binaries being destroyed in dense star clusters and more in sparse clusters so that their resulting period distributions are more similar to the observed field period distribution. This could be achieved

by binaries in denser clusters being exposed shorter to the dynamical evolution of the clusters. Since the evolution ceases as soon as the remnant gas is expelled by the cluster, this means that the time the dense clusters are embedded in gas has to be shorter than for the sparser cluster. This could be achieved in a self-consistent way, since the moment the gas is expelled probably depends on the cluster mass as more massive/dense clusters produce more and heavier stars that explode earlier as supernovae and expel the gas.

The properties of the binary population can therefore help to determine, in which environment most stars form and its potential dependence on the location within the Galaxy. Therefore, knowledge of the properties of binary populations throughout the galaxy would be needed, which are currently only available in the solar neighbourhood and some nearby clusters. However, observations of the GAIA spacecraft, that will launch in 2013, could bring major advances in this context, as it provides exact proper motions of about 1 billion stars, which will allow to detect many wide binaries that have not been detected before. Additionally, with the measurements of GAIA it will be possible to determine many more clusters of stars due to their common proper motions, which could help to decide, which the dominant mode of star formation is.





## Bibliography

Aarseth, S. J., 1963, MNRAS **126**, 223.

Aarseth, S. J., 1971, Ap&SS **13**, 324.

Aarseth, S. J., 1972, in *IAU Colloq. 10: Gravitational N-Body Problem*, edited by M. Lecar, volume 31 of *Astrophysics and Space Science Library*, p. 373.

Aarseth, S. J., 2003, *Gravitational N-Body Simulations*.

Aarseth, S. J., M. Henon, & R. Wielen, 1974, A&A **37**, 183.

Adams, F. C., 2000, ApJ **542**, 964.

Ahmad, A., & L. Cohen, 1973, Journal of Computational Physics **12**, 389.

Allison, R. J., S. P. Goodwin, R. J. Parker, R. de Grijs, S. F. Portegies Zwart, & M. B. N. Kouwenhoven, 2009, ApJ **700**, L99.

Andrews, S. M., & J. P. Williams, 2007, ApJ **659**, 705.

Arons, J., & C. E. Max, 1975, ApJ **196**, L77.

Banerjee, S., P. Kroupa, & S. Oh, 2012, ApJ **746**, 15.

Bastian, N., & S. P. Goodwin, 2006, MNRAS **369**, L9.

Bate, M. R., 2000, MNRAS **314**, 33.

Baumgardt, H., & P. Kroupa, 2007, MNRAS **380**, 1589.

Beck, T. L., M. Simon, & L. M. Close, 2003, ApJ **583**, 358.

Bettis, D. G., & V. Szebehely, 1972, in *IAU Colloq. 10: Gravitational N-Body Problem*, edited by M. Lecar, volume 31 of *Astrophysics and Space Science Library*, p. 388.

Binney, J., & M. Merrifield, 1998, *Galactic Astronomy*.

Binney, J., & S. Tremaine, 2008, *Galactic Dynamics: Second Edition* (Princeton University Press).

Blitz, L., 1993, in *Protostars and Planets III*, edited by E. H. Levy & J. I. Lunine, pp. 125–161.

Bonnell, I. A., M. R. Bate, & S. G. Vine, 2003, MNRAS **343**, 413.

- Bonnell, I. A., P. Clark, & M. R. Bate, 2008, *MNRAS* **389**, 1556.
- Bonnell, I. A., & M. B. Davies, 1998, *MNRAS* **295**, 691.
- Chen, H.-C., & C.-M. Ko, 2009, *ApJ* **698**, 1659.
- Clark, P. C., & I. A. Bonnell, 2004, *MNRAS* **347**, L36.
- Clarkson, W., J. R. Lu, A. M. Ghez, M. R. Morris, N. McCrady, A. Stolte, & S. Yelda, 2011, in *The Galactic Center: a Window to the Nuclear Environment of Disk Galaxies*, edited by M. R. Morris, Q. D. Wang, & F. Yuan, volume 439 of *Astronomical Society of the Pacific Conference Series*, p. 119.
- Connelley, M. S., B. Reipurth, & A. T. Tokunaga, 2008, *AJ* **135**, 2526.
- Crowther, P. A., O. Schnurr, R. Hirschi, N. Yusof, R. J. Parker, S. P. Goodwin, & H. A. Kassim, 2010, *MNRAS* **408**, 731.
- de Grijs, R., R. A. Johnson, G. F. Gilmore, & C. M. Frayn, 2002, *MNRAS* **331**, 228.
- Dias, W. S., B. S. Alessi, A. Moitinho, & J. R. D. Lépine, 2002, *A&A* **389**, 871.
- Djorgovski, S. G., & G. Meylan (eds.), 1993, *Structure and dynamics of globular clusters*, volume 50 of *Astronomical Society of the Pacific Conference Series*.
- Duchêne, G., 1999, *A&A* **341**, 547.
- Duquennoy, A., & M. Mayor, 1991, *A&A* **248**, 485.
- Elmegreen, B. G., Y. Efremov, R. E. Pudritz, & H. Zinnecker, 2000, *Protostars and Planets IV*, 179arXiv:astro-ph/9903136.
- Fischer, D. A., & G. W. Marcy, 1992, *ApJ* **396**, 178.
- Fujii, M. S., & S. Portegies Zwart, 2011, *Science* **334**, 1380.
- Geyer, M. P., & A. Burkert, 2001, *MNRAS* **323**, 988.
- Ghez, A. M., G. Neugebauer, & K. Matthews, 1993, *AJ* **106**, 2005.
- Gieles, M., & H. Baumgardt, 2008, *MNRAS* **389**, L28.
- Gieles, M., & S. F. Portegies Zwart, 2011, *MNRAS* **410**, L6.
- Gieles, M., S. F. Portegies Zwart, H. Baumgardt, E. Athanassoula, H. J. G. L. M. Lamers, M. Sipior, & J. Leenaarts, 2006, *MNRAS* **371**, 793.
- Goldreich, P., & S. Tremaine, 1979, *ApJ* **233**, 857.

- Goodwin, S. P., & N. Bastian, 2006, *MNRAS* **373**, 752.
- Gouliermis, D., S. C. Keller, M. Kontizas, E. Kontizas, & I. Bellas-Velidis, 2004, *A&A* **416**, 137.
- Harris, W. E., 1996, *AJ* **112**, 1487.
- Heggie, D. C., 1975, *MNRAS* **173**, 729.
- Heggie, D. C., & S. J. Aarseth, 1992, *MNRAS* **257**, 513.
- Hénon, M., 1960, *Annales d'Astrophysique* **23**, 668.
- Hénon, M., 1961, *Annales d'Astrophysique* **24**, 369.
- Henon, M., 1969, *A&A* **2**, 151.
- Herbig, G. H., 1960, *ApJS* **4**, 337.
- Herbst, W., & R. Racine, 1976, *AJ* **81**, 840.
- Hillenbrand, L. A., 1997, *AJ* **113**, 1733.
- Hillenbrand, L. A., & L. W. Hartmann, 1998, *ApJ* **492**, 540.
- Hills, J. G., 1975, *AJ* **80**, 809.
- Hills, J. G., 1980, *ApJ* **235**, 986.
- Hoyle, F., 1953, *ApJ* **118**, 513.
- Huff, E. M., & S. W. Stahler, 2006, *ApJ* **644**, 355.
- Hurley, J. R., S. J. Aarseth, & M. M. Shara, 2007, *ApJ* **665**, 707.
- Hut, P., 1983a, *ApJ* **268**, 342.
- Hut, P., 1983b, *AJ* **88**, 1549.
- Hut, P., 1993, *ApJ* **403**, 256.
- Hut, P., & J. N. Bahcall, 1983, *ApJ* **268**, 319.
- Inutsuka, S.-I., & S. M. Miyama, 1992, *ApJ* **388**, 392.
- Ivanova, N., K. Belczynski, J. M. Fregeau, & F. A. Rasio, 2005, *MNRAS* **358**, 572.
- Jeffries, R. D., S. P. Littlefair, T. Naylor, & N. J. Mayne, 2011, *MNRAS* **418**, 1948.
- Jones, B. F., & M. F. Walker, 1988, *AJ* **95**, 1755.
- Kaczmarek, T., C. Olczak, & S. Pfalzner, 2011, *A&A* **528**, A144+.

- Khokhlov, A., E. Mueller, & P. Hoeflich, 1993, *A&A* **270**, 223.
- King, I., 1962, *AJ* **67**, 471.
- King, I. R., 1967, *The Dynamics of Star Clusters*, p. 116.
- Köhler, R., M. G. Petr-Gotzens, M. J. McCaughrean, J. Bouvier, G. Duchêne, A. Quirrenbach, & H. Zinnecker, 2006, *A&A* **458**, 461.
- Kornreich, C., T. Kaczmarek, & S. Pfalzner, 2012, *A&A* **543**, A126.
- Kouwenhoven, M. B. N., A. G. A. Brown, S. F. Portegies Zwart, & L. Kaper, 2007, *A&A* **474**, 77.
- Kouwenhoven, M. B. N., S. P. Goodwin, R. J. Parker, M. B. Davies, D. Malmberg, & P. Kroupa, 2010, *MNRAS* **404**, 1835.
- Kratter, K. M., C. D. Matzner, & M. R. Krumholz, 2008, *ApJ* **681**, 375.
- Kratter, K. M., C. D. Matzner, M. R. Krumholz, & R. I. Klein, 2010, *ApJ* **708**, 1585.
- Kraus, A. L., & L. A. Hillenbrand, 2007, *ApJ* **662**, 413.
- Kroupa, P., 1995a, *MNRAS* **277**, 1491.
- Kroupa, P., 1995b, *MNRAS* **277**, 1522.
- Kroupa, P., 1995c, *MNRAS* **277**, 1507.
- Kroupa, P., 2002, *Science* **295**, 82.
- Kroupa, P., S. Aarseth, & J. Hurley, 2001, *MNRAS* **321**, 699.
- Kroupa, P., & J. Bouvier, 2003, *MNRAS* **346**, 343.
- Kroupa, P., & A. Burkert, 2001, *ApJ* **555**, 945.
- Kroupa, P., M. G. Petr, & M. J. McCaughrean, 1999, *New Astronomy* **4**, 495.
- Kruijssen, J. M. D., T. Maschberger, N. Moeckel, C. J. Clarke, N. Bastian, & I. A. Bonnell, 2012, *MNRAS* **419**, 841.
- Kustaanheimo, P., & E. Stiefel, 1965, *Journal für die Reine und Angewandte Mathematik* **218**, 204.
- Lada, C. J., & N. D. Kylafis (eds.), 1999, *The Origin of Stars and Planetary Systems*.
- Lada, C. J., & E. A. Lada, 2003, *ARA&A* **41**, 57.
- Lada, C. J., M. Margulis, & D. Dearborn, 1984, *ApJ* **285**, 141.
- Larson, R. B., 2003, *Reports on Progress in Physics* **66**, 1651.

- Leinert, C., H. Zinnecker, N. Weitzel, J. Christou, S. T. Ridgway, R. Jameson, M. Haas, & R. Lenzen, 1993, *A&A* **278**, 129.
- Levi-Civita, T., 1920, *Acta Math.* **42**, 99.
- Luhman, K. L., E. E. Mamajek, P. R. Allen, & K. L. Cruz, 2009, *ApJ* **703**, 399.
- Lynden-Bell, D., 1967, *MNRAS* **136**, 101.
- Makino, J., 1991, *PASJ* **43**, 859.
- Makino, J., & S. J. Aarseth, 1992, *PASJ* **44**, 141.
- Makino, J., E. Kokubo, & M. Taiji, 1993, *PASJ* **45**, 349.
- Makino, J., M. Taiji, T. Ebisuzaki, & D. Sugimoto, 1997, *ApJ* **480**, 432.
- Mathieu, R. D., 1983, *ApJ* **267**, L97.
- McCaughrean, M., H. Zinnecker, M. Andersen, G. Meeus, & N. Lodieu, 2002, *The Messenger* **109**, 28.
- Mengel, S., M. D. Lehnert, N. Thatte, & R. Genzel, 2002, *A&A* **383**, 137.
- Mengel, S., & L. E. Tacconi-Garman, 2007, *A&A* **466**, 151.
- Moeckel, N., & J. Bally, 2007, *ApJ* **656**, 275.
- Myers, P. C., & A. A. Goodman, 1988, *ApJ* **326**, L27.
- Offner, S. S. R., R. I. Klein, C. F. McKee, & M. R. Krumholz, 2009, *ApJ* **703**, 131.
- Offner, S. S. R., K. M. Kratter, C. D. Matzner, M. R. Krumholz, & R. I. Klein, 2010, *ApJ* **725**, 1485.
- Olczak, C., S. Pfalzner, & A. Eckart, 2008, *A&A* **488**, 191.
- Olczak, C., S. Pfalzner, & A. Eckart, 2010, *A&A* **509**, A63+.
- Olczak, C., S. Pfalzner, & R. Spurzem, 2006, *ApJ* **642**, 1140.
- Olczak, C., R. Spurzem, & T. Henning, 2011, *A&A* **532**, A119.
- Palla, F., & S. W. Stahler, 2000, *ApJ* **540**, 255.
- Parker, R. J., S. P. Goodwin, P. Kroupa, & M. B. N. Kouwenhoven, 2009, *MNRAS* **397**, 1577.
- Pelupessy, F. I., & S. Portegies Zwart, 2012, *MNRAS* **420**, 1503.
- Petr, M. G., V. Coudé du Foresto, S. V. W. Beckwith, A. Richichi, & M. J. McCaughrean, 1998, *ApJ* **500**, 825.

- Pfalzner, & Kaczmarek, in preparation.
- Pfalzner, S., 2009, A&A **498**, L37.
- Pfalzner, S., & C. Olczak, 2007, A&A **475**, 875.
- Pfalzner, S., C. Olczak, & A. Eckart, 2006, A&A **454**, 811.
- Piskunov, A. E., E. Schilbach, N. V. Kharchenko, S. Röser, & R. Scholz, 2007, A&A **468**, 151.
- Plummer, H. C., 1911, MNRAS **71**, 460.
- Preibisch, T., A. G. A. Brown, T. Bridges, E. Guenther, & H. Zinnecker, 2002, AJ **124**, 404.
- Press, W. H., S. A. Teukolsky, W. T. Vetterling, & B. P. Flannery, 2007, *Numerical Recipes 3rd Edition: The Art of Scientific Computing* (Cambridge University Press, New York, NY, USA), 3 edition, ISBN 0521880688, 9780521880688.
- Prosser, C. F., J. R. Stauffer, L. Hartmann, D. R. Soderblom, B. F. Jones, M. W. Werner, & M. J. McCaughrean, 1994, ApJ **421**, 517.
- Raghavan, D., H. A. McAlister, T. J. Henry, D. W. Latham, G. W. Marcy, B. D. Mason, D. R. Gies, R. J. White, & T. A. ten Brummelaar, 2010, ApJS **190**, 1.
- Reggiani, M., M. Robberto, N. Da Rio, M. R. Meyer, D. R. Soderblom, & L. Ricci, 2011, A&A **534**, A83.
- Reid, I. N., & J. E. Gizis, 1997, AJ **113**, 2246.
- Reipurth, B., M. M. Guimarães, M. S. Connelley, & J. Bally, 2007, AJ **134**, 2272.
- Reipurth, B., & H. Zinnecker, 1993, A&A **278**, 81.
- Rochau, B., W. Brandner, A. Stolte, M. Gennaro, D. Gouliermis, N. Da Rio, N. Dzyurkevich, & T. Henning, 2010, ApJ **716**, L90.
- Sabbi, E., A. Nota, M. Tosi, L. J. Smith, J. Gallagher, & M. Cignoni, 2011, ArXiv e-prints 1106.5974.
- Scally, A., C. Clarke, & M. J. McCaughrean, 2005, MNRAS **358**, 742.
- Simon, M., L. M. Close, & T. L. Beck, 1999, AJ **117**, 1375.
- Smith, L. J., & J. S. Gallagher, 2001, MNRAS **326**, 1027.
- Smith, R., M. Fellhauer, S. Goodwin, & P. Assmann, 2011, MNRAS **414**, 3036.
- Sollima, A., 2008, MNRAS **388**, 307.

- Spitzer, L., 1987, *Dynamical evolution of globular clusters*.
- Spitzer, L., Jr., 1958, ApJ **127**, 17.
- Spurzem, R., 1999, Journal of Computational and Applied Mathematics **109**, 407.
- Sridharan, T. K., H. Beuther, M. Saito, F. Wyrowski, & P. Schilke, 2005, The Astrophysical Journal **634**, L57, URL <http://cdsads.u-strasbg.fr/abs/2005ApJ...634L..57S>.
- Stahler, S. W., 2010, MNRAS **402**, 1758.
- Steinhausen, M., C. Olczak, & S. Pfalzner, 2012, A&A **538**, A10.
- Strom, S. E., K. M. Strom, & G. L. Grasdalen, 1975, ARA&A **13**, 187.
- Sugimoto, D., & E. Bettwieser, 1983, MNRAS **204**, 19P.
- Sugimoto, D., Y. Chikada, J. Makino, T. Ito, T. Ebisuzaki, & M. Umemura, 1990, Nature **345**, 33.
- Tsuribe, T., & S.-I. Inutsuka, 1999, ApJ **523**, L155.
- Tutukov, A. V., 1978, A&A **70**, 57.
- Vesperini, E., S. L. W. McMillan, & S. Portegies Zwart, 2009, ApJ **698**, 615.
- von Hoerner, S., 1960, Z. Astrophys **50**, 184.
- Wolff, S. C., S. E. Strom, D. Dror, & K. Venn, 2007, AJ **133**, 1092.





## A Density-dependence of binary dynamics

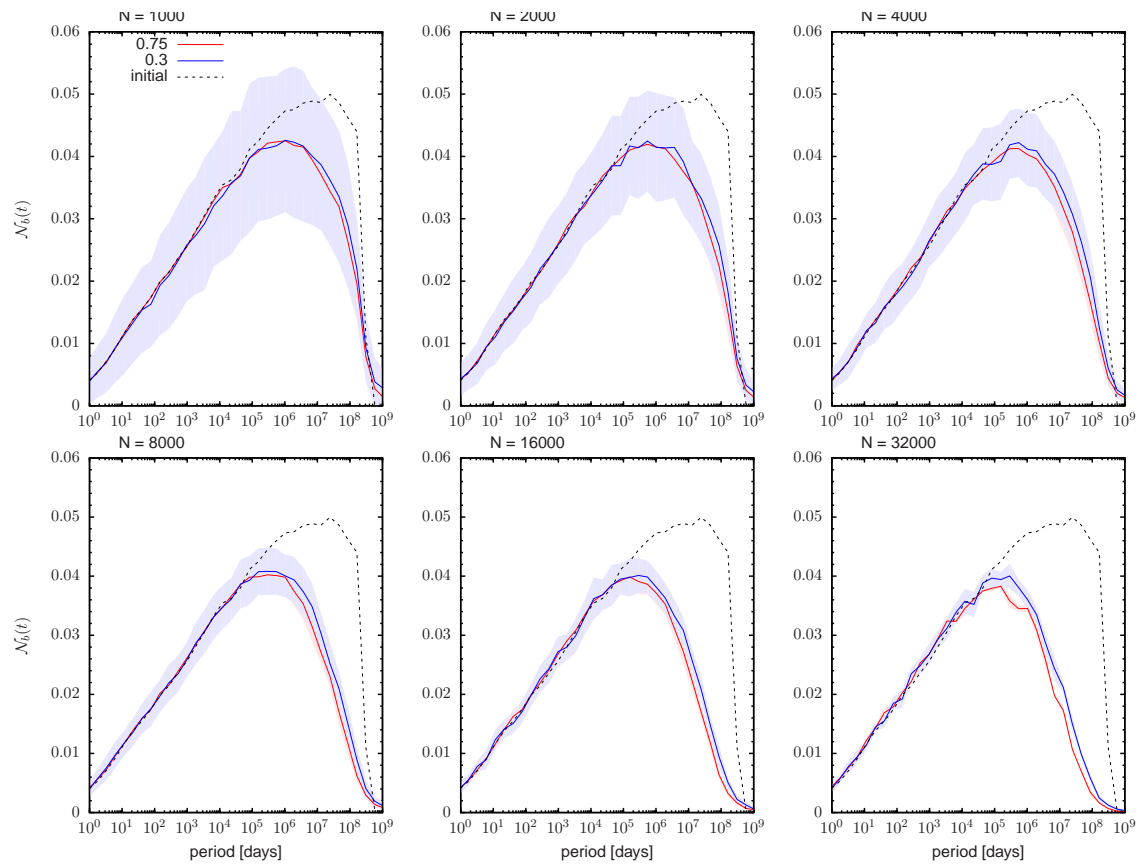


Figure A.1: Normalized period distributions of all clusters after 5Myr.



## B Supervirial Cluster Evolution

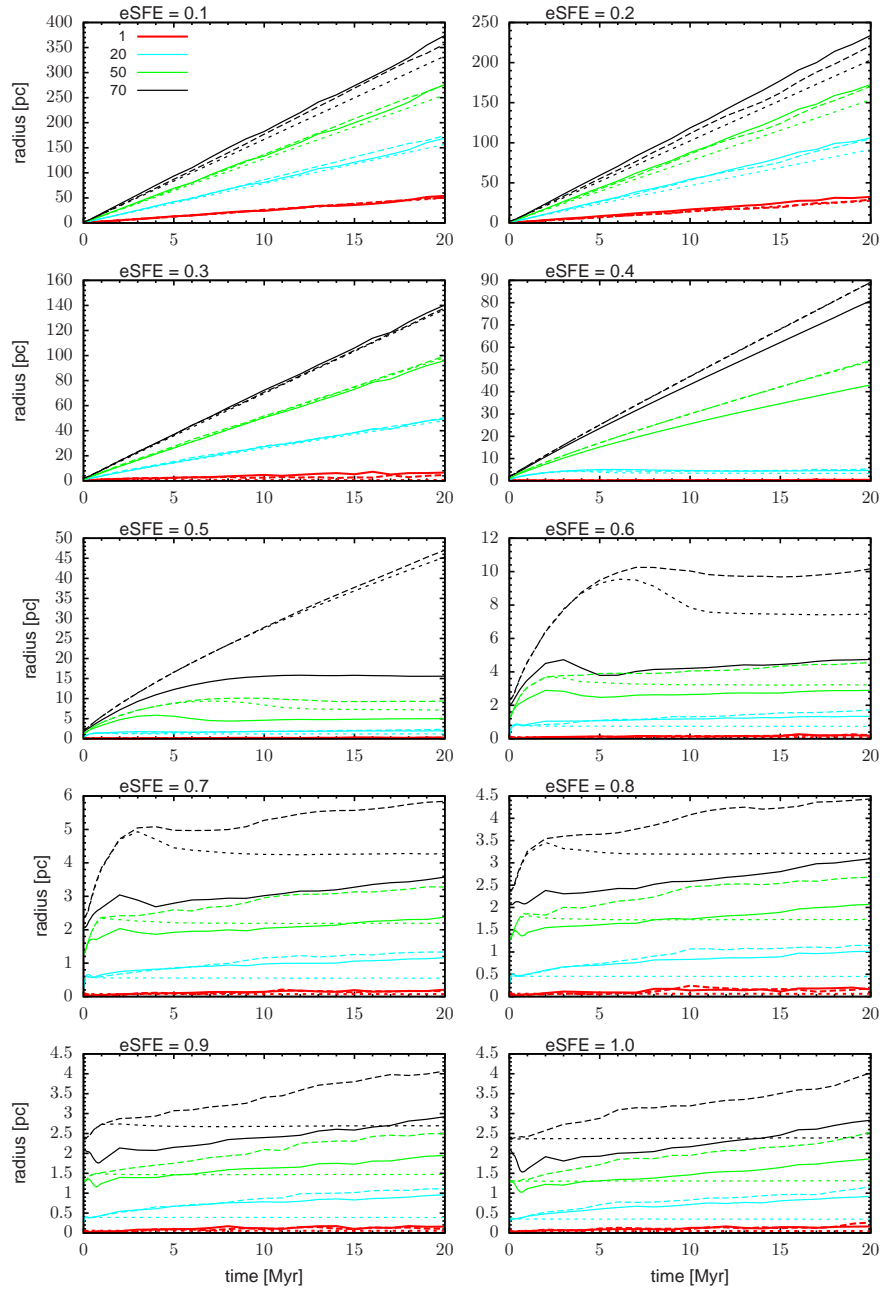


Figure B.1: Evolution of the Lagrangian radii of star clusters with  $\epsilon$  in the range 0.1 – 1.0. Short dashed lines show the evolution of single-mass star clusters, long dashed lines the evolution of star clusters consisting of single stars drawn from the Kroupa (2002) IMF and solid lines the evolution of star cluster set up with a primordial binary population.



## **Acknowledgements**

First I would like to thank Prof. Susanne Pfalzner for giving me the opportunity to write my PhD Thesis in her group and the broad support she has given me over the years.

My thanks also go to Prof. Andreas Eckart from the I. Physalischen Institut der Universität zu Köln and Prof. Karl Menten from the Max-Planck-Institut für Radioastronomie for financing my work in the two institutes.

Next I would like to thank all my colleagues I worked with over the years who were always willing to help me in any situation, may it be professional or during our off-work activities. Especially I would like to thank Christoph Olczak who taught me a lot about cluster dynamics and code development. But also I would like to thank Manuel Steinhausen, Christina Hövel and Andreas Breslau for the help if it was needed.

Last but not least I would like to thank my family, which always supported during my complete studies.



## **Erklärung**

“Ich versichere, dass ich die von mir vorgelegte Dissertation selbständig angefertigt, die benutzten Quellen und Hilfsmittel vollständig angegeben und die Stellen der Arbeit – einschließlich Tabellen, Karten und Abbildungen –, die anderen Werken im Wortlaut oder dem Sinn nach entnommen sind, in jedem Einzelfall als Entlehnung kenntlich gemacht habe; dass diese Dissertation noch keiner anderen Fakultät oder Universität zur Prüfung vorgelegen hat; dass sie – abgesehen von unten angegebenen Teilpublikationen – noch nicht veröffentlicht worden ist sowie, dass ich eine solche Veröffentlichung vor Abschluss des Promotionsverfahrens nicht vornehmen werde. Die Bestimmungen der Promotionsordnung sind mir bekannt. Die von mir vorgelegte Dissertation ist von Frau Prof. Dr. Susanne Pfalzner betreut worden.”

Köln, den





Europass  
Curriculum Vitae



Personal information

Surname(s) / First name(s)	Kaczmarek, Thomas
Address(es)	Maybachstr. 12, 50226 Frechen, Germany
Telephone(s)	02234/17648      Mobile: 0152/53939686
Email(s)	tkaczmarek@mpifr-bonn.mpg.de
Nationality(-ies)	german
Date of birth	09.07.1983
Gender	male

## Education

from May 2011 -	PhD Student Max-Planck-Institut für Radioastronomie Bonn
May 2009 - May 2011	PhD Student I. Physikalisches Institut Universität zu Köln
May 2008 - May 2009	Diploma Thesis: grade 1.4 I. Physikalisches Institut Universität zu Köln “Evolution of the binary population in young dense star clusters”
October 2003 - May 2009	Studies of Physics Universität zu Köln
August 1994 - June 2003	Abitur (final secondary-school examinations): grade 1.9 Gymnasium Frechen

## Experience

August 6 <sup>th</sup> - October 12 <sup>th</sup> 2007	Summer Student programme John von Neumann Institute for computing Jülich
March 2006 - May 2008	Student research assistant I. Physikalisches Institut Universität zu Köln

## Skills and Qualification

Language Skills	German: native English: fluent in writing and speech
Programming skills:	Fortran77, 90, 2003: very good C, Pascal, Python: good MPI and openMP on massively parallel Supercomputers

## Publications

April 2011	Evolution of the binary population in young dense star clusters Kaczmarek, T.; Olczak, C.; Pfalzner, S. (Astronomy & Astrophysics)
May 2012	Towards the field binary population: Influence of orbital decay on close binaries Kornfeld, C.; Kaczmarek T.; Pfalzner S. (Astronomy & Astrophysics)
2012	The evolution of protoplanetary discs in the Arches cluster Olczak, C.; Kaczmarek, T.; Harfst, S.; Pfalzner, S.; Portegies Zwart, S., accepted
2012	Modes of clustered star formation Pfalzner, S.; Kaczmarek, T.; Olczak, C., accepted

